Fusion Energy Engineering Laboratory (FEEL)
Nuclear Engineering Research Group (NERG)
Escola Tècnica Superior d'Enginyeria Industrial de Barcelona
UNIVERSITAT POLITÈCNICA DE CATALUNYA,
BARCELONA, SPAIN

PhD thesis presented by

José Carlos Rivas Reguera

For the degree of doctor at the

UNIVERSITAT POLITÈCNICA DE CATALUNYA

Development of AINA code for the study of loss of plasma control events in ITER and DEMO, and contribution to the systems study of DEMO

Director

Javier Dies
Professor chair of Nuclear Engineering

Para mis padres

To Naoko

I am deeply grateful to Professor Javier Dies, my thesis director, for allowing me to do this thesis and for helping me during the last years, including my participation in several national and international fusion projects.

In developing AINA code, I have been walking on the shoulders of a giant that I never met. This is Takuro Honda, the developer of SAFALY code and author of many publications on ITER safety studies. I can only show my deepest respect for his work.

Werner Gulden, who supported always our activity with AINA code, shared with me many times his scientific and human quality. I am grateful for the opportunity I had to collaborate with him.

I am grateful for the help that I received from Neill Taylor, and also from other scientists working at ITER Safety to solve many questions related to my research.

I am also grateful to Michiya Shimada. He solved during years my questions about plasma and how to implement models in AINA code. No doubt my work would be different without his advice.

I wish to acknowledge to Paloma Castro and Luis Sedano, for the advice and support they gave me at different moments when working at Tecno_FUS project.

David Ward, Richard Kemp, Peter Knight and Michael Kovari helped me to learn a little about PROCESS, a complex code which is a central tool in the design of the European DEMO. Thank you also for your warm hospitality during my stay at Abingdon.

During work in EuroFUSION Safety tasks, I had the opportunity of meeting great scientists working in fusion safety. It is always an endless source of pleasure for me to learn from them about fusion safety. Special thanks to Xue Zhou Jin and Dario Carloni, from KIT, and to Paloma Diaz from CIEMAT.

In JAEA Fusion Reactor Design Group, at IFERC, I found a great group of scientists willing to help in the progress of AINA project. I am deeply grateful to Nakamura-san, Takase-san and Someya-san for their help during the twelve months I spent at Rokkasho-mura.

During these years working in several projects I have found many great scientists, and I tried to learn from them as much as possible, not only science but also human qualities. I will not pretend that my work goes also on their shoulders, but at least I was fortunate enough to follow their steps.

I also found a lot of good friends in the world of nuclear fusion and plasma research, and I find really unfair not to mention all of them. I really enjoyed learning at Madrid, Weert, Karlsruhe and Greifswald, and I can only say that it is great to find old friends whenever I attend a fusion conference. Fusion community has a great spirit, and that is the reason why I am sure this project will succeed.

Framework

This PhD Thesis has been developed in the framework of the following programmes and tasks:

JAPAN-EU collaborative work for development of AINA code in 2014-2015 (C-10321)
Funded by Fusion for Energy in the frame of Broader Approach Activities, 2015-2016
Developed by International Fusion Energy Research Center (IFERC)
Seconded National Expert: Jose Carlos Rivas

EuroFUSION SAE-2.13.1-02 AINA plasma physics module development for DEMO - SAE-2.13.2-01 AINA Breeding blanket module - SAE-2.13.5-01 DEMO-relevant AINA code benchmarking - SAE-2.13.6-01 AINA safety analyses of DEMO scenarios (E-1322)

Funded by EuroFUSION Organisation, 2015
Developed by Departamento de Física e Ingeniería Nuclear, UPC
Principal researcher: Javier Dies

EuroFUSION SAE-2.13.1-01 AINA plasma physics module development for DEMO - SAE-2.13.2-01 AINA Breeding blanket module (E-1322)
Funded by EuroFUSION Organisation, 2014
Developed by Departamento de Física e Ingeniería Nuclear, UPC
Principal researcher: Javier Dies

EFDA WP13-SYS04 Safety - Technical Specification -T07 Development of AINA for DEMO application (E-5033)
Funded by EFDA Organisation, 2013
Developed by Departamento de Física e Ingeniería Nuclear, UPC
Principal researcher: Javier Dies

EFDA WP13-SYS01A System Code - T02: Sensitivity studies of DEMO design to key assumptions (E-5033)
Funded by EFDA Organisation, 2013
Developed by Departamento de Física e Ingeniería Nuclear, UPC
Principal researcher: Javier Dies

Consolider TECNO-FUS Fusion Technology Program (CSD2008-79 TECNO-FUS, V-00111)
Funded by the Innovation and Science Ministry, 2009-2012
Developed by Departamento de Física e Ingeniería Nuclear, UPC
Principal researcher: Javier Dies

ITER Safety Studies: Development of quality management system for AINA code (C-7457)
Funded by ITER Organisation, 2008-2009
Developed by Departamento de Física e Ingeniería Nuclear, UPC
Principal researcher: Javier Dies

ITER: Passive plasma termination for berylium evaporation in LOCA transients (ITER/CT/07/411, C-7155)
Funded by ITER Organisation, 2008
Developed by Departamento de Física e Ingeniería Nuclear, UPC
Principal researcher: Javier Dies

ITER loss of plasma control event evaluations related to the Generic Site Safety Report (UNI607101806289)
Funded by ITER Organisation, 2007
Developed by Departamento de Física e Ingeniería Nuclear, UPC
Principal researcher: Javier Dies

Besides these agreements, this thesis would not be issued without the financial support to the author from the following entities and fellowship programmes:

Chair ARGOS - Funding for the assistance to courses or conferences (2014)
Funded by Consejo de Seguridad Nuclear

Chair ARGOS - Funding for the assistance to courses or conferences (2010)
Funded by Consejo de Seguridad Nuclear

Programa de formación de personal investigador (2009-2012)
Funded by NERG-UPC

Chair ARGOS - Reforma del código Plasma-Pared AINA para estudios de seguridad en ITER (2008-2009)
Funded by Consejo de Seguridad Nuclear

AGAUR- Programa de prestecs per a l'emancipació (2008-2010)
Funded by Generalitat de Catalunya

Significant mention to the Associació d'Enginyers Industrials de Catalunya and the Agrupació Sócio-Cultural dels Enginyers Industrials de Catalunya by the concession of the «Premi-Ajut per la realització de Tesis Doctorals» grant (2010).

Objectives and plan of this thesis

The main objectives of this thesis are as follows:

1. Contribution to the development of AINA code, a safety code for the study of plasma wall transients in nuclear fusion reactors like ITER.
2. Contribution to ITER and DEMO Safety Studies by performing studies of plasma related bounding events with AINA code. The objective is to analyze loss of plasma control transients and thermohydraulic transients by assuming that the plasma control function is lost with the objective of generating results useful to determining if the Emergency Plasma Shut-down System (EPSS) should be a Safety Important Component (SIC).
3. Contribution to the development of a systems code for nuclear fusion reactor conceptual studies.
4. Contribution to generate with a plasma solver rationally justified plasma specifications as input for breeding blanket design: size, shape, neutron source 3D distribution.

In Chapter 1, a brief history of plasma and nuclear fusion research is exposed. In addition, the more important energy issues worldwide are discussed, and nuclear fusion is placed in context with the rest of energy generation alternatives. ITER and the future fusion demonstration reactor characteristics are shown. Safety studies and systems studies are briefly explained.

In Chapter 2, the models and architecture of AINA safety code for ITER and DEMO are described. Numerical, plasma, erosion, blanket and divertor models are exposed. Also explained are all the numerical analyses done in support of the previous models.

In Chapter 3, the ITER safety assessment «Passive plasma termination for beryllium evaporation" is described.

In Chapter 4, the effect of two simultaneous perturbations during a Loss of Plasma Control Transient is described.

In Chapter 5, the Safety Studies of Plasma-Wall Events with AINA code for Japanese DEMO are described

In Chapter 6, the ITER safety assessment «Review of loss of plasma control transients in ITER" is described.

In Chapter 7, the development of a fusion neutron source model for the systems analysis of a tokamak power plant is described.

In Chapter 8, the conclusions and summary are exposed.

In Annex 1, tables of common used terms and variables are included.

In Annex 2, figures resulting from analyses in chapter 6 are presented.

In Annex 3, the Excel macro for automation of AINA execution is presented.

In Annex 4, a code for the calculation of view factors between in-vessel surfaces for arbitrary toroidal configurations is presented.

In Annex 5, the sensitivity analyses done with PROCESS code are presented, and also a python script developed for automation of process execution.

Table of Contents

Figures

Tables

Chapter 1: Magnetic fusion research, a brief history and current context

1.1 Introduction

The history of nuclear fusion research can be traced to an origin in the question about the nature of Sun and its energy. No doubt this question has always accompanied mankind, and many answers were proposed in the past, with uneven success.

However, for the sake of brevity, let's point to a fairly recent milestone in 1939, when the increasingly intensive efforts in astronomy and nuclear physics to unveil Sun's energy secret may well be considered as culminated with the work of the German-American physicist Hans Bethe about the nucleosynthesis in stars.[Beth39]

With his work, a quantitative theory for the energy source of the stars was formulated, that fitted well with the experimental evidence. But also, the general theory of fusion reactions proved as mature enough to allow the beginning of nuclear fusion research, focusing on the exploitation of those reactions to obtain energy.

There was a general optimism in the first years, but from early on, it was evident that the high expectations were unrealistic.[Mead10] Besides, fusion research, as other nuclear research topics, remained as a military secret for several years, and it was not until the conference "Atoms for Peace",[Ener58] in Geneva, that major nuclear power countries declassified it and allowed scientists to share information.

This was a short time after Lawson, in 1957, established the fundamental conditions needed to achieve net power,[Laws57] which are summarised in a minimum

value of the triple product of temperature, density and residence time, in order for the fusion reaction to have a positive energetic balance.

Many different proposals were investigated during these early years, but the efforts quickly focused on a short number of magnetic configurations: tokamak, stellarator, magnetic mirror, and toroidal and linear pinches.[Mead10] The success of one of them, tokamak, in confining plasma,[Tamm58] led to many new experimental facilities all around the world basing their designs on this concept .

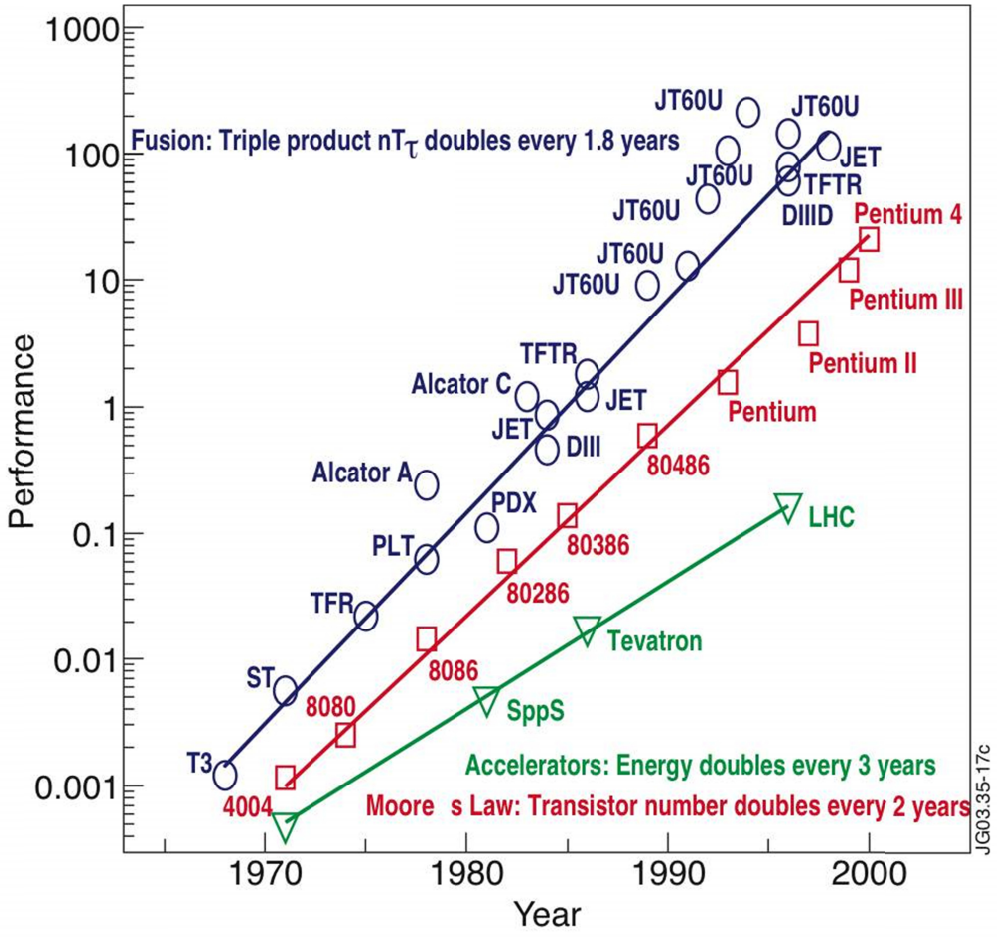

Figure. 1-1: Tokamaks performance evolution compared with Moore's law[Rma15]

Nowadays, tokamaks have a leading position in fusion research.[Elgu10] In 1991, Joint European Torus (JET) tokamak produced a significant amount of fusion power (1.7 MW) from controlled fusion reactions.[Jett92] In 1993, Tokamak Fusion Test Reactor

(TFTR), at Princeton, produced 10 MW from a 50% deuterium-tritium plasma.[Kmmc95] JET owns a current world record of 16 MW, produced in 1997.[KGGL99]

In 1978, in the context of an impending oil crisis, the director general of the IAEA, Sigvard Ecklund, sounded out the member governments sponsoring fusion research about their interest in the development of a next major step.

Yevgeny Velikhov, on behalf of the Soviet Union, proposed that the world's fusion programs join together under the auspices of the IAEA to develop and operate a first Experimental Power Reactor based on the tokamak concept.

The first step was done with the INTOR Workshop, in which fusion scientists and engineers from EURATOM, Japan, the USA, and the Soviet Union worked to assess the readiness of the world's fusion programs to undertake the task.[Stac10]

The collaboration was fruitful in identifying many of the critical issues and in suggesting areas of future research,[Frei07] and thus, on the basis of INTOR results, and in a political context of goodwill between the Soviet Union and USA, General Secretary Gorbachev made the recommendation to President Reagan at the 1985 Geneva summit that led to the formation of the ITER project.

ITER conceptual design activities took place from 1988 to 1991, and produced a consensus on the objectives and operational parameters for the machine.[Inte91] Subsequent engineering design activities produced in 1998 a design proposal[Iter99a] for a 1,500MW reactor, and a budget, which was not accepted by the USA, who withdraw from the project in 1999. This forced the other parties to redesign the project with a lower budget, which led to a new design proposal in 2001 for a 500MW reactor, named ITER-Feat.[Iter01]

The new proposal was accepted, and ITER Project started in 2006, through an agreement signed in Paris by seven parties, EURATOM, Japan, Russia, and the USA, which rejoined the project together with three new signing members: China, India and Korea. ITER Organisation (IO), was established as the institution responsible of the implementation, exploitation and decommissioning of the ITER Project, and the location of ITER was agreed in Cadarache, France, where it is currently being built.

If ITER succeeds, it will demonstrate the viability of magnetic nuclear fusion as a usable energy source. If so, ITER will be followed by a demonstration power plant (DEMO), which should be the last previous step to a commercial power plant (PROTO). However, in the conclusions of the Fusion Fast Track Experts Meeting, held

on 27 November 2001, it was proposed that the last two stages would combine in a single step, in order to achieve energy production in 20-30 years.[King00]

1.2 The ITER project

ITER will be the next step of the long term magnetic fusion research activities, developed during more than sixty years. It is an international project, with parties' population representing more than a half of the whole world population.

Its overall programmatic objective is "to demonstrate the scientific and technological feasibility of fusion energy for peaceful purposes".[Iter01]

To match this goal, ITER should burn deuterium-tritium plasmas with a sufficient net gain Q of generated fusion energy over external energy heating, and with steady-state as an ultimate goal. It also should demonstrate the integration of essential reactor technologies, and allow the integrated testing of the high-heat-flux and nuclear components required. Even though ignition is not a primary objective, it is not precluded "a priori" from the results of ITER operation.

A central goal of ITER is to demonstrate the safety and environmental potential of fusion as an energy source.[Iter01]

The safety principles and criteria for minimising the consequences to the public and the environment from ITER operations are based on internationally recognised safety criteria and radiological limits following ICRP and IAEA recommendations, and in particular on the concept of Defense in Depth and the As Low As Reasonably Achievable (ALARA) principle.[GCMS07]

1.3 Brief introduction to ITER physics and technical basis

1.3.1 Fusion reaction

There are several possible fusion reactions which could be used to obtain energy. However, with the currently available technology, the only practical fusion reaction to be considered is that of deuterium and tritium (Eq. 1.1).

$$ {}_{1}^{2}D \quad + {}_{1}^{3}T \rightarrow {}_{1}^{4}He + n + 17.6\ MeV \qquad \text{Eq. 1.1} $$

In ITER, this reaction will take place mostly in the center of the plasma core, where the conditions of temperature, density and residence time are more favourable.

Although deuterium is abundant in nature, and its supply does not create a major problem, tritium is radioactive, with a half life of 12.32 years, and the only natural source is cosmic rays, so it does not occur naturally on Earth, in practical terms. Thus, it will be externally provided for ITER. Moreover, to guarantee the sustainability of fusion reactor operation, it must be generated as a part of the reactor working cycle.

This will be done through the use of a breeding blanket based on lithium, which can absorb neutrons to produce helium and tritium. Two isotopes of lithium can be used with this purpose: ^{7}Li and ^{6}Li. The ^{7}Li reaction is endothermic and quickly decreases with the slowing energy of neutrons. That is, it works with "fast" neutrons. Its product is a tritium atom and a "slow" neutron (Eq. 1.2).

$$^{7}_{3}Li + n \rightarrow {}^{4}_{2}He + {}^{3}_{1}T + n \; - 2.5\; MeV \qquad \text{Eq. 1.2}$$

The ^{6}Li reaction has a cross section that increases monotonically with slowing neutron energy, that is, it works better with slow neutrons rather than with the fast neutrons produced by D-T fusion reaction. It is an exothermic reaction and produces tritium and helium (Eq. 1.3)

$$^{6}_{3}Li + n \rightarrow {}^{4}_{2}He + {}^{3}_{1}T + 4.8\; MeV \qquad \text{Eq. 1.3}$$

Lithium is also abundant, but the breeding blanket technology must still be developed. A cornerstone of the ITER project will be the testing of different breeding blanket designs, which will provide crucial information to the development of future reactor blankets.

Tritium is a major concern from the safety point of view, and the circuits and devices devoted to its management are an important part of the future ITER facility. The other major concern is the activation of the wall elements by the neutron flux. However, when compared with fission reactors, a low volume of activated products in the medium term is foreseen.[CMDG00]

1.3.2 ITER configuration

ITER experiment will be a tokamak. The tokamak operation is based on the confinement of plasmas with the aid of an externally supplied magnetic field. In ITER, the plasma will be confined and heated to make possible a sustained fusion reaction with net energy gain.

Table 1-1: ITER main parameters, 500 MW inductive scenario[PoSM06a]

ITER Parameters	
Total fusion power	500 MW
Additional heating power	50 MW
Q - fusion power/ additional heating power	≥ 10
Average 14MeV neutron wall loading	≥ 0.5 MW/m^2
Plasma inductive burn time	300-500 s
Plasma major radius (R)	6.2 m
Plasma minor radius (a)	2.0 m
Plasma current (Ip)	15 MA
Toroidal field at 6.2 m radius (BT)	5.3 T
Type of Plasma	D-T
Volume of plasma (m^3)	837

Specifically, ITER will be a long pulse tokamak with elongated plasma and single null poloidal divertor. Its main parameters can be found in several sources,[Iter01, PoSM06] and vary depending on the considered reference scenario. Five design scenarios are specified for ITER in the Plasma Performance Assessment document, from which the inductive, 500 MW scenario parameters are outlined in Table 1-1.

Theoretical MHD equilibrium calculations show that the magnetic field configuration must be toroidally closed,[GrRu58] in order to optimize confinement of the plasma particles, which tend to move spiraling around the direction of the magnetic field. To minimize further drifts, the field must be also twisted.

The particularity of a tokamak is the way it generates this twisted toroidal magnetic field. In other systems, the confining field is entirely generated by external coils or magnets. In a tokamak, an externally driven current through the plasma plays a role in generating the twist of the confining field.

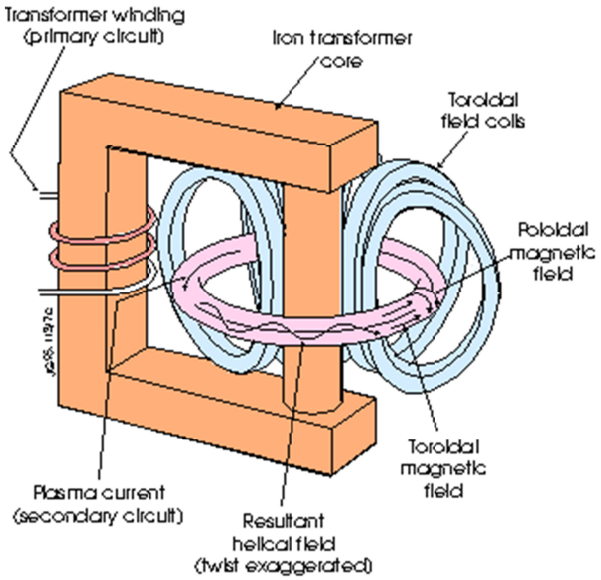

Figure 1-2: Schematic representation of a tokamak fusion device (source: EFDA)

Therefore, the magnetic configuration in a tokamak is mainly generated by a set of poloidal coils, which create a toroidal field and a central solenoid, which drive a current in the plasma by transformer effect, which in turn generates a poloidal component of the field, giving it the mentioned twist.

Stability of the plasma is also a major issue. The most dangerous instabilities for the integrity of the vessel are the vertical displacement events (VDEs), the runaway electrons and the major disruptions, which are linked with ideal MHD instabilities. To deal with these events, the plasma operation must take place within some empirical stability limits which define an operating window. These limits are the upper density limit, the poloidal current limit, the safety factor and the beta limit.[Iter99b]

The confinement that can be achieved for a given magnetic configuration can be expressed by the beta coefficient, which represents the ratio between the plasma pressure and the magnetic pressure. It depends on the external magnetic field, which in turn depends on the technology employed for the coils.

If copper is used as conductor material in the coils, the resistive losses would represent a significant fraction of the consumed power. On the other hand, if superconductor coils are employed, there is a limit in the current that if surpassed will lead to a current quench.

Confinement can be increased by using an elongated and triangularised plasma configuration. Therefore, toroidal coils are used also for shaping the plasma, and to create the single null configuration. They are used also for position control of the plasma, with the main mission of avoiding the VDEs.

Plasma instabilities other than the ideal MHD ones are not so dangerous in terms of disruption risk, but can degrade confinement through different ways. A physical mechanism to increase the confinement is called the high confinement mode, or H-mode. It is a sudden increase in the confinement that happens when the external heating in the plasma core is increased while simultaneously edge turbulence vanishes.

However, the H-mode has a characteristic instability, which is the edge localised modes or ELMs, which show as periodical particle and energy pulses over the scrape off layer (SOL), multiplying the maximum energy over the divertor target. Ergodic field coils have been successfully tested to control the intensity of ELMs and will be installed in ITER.

The ITER plasma will be contained in a vacuum vessel, with the mission of maintaining high vacuum (in turn contained in a cryostat), where blanket modules will be mounted, with the mission of contain neutronic radiation, which will support First Wall slabs, where the plasma facing tiles are mounted. The divertor is a critical element of the wall, because it will receive the maximum surface energy density from the plasma.

All the wall elements will be refrigerated by a high capacity cooling system, with water as coolant fluid. Four independent cooling circuits will be installed; three for the First Wall and blanket, and one for the divertor. Hot water from the outlet of the circuits will be externally cooled in cooling towers, without generation of energy.

However, the burning plasma environment will limit the lifespan of the in-vessel elements, due to radiation damage, disruptions, and other factors like the cyclical operation mode. Therefore, different in-vessel parts must be replaced, and this will be done with a remotely controlled manipulation system, which will work between the Main Vessel and the Hot Cell building, where maintenance will be done. This manipulation system includes a sophisticated robotic arm for in-vessel tasks.

The vacuum vessel will have several ports intended for maintenance, and for the location of the heating and fuelling systems, the test blanket modules (TBMs), and other systems and probes.

Heating and current drive systems will have the mission of providing energy to the plasma and creating a current during the non-inductive scenarios. They can be divided in radiofrequency systems and neutral beam systems.[Iter99b]

There will be two fuelling systems in ITER:[NLFJ98] a gas injection system, with the mission of injecting ions and impurities in the plasma core and also of controlling the particle flux to the divertor; and a pellet injection system, with the mission of injecting ions directly in the plasma core and thus with the capacity of exert isotopic control.

Tritium management will be also a major issue in ITER, because this radioactive, artificially produced element will be supplied externally, and tritium plant balance must be carefully controlled. ITER will be equipped with a tritium management facility[GABC07] which will process divertor cryopumps exhaust to separate hydrogenic ions from helium, and then to separate and store the different hydrogen isotopes. Deuterium and tritium will be later fueled again to the tokamak from the storage device. Tritium permeation fluxes will be recovered also from the coolant circuit and from the ventilation circuits.

There are many other systems in ITER, like the power supply system, or the CODAC (Control, Data Access and Communication), which will be the control system of ITER, but to explain them in detail is beyond the purpose of this introduction. Detailed information can be found in the available literature.[Iter01]

1.4 ITER and DEMO Safety studies

As previous studies have shown in the past, magnetic fusion technology “has very good inherent safety qualities, among which are absence of 'chain reaction' and no production of long-lived, highly radiotoxic products”.[CMDG00]

The inherent safety characteristics of a fusion reactor are due to the very low fuel inventory inside the plasma chamber and to the passive shutdown characteristic of the plasma in case of malfunction.[GuRC00]

Regarding radioactivity, only tritium is radioactive among fuels, and its half-life is 12.32 years. Additionally, the activated materials resulting from the neutronic flux would need less than 100 years to reduce their activity to low levels.[GuRC00]

ITER Safety studies have developed a technical safety basis for the regulatory and licensing of the ITER site, with attention to emissions during normal operation, occupational safety, decommissioning, and potential accidents and incidents.

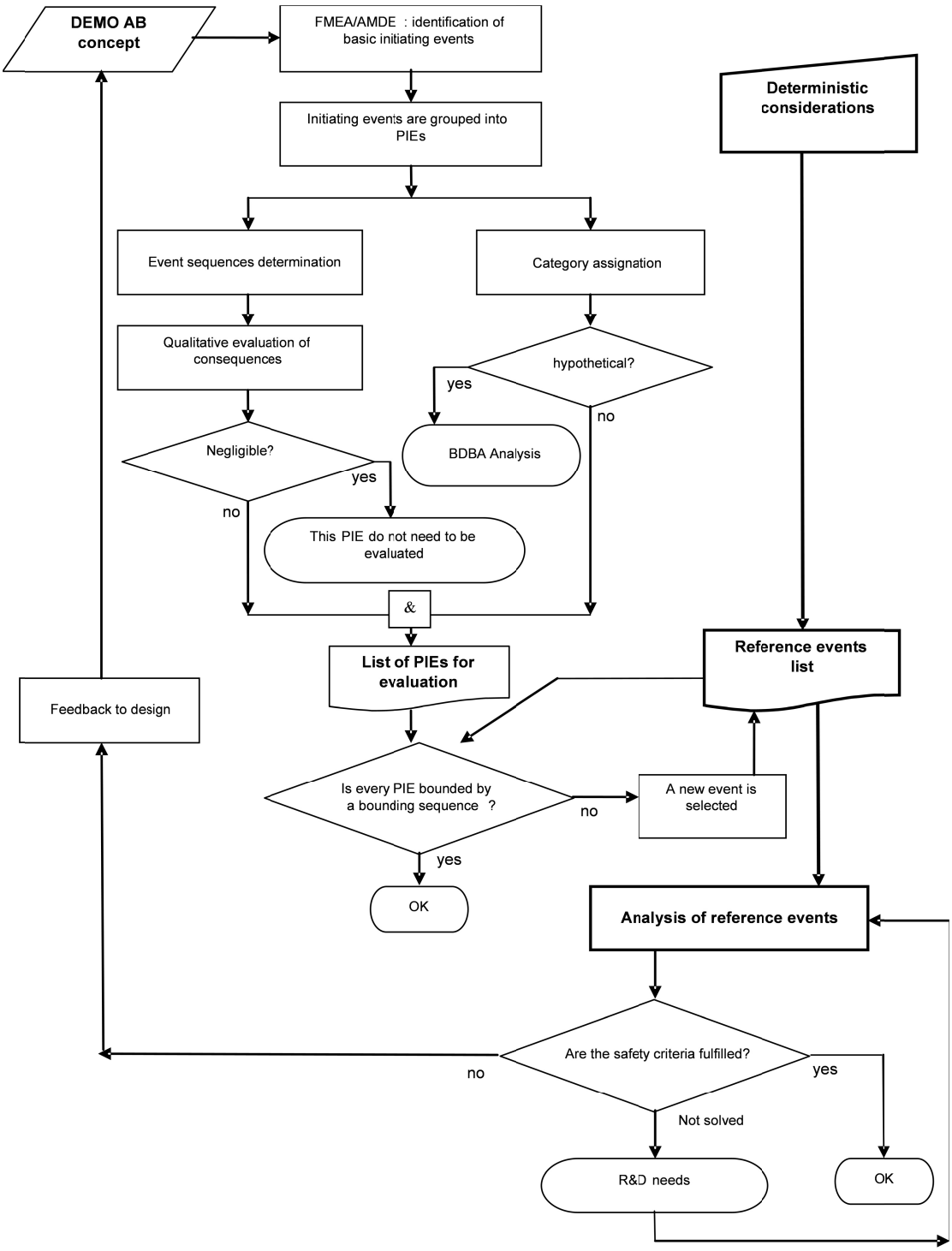

Figure 1-3 Accident analysis process in ITER and DEMO safety studies

DEMO safety studies take benefit from the ITER experience. For the study of accident sequences, the work is based on the methodology developed for ITER safety

studies, which prescribe a combination of top-down and bottom-up approaches to find the accident sequences challenging the confinement. It is outlined in the diagram shown in Figure 1-3.

Top-down and bottom-up strategies are combined through a PIE-PIT diagram. A list of Postulated Initiating Events (PIEs) is produced from a Functional Failure Modes and Effects Analysis (FFMEA) study.

Additionally, the study of the confinement strategy leads to the formulation of a Master Logic Diagram (MLD) where the top event is an excessive off-site release, which allows the determination of several plant confinement states where a release was produced. Reference events producing a release of radioactive materials are postulated for each plant state.

Then, accident sequences are studied for each PIE, determining which plant state is reached at the end of the sequence. The results are then shown in a PIE-PIT matrix.

By assigning frequency category and radiological consequences, it is then possible to determine the bounding events for each plant state in terms of risk.

1.5 DEMO design activities

There are several conceptual DEMO studies around the world.[FZZZ09, KNHC08, MCPL06, TNEK09, Wu08] As for the European approach, EuroFUSION, through its agency Fusion for Energy, is working together with Japan in the Broader Approach project to develop a DEMO reactor, progressing along the following main lines:[Tsun09]

- The development of burning DT plasmas, and the understanding of issues like alpha particle heating efficiency or burning fraction optimisation, which will be pursued during ITER operation.

- The optimisation of stable, steady state plasma operation, which will be explored by means of alternative designs, like advanced tokamaks or stellarators.

- The study of material compatibility with the high neutronic and surface energy loads expected, which will be developed by IFMIF facility, now in EVEDA phase.

- The development of efficient breeding blanket systems, in terms of tritium generation and high temperature heat extraction. This task will be undergone also during ITER operation, through the TBM testing program.

Therefore, the final design will depend on the results from the ITER experiment and from the IFMIF irradiation facility, as well as on the results coming from other fusion experiments, like EAST, K-STAR, SST-1 and Tore Supra.

1.5.1 The TECNO_FUS program

One of the most challenging components of a future fusion reactor is the breeding blanket. ITER will work with externally supplied tritium, but a fusion power plant must generate its own tritium to ensure the viability of the process. Thus, all the ITER Parties (EU, USA, China, Japan, Korea and India) plan to test breeding blanket mock-up modules in ITER.

TECNO_FUS[SSHV09] was a Spanish Fusion Technology Program articulated around the conceptual design of a Breeding Blanket and its Plant Auxiliary Systems. The R&D activities developed in this program were:

- Advanced neutronics for design of fusion technology components,
- Development of production and characterisation capabilities of fusion reactors materials,
- Computational fluid-dynamics for magneto-hydrodynamics for Fusion Technology,
- Component structural thermo-mechanics and electromagnetic design analysis,
- Conception and design of singular plants for the research of auxiliary systems like power or tritium systems,
- Safety and environmental impact studies of fusion technology,
- Development of specific instrumentation for the basic set of design responses,
- Components and systems engineering integration,
- Confined plasma for fusion reactor design and specifications.

The activities are integrated around the design of a Dual Coolant He/Lead-Lithium breeding blanket and plant auxiliary systems for DEMO fusion reactor specifications.[MCPL06]

The activity in relation to the development of plasma specifications for fusion reactor design has been developed in the frame of this thesis work. It included the development and validation of a systems code, able to create plasma equilibria and geometry specifications that can be used as an input for conceptual design activities.

Chapter 2: The AINA 3.0 code

2.1 Introduction

2.1.1 Antecedents of AINA code

AINA, acronym of Analyses of IN-vessel Accidents, is a code that integrates a global balance plasma dynamics model and a radial and poloidal thermal analysis of in-vessel components by considering separately First Wall and divertor modules and performing a thermal analysis for each one in the depth direction. AINA is an evolution of the SAFALY[HBUS97a] code, developed by Takuro Honda at HRL, Hitachi, Ltd. in the frame of a JAERI contract. SAFALY code was built on the basis of simplified models and it was thought to be fully adaptable to the quantitative analysis of accidental sequences of a tokamak. Uncertainties coming up from design of the reactor, from plasma physics or from material properties could be overcome with parametric studies and the adaptability of the code.

In the beginning, it was used to evaluate events of power excursion in the old ITER design of 1.5GW[HBUS97b] and it was gradually improved to analyse different accidental events taking into consideration burning control, confinement mode transition and impurities transport, among others.

Finally in 2001, SAFALY was used to evaluate some accidental sequences of loss of plasma control inside the ITER of 0.5GW.[HBNS01] Since then, no improvement or actualisation of the code was implemented until 2004, when the European Fusion Development Agreement (EFDA) transferred the code to the Fusion Energy Engineering Laboratory (FEEL) of the Technical University of Catalonia-BarcelonaTech, where further development is still being carried out.

The version of the code that arrived to the FEEL is stored as JA001207, that is a modified version by Mr. Neyatani from JAHT in December 2000 as deduced from code comments. From 2004 to 2007, the SAFALY code was upgraded and validated,[DaDI00, Izqu06, Sola05, Tous00] and the evolved code received the name of AINA.

Since 2009, in the frame of a contract between ITER and the Technical University of Catalonia-Barcelona Tech, a new code has been developed, on the basis of the same 0D plasma algorithms and 1D wall thermal algorithms, receiving the name of AINA 2.0.[DiRB10a, DiRB10b, DRBD10a, DRBD10b]

The current number for stable version is 3,[RiDi13] and has two sub-versions, 3.0 for ITER and 3.1 for DEMO water cooled pebble bed blanket. Versions 3.2, 3.3, 3 .4 and 3.5 are foreseen for European next step blankets.

2.1.2 AINA requirements definition

AINA is a code used for tokamak safety studies, specifically for the study of the effect of off-normal plasma events over the integrity of in-vessel components, from a thermal point of view.

The considered accidents that can lead to these plasma transients are perturbations in fuelling or external heating systems of plasma, or thermohydraulic accidents without in-vessel leak, or a combination of both, and always assuming the complete loss of the plasma control function, until a passive shutdown ends the plasma discharge.

The devices that are susceptible to be studied with AINA code are ITER and DEMO fusion reactors. The safety studies to be done with this code are intended to provide information useful as input for other calculations in the frame of accident sequence analyses. Also in the frame of conceptual design activities, for the design of the plasma control system, to decide about the maximum recovery time in case of malfunction, and whether or not the Emergency Plasma Shut-down System (EPSS) should be a Safety Important System (SIC) for a specific fusion reactor design.

AINA code uses simplified models for plasma dynamics, plasma-wall interaction and wall thermal evolution. Its purpose is to establish an envelope for the worst effects that such transients can cause, useful to extract conclusions in a safety analysis.

Therefore, its models must be conservative from a safety point of view. This goal is achieved by entering margins in the physical models that guarantee a maximum in the final effects over the wall that is over the expected results from a more realistic physical model.[UPWB96]

At the same time, the models should predict as accurately as possible the behavior of the studied system. This means that the safety envelope of the physical system should be as close as possible to the realistic physical results to minimize the error induced by the safety margins.

2.1.3 AINA application structure

AINA code is contained in a dll that is called from a graphical interface. It consists of two different class hierarchies:

- Numerical calculation classes: They are intended to perform numerical calculations on the basis of the system's derivatives, in order to predict the time evolution or the static equilibrium. It has been preferred to use standard and verified algorithms, because convergence, stability and accuracy can be verified.

- System modelling classes: With the purpose of embedding the data structures and calculation functions that form the different physics and engineering models of the system. From these classes, the necessary values of the differential equations can be obtained in order to perform the numerical calculations.

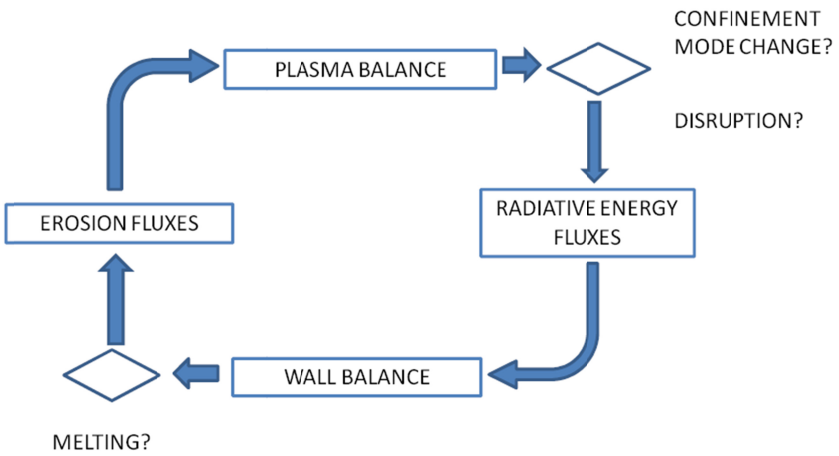

Figure 2-1 AINA CORE main loop schematics

The execution of a simulation uses two processes:

- Calculation of steady state equilibrium. It is used in determining the limits of the plasma operating window and in establishing the initial condition for a transient simulation.

- Propagation of a transient in time. It takes the steady state equilibrium as the initial condition and, on the basis of programmed perturbations, calculates the time evolution of the system.

For both simulation processes, the flux diagram in Figure 2-1 explains the calculations that are done.

2.1.4 Interface applications

The graphical interface is called AINA_GUI.[1] It is a Windows application that allows the configuration of input parameters and the rendering of output parameters. It is described in a previous work,,[IDEU08] and is not included here.

For advanced studies with AINA an Excel macro in Visual Basic has been developed. It allows the execution of a list of simulations with AINA code and the processing of the results, extracting useful statistics like maxima, minima or average values for each of the solution variables. It is described in Annex 3.

[1] There is also an interface library which is necessary to deal with the link between the c# managed code of AINA_GUI and the c++ unmanaged code of AINA_CORE.

2.2 The plasma core model

In AINA code, a 0D multi-fluid approach is used to solve the mass and energy balance of the plasma core. The terms of the balance equations are calculated through volume integrals which use a simplified toroidal geometry and radial profiles of plasma density and temperature. MHD equilibrium results are determined by external input parameters. The heat conduction losses are calculated using an overall confinement time scaling.

AINA code can calculate the steady state equilibrium from a specified fusion power and average ion temperature. If a perturbation is introduced in the plasma for a safety analysis, the code can calculate the time evolution of the plasma variables.

The 0D, or "overall balance" model of the plasma core, calculates the solution of the conservation equations of mass and energy considered in the overall plasma core system. The transport problem is avoided by using a value for the global confinement time and energy particles, which can be extracted from theoretical considerations or using an empirical or semi-empirical scaling. IPB98 scaling, based on multi-machine database,[Iter99b] which was used for ITER design, is also used in AINA code.

The advantage of using a 0D approach is its lower computational requirement. That is why 0D codes are still used for sensitivity or optimisation studies where a large number of simulations are required, and where there is often a significant theoretical uncertainty.

A drawback of 0D codes, when compared with transport codes, is that radial profiles are not calculated, but must be provided as an input argument to the calculations. In the case of ITER, safety analyses are performed over a set of reference design and plasma scenarios.[PoSM06a]

2.2.1 Geometry of plasma used in AINA code

An axisymmetric torus is considered, with a poloidal section shape of the LCMS composed by four elliptical arcs.

To define these arcs, two elongations $\kappa_X^{(u)}$, $\kappa_X^{(l)}$ and two triangularities $\delta_X^{(u)}$, $\delta_X^{(l)}$, plus the value of minor toroidal radius are used. To determine volume and surface of plasma, the major toroidal radius is needed also.

Volume and surface results are shown in Eq. 2.1 and Eq. 2.2

$$V = \pi^2 a^2 R\left(\kappa_X^{(u)} + \kappa_X^{(l)}\right) \quad \text{Eq. 2.1}$$

$$S = 2\pi \times \sum_i^4 R_i \times p_i \quad \text{Eq. 2.2}$$

With p_i the approximate poloidal perimeter,[Rama14] of each of the four ellipse arcs, and R_i the radii of the centroids of each of the quarter elliptical areas. The external area is obtained then by applying Pappus theorem.[KeBl46] (Eq. 2.3, Eq. 2.4, Eq. 2.5, Eq. 2.6, Eq. 2.7, Eq. 2.8, Eq. 2.9, Eq. 2.10).

$$p_1 = \pi a\left[3\left(1 + \delta_X^{(u)} + \kappa_X^{(u)}\right) - \sqrt{\left(1 + \delta_X^{(u)} + 3\kappa_X^{(u)}\right)\left(3 + 3\delta_X^{(u)} + \kappa_X^{(u)}\right)}\right] \quad \text{Eq. 2.3}$$

$$p_2 = \pi a\left[3\left(1 - \delta_X^{(u)} + \kappa_X^{(u)}\right) - \sqrt{\left(1 - \delta_X^{(u)} + 3\kappa_X^{(u)}\right)\left(3 - 3\delta_X^{(u)} + \kappa_X^{(u)}\right)}\right] \quad \text{Eq. 2.4}$$

$$p_3 = \pi a\left[3\left(1 + \delta_X^{(l)} + \kappa_X^{(l)}\right) - \sqrt{\left(1 + \delta_X^{(l)} + 3\kappa_X^{(l)}\right)\left(3 + 3\delta_X^{(l)} + \kappa_X^{(l)}\right)}\right] \quad \text{Eq. 2.5}$$

$$p_4 = \pi a\left[3\left(1 - \delta_X^{(l)} + \kappa_X^{(l)}\right) - \sqrt{\left(1 - \delta_X^{(l)} + 3\kappa_X^{(l)}\right)\left(3 - 3\delta_X^{(l)} + \kappa_X^{(l)}\right)}\right] \quad \text{Eq. 2.6}$$

$$R_1 = R - a\delta_X^{(u)} - \frac{4}{3\pi}a\left(1 + \delta_X^{(u)}\right) \quad \text{Eq. 2.7}$$

$$R_2 = R - a\delta_X^{(u)} - \frac{4}{3\pi}a\left(1 - \delta_X^{(u)}\right) \quad \text{Eq. 2.8}$$

$$R_3 = R - a\delta_X^{(l)} - \frac{4}{3\pi}a\left(1 + \delta_X^{(l)}\right) \quad \text{Eq. 2.9}$$

$$R_4 = R - a\delta_X^{(l)} - \frac{4}{3\pi}a\left(1 - \delta_X^{(l)}\right) \quad \text{Eq. 2.10}$$

2.2.2 Volume integrals, volume average values, linear average values

Parabolic functions are used to model radial profiles of density, temperature and current, as shown in Eq. 2.11.

$$\mathrm{x(r)} = \mathrm{x_{max}}\left(1 - \left(\frac{\mathrm{r}}{\mathrm{a}}\right)^2\right)^{\alpha\,\mathrm{x}} \qquad \text{Eq. 2.11}$$

The volume average of a magnitude is calculated as shown in Eq. 2.12 whereas the line average is calculated as shown in Eq. 2.13.

$$\langle x \rangle = \int_V x(\vec{r})\overrightarrow{dr} \qquad \text{Eq. 2.12}$$

$$\bar{x} = \int_0^a x(r)dr \qquad \text{Eq. 2.13}$$

In the case of a parabolic profile, the results are shown in Eq. 2.14 and Eq. 2.15.

$$\langle x \rangle = x_{max}\beta(1, \alpha_x + 1) \qquad \text{Eq. 2.14}$$

$$\bar{x} = x_{max}\beta\left(\frac{1}{2}, \alpha_x + 1\right) \qquad \text{Eq. 2.15}$$

All the variables included in the 0D plasma balance equations are calculated as volume integrals of quantities that are taken as constant in every isoflux surface. This in practice means that they are functions of local variables that in this model are calculated by parabolic radial profiles and not of by actual geometrical position.

With this consideration in mind, the volume integral of a function is calculated as shown in Eq. 2.16, with $\rho = \frac{r}{a}$.

$$F(x) = \int_V f\big(x(\vec{r})\big)\,\overrightarrow{dr} = V \times \int_0^1 f\big(x(\rho)\big)\rho d\rho \qquad \text{Eq. 2.16}$$

2.2.3 Particles and power balance

As it was mentioned before, the code contains a global balance model for plasma dynamics. This model is able to determine the steady state parameters of the plasma, taking as input parameters volume averaged ionic temperature, and fusion power.

Besides, it is able to calculate the time evolution of the initial equilibrium when some perturbation in plasma equilibrium is configured.

The principles of conservation of mass and energy are used to formulate the balance equations of the system.

2.2.4 Particles balance in the main plasma

The mass balance equations for core plasma are shown in Eq. 2.17.

$$\frac{dn_H}{dt} = S_H - 2S_\alpha - \frac{n_H}{\tau_{p,H}} \qquad \text{Eq. 2.17}$$
$$\frac{dn_\alpha}{dt} = S_\alpha - \frac{n_\alpha}{\tau_{p,\alpha}}$$
$$\frac{dn_{Z,j}}{dt} = S_{Z,j} - \frac{n_{Z,j}}{\tau_{p,Z}}$$

Electric charge conservation assumption allows the calculation of the electron density. A complete ionisation is assumed for all the considered species (Eq. 2.18).

$$n_e = n_i + 2n_\alpha + \sum_i (Z_i n_z) \qquad \text{Eq. 2.18}$$

The total alpha particles source is calculated by volume integration of the specific alpha particle source (Eq. 2.18).

$$\mathrm{S}_\alpha = \int_V s_\alpha dV \qquad \text{Eq. 2.19}$$

The percentage of both deuterium and tritium is assumed to be 50%. Thus, the specific alpha source term is given by Eq. 2.20.

$$n_D = n_T = \frac{n_H}{2} \qquad \text{Eq. 2.20}$$
$$\mathrm{s}_\alpha = \mathrm{n}_\mathrm{D} n_T \langle \sigma v \rangle_{DT} = \frac{1}{4} n_H^2 \langle \sigma v \rangle_{DT}$$

The velocity averaged cross-section of the deuterium-tritium nuclear fusion reaction is calculated with the Bosch-Hale fit (Eq. 2.21).[HsGm92]

$$\langle\sigma v\rangle_{DT} = 10^{-6}\times C1\times\theta\times e^{-3\xi}\times\left[\xi/m_r c^2 T^3\right]^{0.5} \qquad \text{Eq. 2.21}$$

$$\theta = T/\left(1 - T\left(C2 + T\left(C4 + T\times C6\right)\right)/\left(1 + T\left(C5 + T\times C7\right)\right)\right)$$

$$\xi = \left[B_G^2/4\theta\right]^{1/3}$$

$$B_G = 34.3827 \qquad m_r c^2 = 1.124656\times10^6 \qquad C1 = 1.17302\times10^{-9}$$

$$C2 = 1.51361\times10^{-2} \qquad C3 = 7.51886\times10^{-2} \qquad C4 = 4.60643\times10^{-3}$$

$$C5 = 1.35\times10^{-2} \qquad C6 = -1.06750\times10^{-4} \qquad C7 = 1.366\times10^{-5}$$

For the initial equilibrium, Eq. 2.17 transforms in Eq. 2.22.

$$S_H = 2S_\alpha + \frac{n_H}{\tau_{p,H}} \qquad \text{Eq. 2.22}$$

$$n_\alpha = S_\alpha \tau_{p,\alpha}$$

$$n_{Z,j} = S_{Z,j}\tau_{p,Z}$$

Which is solved when we define the confinement times (Eq. 2.38, Eq. 2.40), the impurity sources (Eq. 2.79) and the value of the hydrogen density, that can be calculated if we assume known the ion temperature profile and the isotopic composition (Eq. 2.20) by just specifying the fusion power.

$$P_{FUS} = S_\alpha E_{FUS} \qquad \text{Eq. 2.23}$$

2.2.5 Power balance in the main plasma

The power balance equations for core plasma are shown in Eq. 2.24.

$$\frac{3}{2}\frac{d(n_i T_i)}{dt} = P_{ext,i} + P_{\alpha,i} - P_{ie} - \frac{3}{2}\frac{n_i T_i}{\tau_{E,i}} \qquad \text{Eq. 2.24}$$

$$\frac{3}{2}\frac{d(n_e T_e)}{dt} = P_{ext,e} + P_{\alpha,e} + P_\Omega + P_{ie} - P_{br} - P_{syn} - P_{li} - \frac{3}{2}\frac{n_e T_e}{\tau_{E,e}}$$

The *power* exchanged *between ions and electrons* is shown in Eq. 2.25.[HBUS97b, WeCa04]

$$p_{ie} = -\frac{3}{2} n_e \frac{dT_e}{dt} = \frac{3}{2} n_e \frac{T_i - T_e}{\tau_{i,e}} \qquad \text{Eq. 2.25}$$
$$\tau_{i,e} = \sum_k \frac{m_{i,k}}{2m_e} \tau_{e,k}$$

Where $\tau_{i,e}$ is the heat exchange time[WeCa04] and $\tau_{e,k}$ is the electron collision frequency, given by Eq. 2.26.

$$\tau_{e,k} = 3(2\pi)^{3/2} \frac{\varepsilon_0^2 m_e^{1/2} T_e^{3/2}}{n_{Z,k} Z_k^2 e^4 \ln \Lambda} \qquad \text{Eq. 2.26}$$

The frequency of collisions is determined by the faster electrons. The energy is transferred to the ions by a fraction m_e/m_i.[WeCa04]

The final result is shown in Eq. 2.27.

$$p_{ie} = 1.5 \cdot 10^{-19} \cdot \ln \Lambda \cdot n_e \cdot \sum_k \frac{Z_k n_k}{A_k} \frac{T_i - T_e}{T_e^{1.5}} \qquad \text{Eq. 2.27}$$

Where A_k is the atomic mass, Z_k the atomic number and ln Λ is the Coulomb logarithm.

2.2.6 Heating

The *alpha power sources* are calculated with Eq. 2.28. It is assumed also that alpha particles remain confined until they get thermalised, except for those *ripple lost*. Therefore, the P_α term represents the alpha power which effectively thermalizes inside the plasma. The ripple factor is an input parameter of the simulation.

$$S_\alpha = \frac{1}{4} \int_V n_H^2 \langle \sigma v \rangle_{DT} \, dV \qquad \text{Eq. 2.28}$$
$$P_\alpha = S_\alpha \left(E_\alpha - \frac{3}{2} T_i \right) (1 - f_{ripple})$$

The *fraction of alpha power absorbed by electrons* is shown in Eq. 2.29.[HBUS97a]

$$f_\alpha = 1 - \left(\frac{T_e}{50}\right) - 0.37\left(\frac{T_e}{50}\right)^{1.75} \qquad \text{Eq. 2.29}$$

The ohmic heating power density is[AJDU01] shown in Eq. 2.30.

$$p_\Omega = \eta\, j_\Omega^2 \qquad \text{Eq. 2.30}$$

To obtain the ohmic current from the total poloidal current, the bootstrap and current drive components must be substracted (Eq. 2.31).

$$j_\Omega = j_P - j_{BS} - j_{CD} \qquad \text{Eq. 2.31}$$

And the plasma resistivity parallel to the magnetic field is given by the product of the Spitzer resistivity corrected for impurities η_S, and the neoclassical correction factor γ_{NC} (Eq. 2.32).

$$\eta_\parallel = \eta_S\, \gamma_{NC} = \eta_0 \frac{Z_{eff} \ln\Lambda}{T_e^{1.5}} \gamma_{NC} \qquad \text{Eq. 2.32}$$

$$\eta_0 = 0.51 \frac{m_e^{1.5} e^2}{3\varepsilon_0^2 (2\pi)^{1.5}} \cong 1.66 \times 10^{-9}$$

$$\gamma_{NC} = \frac{1}{1 - 1.95\left(\frac{\rho}{A}\right)^{0.5} + 0.95\frac{\rho}{A}}$$

2.2.7 Power losses

The power losses in the plasma core can be summarised as radiation losses and confinement losses. Radiation losses originate in charged particles' acceleration. Because of their lighter mass, electrons suffer harsher accelerations, so only their effects are considered here.

Depending on the origin of the acceleration of the electrons, the core radiation can be divided in bremsstrahlung and synchrotron radiation. Bremsstrahlung radiation is emitted in the range of the X-rays' wavelengths mainly due to the electron-ion collisions.

Power losses by Bremsstrahlung are calculated in code by means of the expression[GoRu95] in Eq. 2.33.

$$p_{br} = 3.34 \cdot 10^{-21} n_e \sum_k Z_k^2 n_k T_e^{0.5} \qquad \text{Eq. 2.33}$$

Synchrotron radiation has its origin in the gyromotion of the electrons around the direction of the magnetic field confining the plasma. Because of the complexity of the exact calculation, synchrotron radiation losses are roughly calculated by expressions deduced for homogeneous cylindrical plasmas[TrKu58]. The emission is in the millimetre wavelength region. Consequently, the emmited radiation is both absorbed by the plasma itself and reflected by the First Wall.

Synchrotron power losses are computed through the Albajar fit (Eq. 2.34).[AlJG01]

$$\begin{aligned} P_{syn,r}(MW) &= 3.84 \times 10^{-8} (1-r)^{1/2} Ra^{1.38} k^{0.79} \\ &\times B_t^{2.62} n_{e_0(20)}^{0.38} T_{e_0} \left(16 + T_{e_0}\right)^{2.61} \\ &\times \left(1 + 0.12 \frac{T_{e_0}}{p_{a_0}^{0.41}} \right)^{-1.51} \\ &\times K(\alpha_n, \alpha_T, \beta_T) G(A) \end{aligned} \qquad \text{Eq. 2.34}$$

where

$$\begin{aligned} K(\alpha_n, \alpha_T, \beta_T) &= (\alpha_n + 3.87\alpha_T + 1.46)^{-0.79} \\ &\times (1.98 + \alpha_T)^{1.36} \beta_T^{2.14} \\ &\times \left(\beta_T^{1.53} + 1.87\alpha_T - 0.16\right)^{-1.33} \end{aligned}$$

$$G(A) = 0.93\left[1 + 0.85 \exp(-0.82A)\right]$$

$$p_{a_0} = 6.04 \times 10^3 \frac{a n_{e_0(20)}}{B_t}$$

Because of the presence of impurities, power losses are enhanced. On the one hand, the bremsstrahlung radiation increases because of the higher value of the effective charge of the plasma. On the other hand, several atomic physical processes such as ionisation by electron collisions, radiative recombination, charge exchange recombination and excitation produce the so-called line radiation.

The line radiation is maximal at low temperatures, i.e. of the order of tens of eV, for the low Z impurities, and of the order of 1 keV for medium Z impurities, and it vanishes for core temperatures in which such species are fully ionised. Heavy impurities (metals) and their associated line radiation must be absolutely avoided in a thermonuclear plasma core.

With the previous statements, it seems obvious that line radiation losses will be only important at the plasma edge, where they contribute to dissipate the conductive-convective heat flux. Thus, radiation losses at the plasma core power balance are dominated by bremsstrahlung radiation.[AJDU01]

Line power losses, due to electronic transitions in not completely ionised atoms in the plasma, are expected to be important only in the relatively cold plasma edge. Near the plasma axis, only high Z impurities like tungsten would radiate, but they are expected to be marginal in the plasma core.

Three options have been used in AINA code. The first one, due to Uckan,[UPWB96] was inherited from SAFALY code, and is shown in Eq. 2.35. It requires the steady state value to be introduced as input.

$$\frac{P_{edge}}{P_{edge}^{0}} = \left(\frac{f_{z-edge}}{f_{z-edge}^{0}}\right)^{0.75} \times \left(\frac{n_{edge}}{n_{edge}^{0}}\right)^{1.5} = \left(\frac{n_{z-edge} \times n_e}{n_{z-edge}^{0} \times n_e^{0}}\right)^{0.75} \qquad \text{Eq. 2.35}$$

Where P_{edge}^{0} is the steady state value of edge radiation, which can be specified by input, $f_{z-edge} = n_{z-edge} / n_{edge}$ the impurity fraction at the edge and $n_{edge} = k \cdot n_e$ the electron density at the edge calculated by the fraction of n_{edge} / n_e, given by input.

The second one is due to Matthews et al.[MAAG97] It was obtained through a multi-machine regression, and fits reasonably well with the current experimental evidence. It is shown in Eq. 2.36 and was used in the AINA 2.0 version.

$$P_{edge} = \frac{10^{-33}}{5.6} n_e^{1.95} S^{1.03} \frac{Z_{eff}^{*} - 1}{Z_r^{0.19}} \qquad \text{Eq. 2.36}$$

$$Z_{eff}^{*} = 1 + f_r Z_r (Z_r - 1)$$

$$\frac{P_{edge}}{P_{edge}^{0}} = \left(\frac{n_e}{n_e^{0}}\right)^{1.95} \times \frac{Z_{eff}^{*} - 1}{Z_{eff}^{*\,0} - 1} \times \left(\frac{Z_r^{0}}{Z_r}\right)^{0.19}$$

However, the previous expressions do not take into account the possible variations in the temperature and radial profiles of the plasma during a transient. Therefore, in the 3.0 version of AINA code, the line power is evaluated following the method exposed by Post and Jensen,[PJTG77] as it was proposed also in a previous work,[Izqu06] but now the line power losses are effectively integrated over the plasma volume, thus taking into account the local variations in temperature, density and impurity fraction (Eq. 2.37),

$$p_{line} = n_e \times n_z \times Lz \qquad \text{Eq. 2.37}$$
$$with$$
$$\log_{10} Lz = \sum_{i=0}^{5} A(i) \times \left\{\log_{10}\left[T_i(keV)\right]\right\}^i$$

where $A(i)$ are the polynomial fitting coefficients for each of the impurity species.

2.2.8 Confinement time, confinement mode transition

The transport problem in a 0-D code is solved by using a global scaling for particle and energy confinement times. This way, the conductive losses are calculated as the quotient between the plasma mass, or energy, and the corresponding confinement time.

For the energy confinement time, empirical scalings based on a multi-machine database[Iter99b] are used to determine the corresponding values in H or L mode. In Eq. 2.38, the equations used in AINA code for H-mode and L-mode scalings are shown.

ITER98(y) updated law H - mode

$$\tau_{\mathrm{E,e}} = 0.0562 I^{0.93} R^{1.97} \left(\frac{a}{R}\right)^{0.58} k_{H5,6}^{0.78} n_{19}^{0.41} B^{0.15} A_i^{0.19} P^{-0.69} F \qquad \text{Eq. 2.38}$$

ITER98(y) updated law L - mode

$$\tau_{\mathrm{E,e}} = \frac{0.023 I^{0.96} R^{1.83} k_{H5,6}^{0.64} n_{19}^{0.4} B^{0.03} A_i^{0.2}}{\left(\frac{a}{R}\right)^{0.06} P^{0.73}} F$$

These scalings have a limited range of validity, and thus, during the simulation of a plasma transient, can yield physically implausible results. Therefore, they are bounded with a scaling based on theoretical considerations (Eq. 2.39), as prescribed by Uckan.[UPWB96]

$$\tau_E = \min\left\{\tau_E(neoclassical); \tau_E(\Omega); \tau_E(ELMy\ H\ mode)\right\} \qquad \text{Eq. 2.39}$$
$$\approx \min\left\{\tau_E(\Omega); \tau_E(ELMy\ H\ mode)\right\}$$
$$\tau_E(\Omega) = 0.07\left[n_{20}\right] a R^2 q_\Psi \qquad \text{"}Neo\ Alcator\ scaling\text{"}$$

The value of the energy confinement time at steady state is required for the calculation of plasma energy conductive losses. The scaling law for particle confinement time τ_p is not sufficiently established compared with that of the energy

confinement time, mainly due to existence of two dominant particle sources, i.e. central fuelling by NBI and pellet injection; and edge fuelling by gas puffing and recycling. Scaling laws for particle confinement time in ELMy H-mode plasmas of JT-60U and DIII-D were proposed with separately defined confinement times for central fuelling and edge fuelling[HKAN99, TaMB01]. However, there is not yet a database with data from many machines like the one for the energy confinement time.[Kike07].

Therefore, assumptions for the relative magnitude of $\tau_{E,i}$and $\tau_{p,i}$ are used on the basis of the energy confinement time of the electrons[HBUS97b] (Eq. 2.40),

$$\tau_{E,i} = C_i \tau_{E,e} \ , \tau_{P,i} = \tau_{P,imp} = C_P \tau_{E,e} \ , \tau_{P,\alpha} = C_\alpha \tau_{E,e} \qquad \text{Eq. 2.40}$$

where C_i, C_P and C_α are constants. Ion energy confinement time is taken as the same as the electron energy confinement time.

The transition between confinement modes H and L is considered to take place when the power crossing the separatrix by loss of confinement goes beyond or falls below a certain threshold power.

We take the expressions in Eq. 2.41 for transitions from *H* to *L* and from *L* to *H* being as conservative as possible from the maximum achievable fusion power point of view,[UPWB96]

$$\begin{aligned} &if\left(P_{SEP} < P_{THR}\right) \longrightarrow Transition \quad H-L \\ &\quad P_{THR} = 0.2 \times \min\left(P_{THRi}\right) \quad i = 1 \ldots 5 \\ &if\left(P_{SEP} > P_{THR}\right) \longrightarrow Transition \quad L-H \\ &\quad P_{THR} = 0.5 \times \min\left(P_{THRi}\right) \quad i = 1 \ldots 5 \end{aligned} \qquad \text{Eq. 2.41}$$

where the threshold values (Eq. 2.42) are calculated as prescribed in the “Plasma Performance Assessment” ITER document.[PoSM06a]

$$P_{THR0} = 0.1 \times n_{e,20}{}^{0.46} \times B_T{}^{0.87} \times S^{0.84} \times M^{-1} \qquad \text{Eq. 2.42}$$

$$P_{THR1} = 0.084 \times n_{e,20}{}^{0.73} \times B_T{}^{0.74} \times S^{0.98} \times M^{-1}$$

$$P_{THR2} = 0.144 \times n_{e,20}{}^{0.7} \times |B|_{out}^{0.7} \times S^{0.9} \times M^{-1} \times \left(Z_{eff}/2\right)^{0.7} \times F(A)^{\gamma}$$

with :

$$S = 4\pi^2 aR\left(\left(1+\kappa^2\right)/2\right)^{0.5}$$

$$|B|_{out} = \left(B_{t,out}^2 + B_{p,out}^2\right)^{0.5}$$

$$B_{t,out} = B \times A/(A+1), \quad B_{p,out} = \left(\mu_0 I/2\pi a\right) \times \left(1 + A^{-1}\right), \quad A = R/a$$

$$F(A) = 0.1A/f(A), \quad f(A) \approx 1 - \left[1/(1+A)\right]^{0.5}, \quad \gamma = 0.5 \pm 0.5$$

The power value used for both the confinement time scalings and the L-H mode transitions (Eq. 2.43) is also calculated as prescribed in the "Plasma Performance Assessment" ITER document, and is estimated to be about 30% more conservative.[PoSM06a]

$$P = P_{\alpha} + P_{aux} + P_{oh} - P_{br} - P_{sy} - P_{li}/3 \qquad \text{Eq. 2.43}$$

2.2.9 Other plasma parameters and models

The *bootstrap current* ratio, the fraction of the toroidal current which is self-generated due to the bootstrap effect, is calculated as shown in Eq. 2.44.[AERG92]

$$f_{bootstrap} = \frac{I_{boot}}{I_p} = C_{bs}\left(\varepsilon^{1/2}\beta_p\right)^{1.3} \qquad \text{Eq. 2.44}$$

$$C_{bs} = 1.32 - 0.235\left(q_{95}/q_0\right) + 0.0185\left(q_{95}/q_0\right)^2$$

$$\beta_p = \beta_T \times 10^{-2} \times \left(\frac{B_T \cdot 5.0 \cdot a \cdot \sqrt{k_{95}}}{I_P}\right)^2$$

The resistive loop voltage (Eq. 2.45) can be calculated using the previously defined neoclassical resistivity.[UcOC91]

$$e_\Omega = \eta\, j_\Omega \qquad \text{Eq. 2.45}$$
$$V_{Loop} = \int_L E dl = \int_L \langle e_\Omega \rangle_S dl = \int_L \langle \eta\, j_\Omega \rangle_S dl$$
$$with \quad \langle \circ \rangle_S = \frac{\int \circ\, ds}{S}$$

2.2.10 Instabilities driving to plasma termination

The termination of the plasma discharge due to a disruption means the end of the simulation in AINA code. The following ways of plasma termination have been implemented:

- *Beta limit (Troyon limit),*[FRHS84]

$$\beta_t \geq \beta_{lim} \qquad \text{Eq. 2.46}$$
$$\beta_{lim} = g_{Troyon} \frac{I\,[MA]}{a\,[m] B_t[T]}$$

  Where, in Eq. 2.46, g_{Troyon} is an empiric coefficient. *Beta* is the ratio between kinetic and magnetic pressure: when plasma's kinetic pressure is greater than magnetic confinement there's a disruption, but if kinetic pressure isn't enough to withstand magnetic pressure to a certain degree it shrinks to the point of collapse as well.

- *Density limit (Greenwald limit:)*[Mart02] there is a limit on the mean density of electrons before a disruptive plasma ending, given by Eq. 2.47

$$\bar{n}_e \left[10^{20} m^{-3}\right] \geq \frac{I[MA]}{\pi \cdot a^2 [m^2]} \qquad \text{Eq. 2.47}$$

  A value of *2·Greenwald limit* has been specified as conservative enough from the safety point of view.

- *Radiative collapse*. If, during a transient simulation, the radiated power exceeds the input power supplied by means of external heating (NBI

and RF) and α-power, fusion can't be self-sustained any more (Eq. 2.48). Hence, the plasma finishes disruptively.

$$P_{\alpha} + P_{aux} + P_{oh} - P_{br} - P_{sy} - P_{li} \leq 0 \qquad \text{Eq. 2.48}$$

- *Locked modes*: these are instabilities susceptible to drive the plasma to a sudden disruption. They are very likely to appear during the low density phase required for H-mode access, although they might also be present in other transients.[HBNS01] A lower bound (Eq. 2.49) has been specified in code based on ITER Physics Basis document.[Iter99b]

$$\bar{n}_e \leq 2 \cdot 10^{19} \ m^{-3} \qquad \text{Eq. 2.49}$$

2.3 The plasma-wall interaction model

2.3.1 Introduction

The tokamak plasma, although confined by a magnetic field, is still in contact with a solid wall that strongly influences its characteristics. To minimize contact with the wall, limiters or divertors are used.

ITER uses a poloidal divertor with a single null configuration. This means that most of the plasma-wall interaction takes place in the divertor. In the First Wall, nevertheless, non-negligible processes develop, where neutral recombination plays a central role. Impurities flows produced by erosion of the First Wall have the drawback that they have a particularly high efficiency to enter in the central plasma compared with those produced in the divertor.[Stan00]

Divertor operation is taken as defined in the Plasma Performance Assessment document,[PoSM06a] in a semi-detached regime. However, the model allows the divertor operation regime to change during a transient.[THNH98]

The plasma wall interaction model implemented in AINA focuses on two aspects:

- Calculation of energy fluxes, necessary for the thermal equilibrium calculation of the wall. These energy fluxes include the fluxes coming from the plasma and the fluxes emitted from the wall. The fluxes coming from the plasma can be classified as:
    1. Neutron power deposition. Neutrons penetrate the wall, so the deposition has volumetric nature.
    2. Surface wall loading at First Wall. It is considered, for the purposes of modelling in AINA code, to happen at the wall surface. Its origins are electromagnetic power losses at plasma core and the energy of the particles colliding with First Wall.
    3. Surface wall loading at divertor. At the targets, surface wall loading is considered to come exclusively from the colliding particles. At the rest of the divertor, it comes from EM power and also from colliding particles. The behaviour, however, depends on the regime of the divertor: attached, detached or semidetached.

The fluxes emitted from the wall are used for wall thermal equilibrium calculation. The radiative balance between surfaces is calculated taking into account the view factor, which is calculated with an external code developed in the frame of this thesis.[RiDF15]

– Calculation of surface erosion and impurity fluxes to core plasma, on the basis of particle fluxes hitting the wall. The calculation process is as follows:

1. Particle fluxes wall loading obtained on the basis of data from SOLPS simulation[KLKR09] is used to interpolate during plasma transient to obtain particle fluxes. Then, the energy of particles at the wall surface is calculated with a sheath model.
2. Erosion of surfaces is calculated from the previous result, taking into account physical sputtering and radiation enhanced sublimation.
3. Impurity flux to core plasma is then calculated from erosion data with a simple model that uses a screening factor and a time delay as main modelling parameters. [HBUS97a]

Surfaces for the calculation regions cover the entire wall surface, except for the targets area, which is variable. For each calculation region, the maximum flux value is taken in order to make the result more robust.

2.3.2 AINA model of power deposition in in-vessel components

2.3.2.1 Surface heat fluxes

The equation for the surface heat fluence calculation at a generic module of First Wall is shown in Eq. 2.50, where $P_{rad,core}$ is the total electromagnetic power radiated from the plasma core, $f_{wall\ loading}$ is the peaking factor in the calculation region and surface is the wall surface of the corresponding module:

$$\dot{q}_{radiative}^{surface\ j} = P_{rad,core} \times \frac{\int_{surface\ j} f_{wall\ loading}\ ds}{surface_j} \qquad \text{Eq. 2.50}$$

In the case of ITER radiative surface load at First Wall, due to the difficulty and uncertainties to determine a poloidal wall loading, a peaking value is assumed for all the poloidal section.[Loar08]

In the case of Japanese DEMO, a tentative wall loading was produced on the basis of SONIC code simulation data.[HASN14]

At targets, peak power flux is calculated with parametric equations based on SOLPS simulations[AHGG03, GHGA07, PKPJ07] and at the rest of divertor, heat fluxes are calculated on the basis of a wall loading for the remainder of power flux to divertor.

$$\dot{q}_{radiative}^{surface\ j} = \left(P_{separatrix} - P_{targets}\right) \times \frac{\int_{surface\ j} f_{wall\ loading}\, ds}{surface_j} \qquad \text{Eq. 2.51}$$

The wetted area of divertor target is adjusted to keep the energy balance in divertor. The poloidal width of the wetted area tends to decrease with the increase in $q_{div\text{-}target}$, a tendency which is consistent with the experimental results.[Ayma01a]

Finally, to calculate the flux boundary condition for the thermal equilibrium at in-vessel walls, the energy of colliding particle fluxes (ions, electrons, neutrals) is added, the sublimation energy is substracted, and finally 3D radiative thermal equilibrium with other in-vessel surfaces is calculated.

$$\dot{q}_{TOTAL}^{surface\ j} = \dot{q}_{radiative}^{surface\ j} + \dot{q}_{particles}^{surface\ j} - \dot{q}_{sublimation}^{surface\ j} + \sum_{k \neq j} \dot{q}_{exchange}^{k,j} \qquad \text{Eq. 2.52}$$

2.3.2.2 Neutronic heat flux

The AINA model for thermal load in a generic wall module due to incoming fusion neutrons is shown in Eq. 2.53, where S_α is calculated in Eq. 2.28, E_n is the mean energy of neutrons, $f_{wall\ loading}$ is the wall loading function in the surface of the module, and $surface_j$ is the wall surface of the corresponding calculation region:

$$\dot{q}_{NEUTRON}^{surface\ j}(0,0) = S_\alpha \times E_n \times \frac{\int_{surface\ j} f_{wall\ loading}\, ds}{surface_j} \qquad \text{Eq. 2.53}$$

To obtain the radial, or volumetric heat flux deposition during transient, a weighting coefficient based on the variation of fusion power with respect to initial equilibrium is used.

$$\dot{q}_{NEUTRON}^{surface\ j}(r,t) = \dot{q}_{NEUTRON}^{surface\ j}(0,0) \times \frac{P_{FUSION}(t)}{P_{FUSION}(0)} \times weighting(r) \qquad \text{Eq. 2.54}$$

In the case of ITER, neutron wall loading has been taken from the ITER Safety Analysis Data List document.[Topi08] In Figure 2-2 the steady state neutron wall loading of the ITER 500MW inductive scenario is shown.

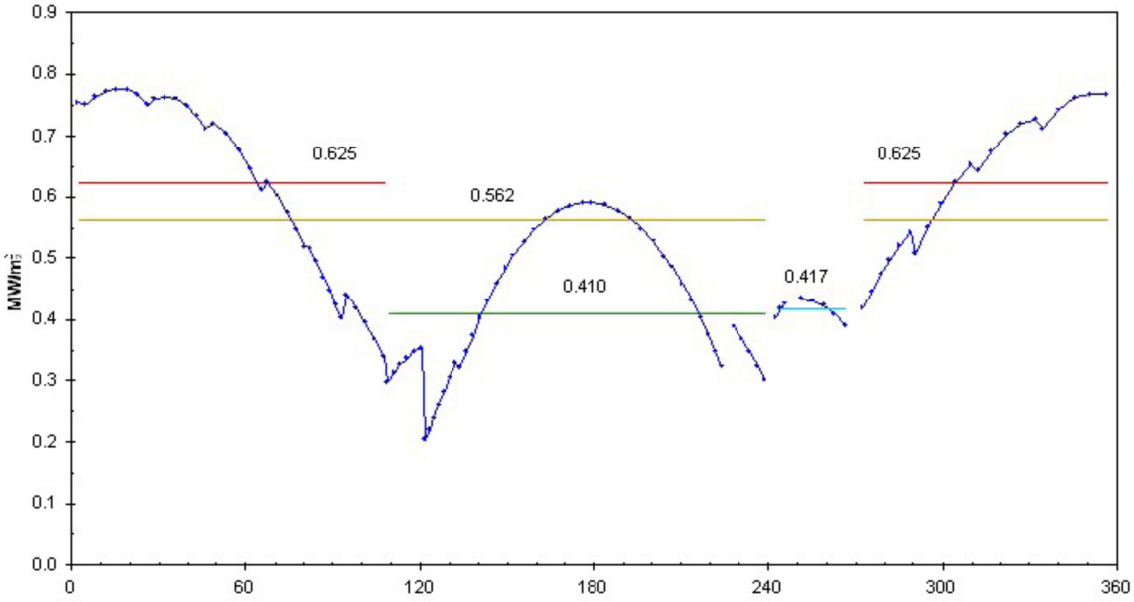

Figure 2-2 Neutronic load per calculation region (First Wall, configured in 9 calculation regions) for 500MW inductive ITER reference scenario[Topi08]

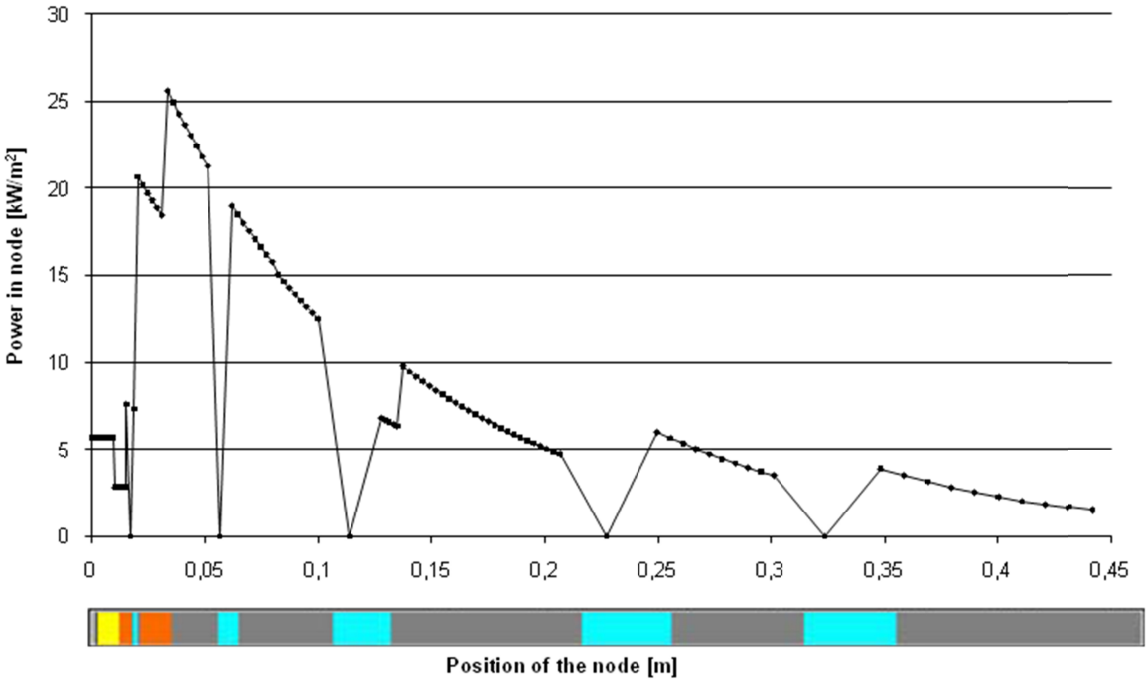

Figure 2-3 Profile of energy deposition of AINA 3.0 for the 2nd module in the steady state of the 500 MW inductive scenario[Sola05]

Regarding the weighting of neutronic heat load, an inverse exponential function is used (Eq. 2.55).

$$\dot{q}_{tot,module}(r,t) = \dot{q}_{tot,module}(t) \times K(r) \qquad \text{Eq. 2.55}$$
$$K(r) \propto k \cdot e^{-\mu r}$$

As an example, Figure 2-3 is included. It shows the radial profile of deposited energy by neutrons in region 2 for the reactor operating at in the inductive 500 MW scenario.

In the case of Japanese DEMO, the poloidal wall loading of neutron power and the radial profile of power deposition at the outer midplane position are input data for AINA, obtained by external neutronics analysis performed for a reference equilibrium scenario by JAEA Fusion Reactor Design Group[STUT15] and UPC-FEEL group.[Fabb14]

In Figure 2-4, poloidal neutron wall loading data for the Japanese DEMO design is shown.

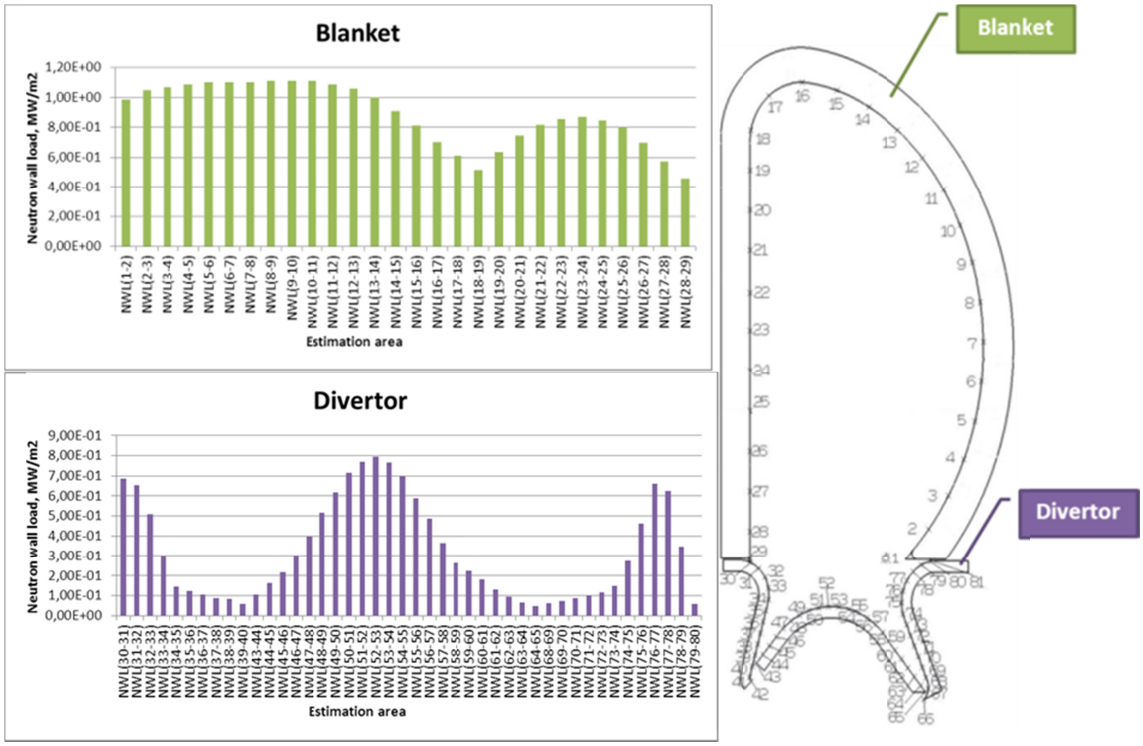

Figure 2-4 Neutron wall load distribution in the poloidal section for Japanese WCPB DEMO design.[STUT15]

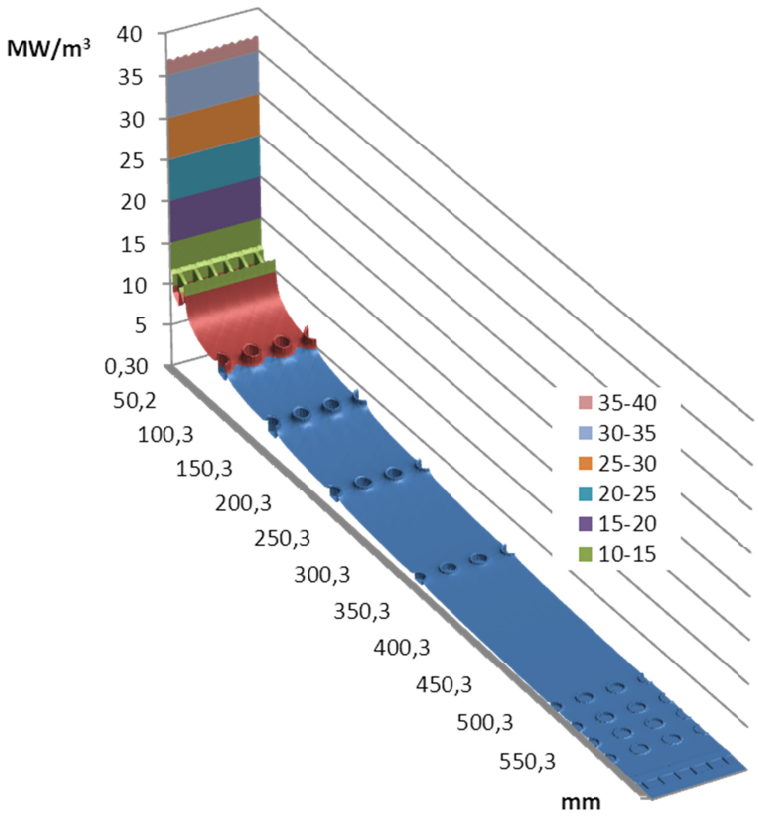

Figure 2-5 Radial profile of neutron power deposition density in radial direction at outer equatorial location

In the case of divertor, an inverse exponential function is also used, like in the case of ITER.

As an example Figure 2-5 is included. It shows the radial profile of neutron power deposition density at outer equatorial location for the reactor operating in the reference steady state.[STUT15]

This model assumes that the radial profile of neutron energy deposition doesn't change during the simulation. This hypothesis can give rise to errors because the variation of blankets' temperature changes the cross section for interactions with neutrons.

2.3.2.3 Particle fluxes for erosion calculation

Particle fluxes are used as input data to calculate wall loading over each of the 27 calculation regions that compose the poloidal in-vessel configuration in AINA code (first-wall + divertor).

For each region, a poloidal angular range is defined, with center in the plasma axis, and input particle data is integrated to obtain an averaged wall-loading. These averaged particle fluxes are used in steady state equilibrium calculations.

For transient calculations, the model assumes that the poloidal weighting of wall loading does not change but the total magnitude of flux does.

Therefore, a weighting coefficient is applied over the initial value of particle fluxes to obtain the value at some instant of the transient.

This coefficient is calculated by dividing the particle losses (of each respective j species) at instant t over the particle losses at initial equilibrium.

$$\Gamma_{j,t} = \Gamma_{j,0} \times \frac{\left(\frac{n}{\tau}\right)_{j,t}}{\left(\frac{n}{\tau}\right)_{j,0}} \qquad \text{Eq. 2.56}$$

In the case of particle temperatures, the coefficient applied is calculated with the temperature of the respective species j in plasma.

$$\mathrm{T}_{\mathrm{j,t}}^{\mathrm{surface}} = \mathrm{T}_{\mathrm{j,0}}^{\mathrm{surface}} \times \frac{\mathrm{T}_{\mathrm{j,t}}^{\mathrm{plasma}}}{\mathrm{T}_{\mathrm{j,0}}^{\mathrm{plasma}}} \qquad \text{Eq. 2.57}$$

In the case of neutral energies, the coefficient applied is calculated as a composition of the two previous coefficients, which also represents a proportion between conductive losses at instant t and at the initial equilibrium. Letter j represents the different species.

$$\mathrm{E}_{j,t}^{neutral} = \mathrm{E}_{j,0}^{neutral} \times \frac{\frac{n_{j,t}T_{j,t}}{\tau_{j,t}}}{\frac{n_{j,0}T_{j,0}}{\tau_{j,0}}} \qquad \text{Eq. 2.58}$$

In the case of ITER, the particle fluxes used for the calculation of erosion over the First Wall have been taken from published data of a SOLPS simulation.[KLKR09]

In the case of Japanese DEMO design, data was provided by simulations made with SONIC code.[HASN14]

Erosion at divertor uses fluxes from the divertor model, which use different variables for calculation, like edge density or conductive losses.

2.3.2.4 Plasma sheath model

For the calculation of the energies that the particles have when they collide with the wall, a collisionless 1-D sheath model is used, based on the results of various studies on the plasma sheath which have been compiled by Stangeby.[Stan00]

The incident energy of ions on the surface is equal to the sum of the energy with which ions enter the pre-sheath, the energy gained in the pre-sheath and the energy gained in the assumed collision-less sheath (Eq. 2.59).

$$E_i = T_e + \left(\frac{3}{2} + \gamma\right) T_i + Z_i \Phi \qquad \text{Eq. 2.59}$$

The incident ion flux on the surface is the same as the ion flux entering the sheath from the pre-sheath (Eq. 2.60).

$$\begin{gathered} \Gamma_s = n_s C_s \\ n_s = n_e = n_i Z_i \\ C_s = \sqrt{\frac{T_e + \gamma T_i}{m_i}} \end{gathered} \qquad \text{Eq. 2.60}$$

And finally, the energy fluxes over the surface are shown in Eq. 2.61.

$$\begin{gathered} q_i = \Gamma_s E_i \cos\psi \\ q_e = 2 T_e \Gamma_s \cos\psi \end{gathered} \qquad \text{Eq. 2.61}$$

2.3.2.5 Target peak heat flux calculation during transients

In past calculations, only parabolic radial profiles were used for plasma core calculations. Besides, divertor model consisted in a very rough interpolation.[THNH98]

In this work, an integrated pedestal and SOL model has been implemented in AINA code, based on SOL scalings[AHGG03, GHGA07, PKPJ07] and pedestal scalings.[John11]

By using the $\mu_{\#}$ constant normalised to 1 at incipient detachment to define the divertor regime, it is possible to estimate the initial equilibrium and the transient evolution of the SOL-core plasma coupled model.

At every initial equilibrium of plasma, target power flux can be specified at a design value, that in present calculations was 10 MW/m^2. This target power flux, together with values at the interface pedestal-SOL, define a regime represented by the $\mu_{\#}$ parameter.[AHGG03]

- During a plasma transient, as core plasma conditions change, also divertor conditions and target power flux evolve, causing change in target thermal equilibrium.

Parametric equations were used to estimate divertor evolution during a plasma-wall transient. The flux diagram for calculations is as follows:

Initial equilibrium:

- Prescribe an initial value for $q_{tar,peak}$
- Calculate the corresponding mu value
- calculate pressure at entrance of private area
- Calculate throughput from plasma core data
- Calculate pumping speed, check it is under the engineering limit
- Calculate upstream values for n_{sep}, T_{sep} and feedback calculation of plasma core equilibrium
- Repeat the loop until equilibrium is found

Transient:

- The pumping speed is a constant during transient (loss of control assumed)
- Variation in throughput induces variation in divertor pressure and thus in divertor regime ($\mu_{\#}$)
- Rest of calculations similar to initial equilibrium

2.3.3 Impurity production

2.3.3.1 Introduction

The Plasma Facing Components (PFC) elements of First Wall and divertor are designed to withstand severe conditions in contact with plasma. High temperatures, radiation and interaction with the scrape-off layer and other particle fluxes degrade and erode the PFC tiles.

Erosion produces a flux of particles which can enter the plasma as impurities. This behaviour is inherent to the nature of plasma wall interaction, but it can be cause of several undesirable effects. On one hand, impurities can affect plasma cooling it down due to Bremsstrahlung and line radiation. On the other hand, the sustained erosion of the wall will lead to reactor maintenance halts in order to replace some of the PFC elements.

Nevertheless, erosion process can give rise to beneficial effects. It can help to shut down the fusion, becoming a passive safety mechanism. For instance, if a *LOCA* occurs, the overheating of the wall will lead to an increase of the impurity production, and hence to plasma ending.[Aman96]

2.3.3.2 Description of the model

The impurity production model is composed by two main sources. The first one is the thermal sublimation source and only depends on PFC temperature. The second one is the erosion source; it's composed by several different processes and depends on both the PFC temperature and the ion and neutral fluxes (as in the case of RES) or only in particle fluxes (as in the case of physical sputtering).

Plasma-wall interaction models included in the new module are, first:

- Thermal sublimation: Model described by Uckan[UPWB96]
- Physical sputtering: Updated model from Bohdansky - Yamamura[GaER95]
- Chemical erosion: Roth's model for the graphite[Roth99]
- Radiation enhanced sublimation: Model described by Doerner[DBKS05]

Secondly, the sheath is modelled on the basis of the one-dimensional acollisional model described by Stangeby.[Stan00] In this version, only the Debye sheath is considered for the model.

Distribution of particle fluxes (ions and neutrals) and energies along the First Wall, baffles, and dome in ITER were obtained from B2-Eirene modelling with a full,

non-linear model of the neutral transport, taking into account the neutral-neutral and molecule-ion collisions.[KLKR09, KPKR05]

Available data were integrated over the poloidal length for each of the 27 modules corresponding to the blanket modules in the poloidal section (without ports) (Figure 2-6) to yield averaged data over which calculations were made.

2.3.3.2.1 Thermal sublimation:

Thermal sublimation source is calculated as a function of the PFC temperature with the Knudsen model (Eq. 2.62),

$$\dot{\delta}_{\text{sublimation}} = \alpha C \frac{1}{\sqrt{T}} e^{\left(-\frac{\Delta H}{\kappa T}\right)} \qquad \text{Eq. 2.62}$$

where
T = surface temperature of material $[\mathrm{K}]$
$\frac{\Delta H}{\kappa}$ = activation energy $[\mathrm{K}]$
α = vaporization (sublimation) coefficient
C = constant depending on material properties
$\dot{\delta}$ = vaporization rate of PFC $\left[\frac{\mathrm{m}}{\mathrm{s}}\right]$

On the other hand, the erosion source is based on the following models:

2.3.3.2.2 Physical sputtering:

The physical sputtering yield Y^{phy} calculation is based on empirical formulas.[GaER95] The Bohdansky formula[Bohd84] is used to determine the sputtering yield for normal incidence of a projectile on a target and the procedure specified by Yamamura[YaII83] is used to specify the angular dependence (Eq. 2.63),

$$Y^{phy}(E_0) = QS_n(\varepsilon)\left[1-\left(E_{th}/E_0\right)^{2/3}\right]\left(1-E_{th}/E_0\right)^2\left(\cos\alpha\right)^{-f}\exp\left(f\left[1-\left(\cos\alpha\right)^{-1}\right]\cos\alpha_{opt}\right)$$

Eq. 2.63

where Q and the threshold energy E_{th} are fitting parameters, E_0 is the incident particle energy (eV) and $\varepsilon = E_0 / E_{TF}$ is the reduced energy.
E_{TF} is the Thomas-Fermi energy (eV) (Eq. 2.64),

$$E_{TF} = 30{,}74\frac{M_1 + M_2}{M_2} Z_1 Z_2 \left(Z_1^{2/3} Z_2^{2/3}\right)^{1/2} \qquad \text{Eq. 2.64}$$

where Z_1, Z_2, M_1, M_2 are the nuclear charge and atomic mass of the projectile and target respectively.
S_n is the nuclear stopping cross section based on the Kr-C potential, which is approximated by Eq. 2.65.

$$S_n(\varepsilon) = \frac{0{,}5\ln\left(1+1{,}2288\varepsilon\right)}{\varepsilon + 0{,}1728\varepsilon^{1/2} + 0{,}008\varepsilon^{0{,}01504}} \qquad \text{Eq. 2.65}$$

Q and E_{th} are given by Eq. 2.66 and Eq. 2.67,

$$QE_s^{2/3} = 1{,}633 Z_1^{2/3} Z_2^{2/3} \left(Z_1^{2/3} + Z_2^{2/3}\right)^{1/3} \frac{M_1^{5/6} M_2^{1/6}}{M_1 + M_2} \frac{0.15 + 0.05 M_2 / M_1}{1 + 0.05\left(M_2 / M_1\right) 1^{1.6}} \qquad \text{Eq. 2.66}$$

$$\frac{E_{th}}{E_s} = 7{,}0\left(M_2 / M_1\right)^{-0{,}54} + 0{,}15\left(M_2 / M_1\right)^{-1/2} \qquad \text{Eq. 2.67}$$

where E_s is the surface binding energy (heat of sublimation), and α is the angle made by the incident projectile with the normal to the target surface. Yamamura's analytical fit formulas for f and α_{opt} are shown in Eq. 2.68.

$$f = \sqrt{E_s}\left(0{,}94 - 1{,}33x10^{-3} M_2 / M\right. \qquad \text{Eq. 2.68}$$

$$\alpha_{opt} = \pi / 2 - a_l n^{-1/3}\left(2\varepsilon\sqrt{E_s / \gamma E_0}\right)$$

where, a_l is the Lindhard screening length $a_l = 0{,}4685\sqrt{Z_1^{2/3} + Z_2^{2/3}}$, n is the target density given in units of atoms / m^3 and γ is the maximum energy transfer factor given by $\gamma = 4M_1 M_2 / \left(M_1 + M_2\right)^2$.

2.3.3.2.3 Chemical erosion:

Chemical erosion consists of two contributions, as shown in Eq. 2.69, one thermal part Y^{therm} and one surface part Y^{surf}.[Roth99]

$$Y^{chem} = Y^{therm}\left(1 + DY^{dam}\right) + Y^{surf} \qquad \text{Eq. 2.69}$$

The thermal erosion is enhanced by the damage production due to incident ions Y^{dam}. D is given by $250/M_1$, where M_1 is the mass of the incident hydrogen isotope. The thermal erosion is obtained by the formula shown in Eq. 2.70,

$$Y^{therm} = c^{sp^3}\frac{0{,}033e^{\frac{-E_{therm}}{KT}}}{2\text{x}10^{-32}\varphi + \left[1 + \frac{2\text{x}10^{29}}{\varphi}e^{\frac{-E_{rel}}{KT}}\right]e^{\frac{-E_{therm}}{KT}}} \qquad \text{Eq. 2.70}$$

where KT is the target surface temperature in eV and C^{sp3} is given by Eq. 2.71.

$$C^{sp^3} = \frac{C\left[2\text{x}10^{-32}\varphi + e^{\frac{-E_{therm}}{KT}}\right]}{2\text{x}10^{-32} + \left[1 + \frac{2\text{x}10^{29}}{\varphi}e^{\frac{-E_{rel}}{KT}}\right]e^{\frac{-E_{therm}}{KT}}} \qquad \text{Eq. 2.71}$$

The value of C is calculated with Eq. 2.72,

$$C = \frac{1}{1 + 3\cdot 10^{7} e^{\frac{-1.4}{KT}}} \qquad \text{Eq. 2.72}$$

with its value for high ion fluxes (Eq. 2.73) where a possible influence of hydrogenation time is taken into account

$$C = \frac{1}{1 + 3\cdot 10^{-23}\varphi} \qquad \text{Eq. 2.73}$$

in order to make a transition from low incident ion fluxes to high incident ion fluxes smoothly.

The term Y^{dam} due to damage caused by incident ions is given by Eq. 2.74.

$$Y^{dam}\left(E_0\right)=QS_n\left[1-\left(\frac{E_{dam}}{E_0}\right)^{2/3}\right]\left(1-\frac{E_{dam}}{E_0}\right)^2 \qquad \text{Eq. 2.74}$$

The surface erosion term is given by Eq. 2.75,

$$Y^{surf}\left(E_0,T\right)=C^{sp^3}=\frac{Y^{des}\left(E_0\right)}{1+e^{\frac{E_0-65eV}{40}}} \qquad \text{Eq. 2.75}$$

Where Y^{des} is calculated with Eq. 2.76.

$$Y^{des}\left(E_0\right)=QS_n\left[1-\left(\frac{E_{de}}{E_0}\right)^{2/3}\right]\left(1-\frac{E_{de}}{E_0}\right)^2 \qquad \text{Eq. 2.76}$$

The values tabulated in the bibliography[Roth99] are used for Q, E_{des} and E_{dam}. For $E_{rel,}$ the value for pure carbon (=1,8 eV) is used. E_{th}, E_{TF} and S_n are calculated from Eqns.4.9,4.10,4.11 y 4.12. E_{therm} is taken as 1,7 eV.

2.3.3.2.4 Radiation enhanced sublimation:

The Radiation Enhanced Sublimation Yield Y^{RES} calculation (Eq. 2.77) is based on the empirical formulas described by Doerner,[DBKS05]

$$Y^{RES}=\frac{Y^{ad}}{1+A\exp\left(\frac{E_{eff}}{T}\right)} \qquad \text{Eq. 2.77}$$

where $E_{eff}=2\ eV$, $A=2\cdot10^{-7}eV$ and $Y^{ad}/Y^{phys}=50$ for beryllium.

The total erosion flux is calculated with Eq. 2.78.

$$\dot{\delta}_{TOTAL}(t)=\dot{\delta}_{SUBLIMATION}+\Gamma_{EROSION}\times\left(Y^{phy}+Y^{chem}+Y^{RES}\right) \qquad \text{Eq. 2.78}$$

2.3.3.3 Improvements done for Japanese DEMO

In the case of Japanese DEMO, the erosion model calculates sputtering of tungsten, taking into account different ion species present in plasma core, plus impurities injected in scrape off layer. Both ions and neutrals are considered in targets, while only neutrals are considered in First Wall.

The particle flux coming to surface from plasma is modeled on the basis of a poloidal wall loading calculated with SONIC code.[HASN14] During a plasma transient, this poloidal wall loading is weighted with the variation of plasma core temperature and density in the case of First Wall, and with the variation of SOL power, density and temperature in the case of divertor. The energies of particles at the wall used for calculating erosion undergo a further transformation when a maxwellian distribution is applied to them, so erosion calculation can account for the high energy particles from the distribution tail that can produce erosion even at low average energies.

Self-sputtering is taken into account only in divertor, and two sources are considered, one from main plasma, with the same temperature as the rest of the ions, and the other composed by thermalised neutrals coming from recent sputtering processes.

2.3.3.4 Impurity Transport

The transport model is based on two screening factors that are calculated to fit the impurity content of plasma in reference scenarios. One of them is for the divertor flux of generated particles and the other for the First Wall flux, yielding in this way the impurity flux entering the core plasma through the SOL.[HBUS97b] In the model, the time delay for the transport is assumed to be the energy confinement time of plasma, which is a conservative assumption, accounting to plasma ablation experimental results (Eq. 2.79),

$$S(t)_{imp} = C_{screen} Y(t-\tau)_e \qquad \text{Eq. 2.79}$$

where

$Y(t)_e$ = impurity production rate
C_{screen} = screening coefficient
τ_d = duration of impurity transport
$S(t)_{imp}$ = impurity source

Due to changes in confinement time, delay time also changes. To model impurity flux in these circumstances, an intermediate discrete buffer is used. However, the result can produce peaks in impurity flux into plasma. To avoid this, the impurity flux is smoothened by applying a normal distribution over the delay time for particles eroded at some instant. This way, the impurity flux into core plasma becomes continuous.

2.4 The wall model

2.4.1 First Wall geometry

Eighteen poloidal blanket modules are configured for safety calculations. The rest of poloidal modules correspond to the divertor, which has been divided in nine calculation points. Thus, the poloidal section is modelled as a set of twenty seven calculation regions, as shown in Figure 2-6. Toroidal symmetry and no ports configuration are assumed.

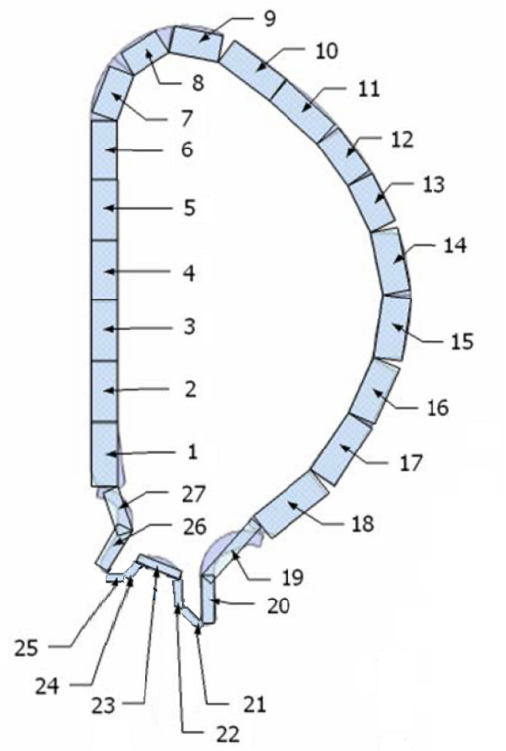

1-8: Inner Blanket
9-18: Outer Blanket
19) Upper Outer Vertical Target
20) Lower Outer Vertical Target
21) Lowest Wing Outer Divertor
22) Highest Wing Outer Divertor
23) Divertor Dome
24) Highest Wing Inner Divertor
25) Lowest Wing Inner Divertor
26) Lower Inner Vertical Target
27) Upper Inner Vertical Target

Figure 2-6 Twenty seven poloidal regions distribution

Each poloidal module is configured with an angular range measured from a specified plasma axis, for the purpose of assigning the corresponding values of particle and neutronic heat wall loadings.

2.4.2 General description of the in-vessel modules

In order to obtain the distribution and evolution of temperatures, a 1D calculation model is derived from the 3D design of each considered module by making strong simplifications and assumptions, but always maintaining the robustness from the point of view of safety.

Thus, the 1-D model results in a radial segment where the different thicknesses and materials are represented, as shown in Figure 2-7, where it can be seen how blanket and divertor have been modelled alternating layers of tungsten, beryllium, copper, stainless steel and coolant channels.

ITER blankets are composed by two different parts, the First Wall and the shielding. The First Wall is in turn composed by the PFCs, which is a tiled surface in contact with plasma, and a heat sink made of copper, with coolant tubes inside. The shielding has also coolant tubes, arranged in both radial and tangential to surface directions.

ROW	Thickness [cm]
Be	1.0000
Cu	0.5000
SS	0.0625
Coolant	0.2840
SS	0.0625
Cu	1.2910
SS	2.0410
Coolant	0.8180
SS	2.0410
SS	2.0000
Coolant	2.5900
SS	0.9100
SS	7.2000
Coolant	3.8875
SS	5.7250
Coolant	3.8875
SS	10.4000

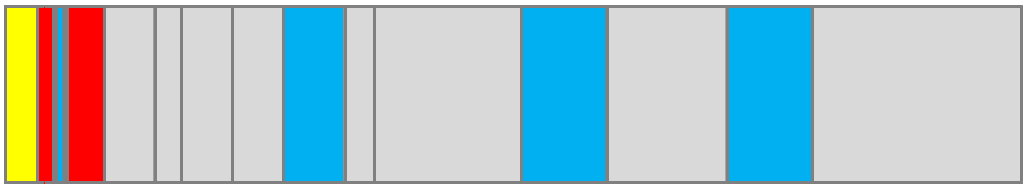

Figure 2-7 Cconfiguration of 1D model of ITER blanket in AINA

Initially, AINA code was intended for ITER safety analyses, but currently it is used also for safety analyses in next step designs.[RNSH15, RNST14]

In the case of Japanese DEMO, the 1-D model results in a radial segment where the different thicknesses and materials are represented, as shown in Figure 2-8.

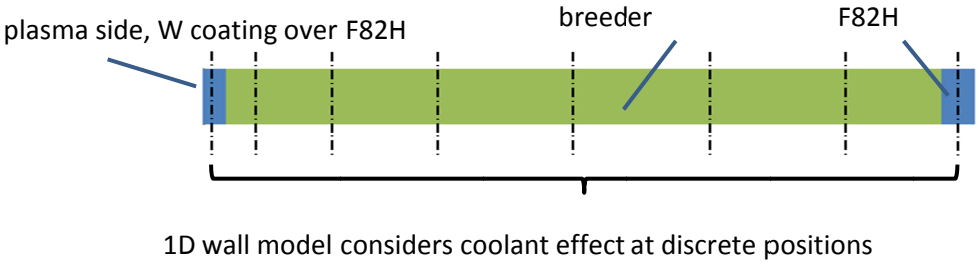

Figure 2-8 Scheme of the configuration of 1D model of next step blanket module in AINA

The resulting configuration can be described as follows:

- First Wall 1D model is configured with tungsten layers for the PFCs and low activation F82H steel for the structure and coolant channels.
- Breeding blanket uses F82H steel for the structural layers and average properties of helium and of the mixed breeder for the breeding area.
- Divertor uses layers of tungsten and of F82H steel. In the volume under targets, a copper heat sink is foreseen.

Material	Width (mm)
W	8.43
Cu	0.91
CuCrZr	0.71
water	2.89
CuCrZr	0.71
Cu	0.86
W	7.49
F82H	37.86
water	2.28
F82H	37.86

Material	Width (mm)
W	8.43
F82H	0.79
Water	3.57
F82H	0.79
W	8.42
F82H	37.86
water	2.28
F82H	37.86

Figure 2-9: Divertor configuration for Japanese DEMO design

In the case of divertor, the thermal model is the same as for ITER and for Japanese DEMO. The configuration resulting from design data includes a layer of tungsten for the PFCs, layers of copper and copper alloy for the heat sink and coolant tubes in target area, and layers

of F82H steel for structure and also for coolant tubes not under the targets (Figure 2-9).

The code allows different combinations of materials and thermal gaps or heat transfer by radiation between cooling channel walls in case of coolant drainage (loss of coolant accidents, etc.)

2.4.3 Continuous model

For the loads described in subsection 2.3.2, thermal behaviour of vacuum vessel's internals is calculated using a dynamic one-dimensional model in the radial direction for each of the regions described above.

The simplification from 3D to 1D is made by first considering each region as a cuboid, where the only conducting surfaces are the one facing the plasma and the one opposite, so the rest can be seen (at least by symmetry considerations) as roughly adiabatic.

It must be added to the previous statements that the different materials in each module are arranged in layers parallel to the inner surface, and that coolant tubes are considered also arranged in layers at different depths and also parallel to the surface in contact with plasma.

Thus, a 1D parabolic, non-linear and inhomogeneous partial differential equation results from the previous statements (Eq. 2.80),

$$\rho(T,x)\cdot c(T,x)\cdot\frac{\partial T}{\partial t}=\frac{\partial}{\partial x}\left(\kappa_T(T,x)\frac{\partial T}{\partial x}\right)+Q_n(x,t) \qquad \text{Eq. 2.80}$$

where ρ is the density, c the heat capacity, κ_T the thermal conductivity and Q_n the volumetric heat deposition, of neutronic origin. The boundary conditions are shown in Eq. 2.81.

$$\begin{aligned} -\kappa(0,t)\frac{\partial T}{\partial x}(0,t) &= \dot{q}_h(t)-\sum\dot{q}_r(t)-\dot{q}_{ev}(t) && x=0 \\ T(L,t) &= const && x=L \\ T(x,0) &= T_0(x) && t=0 \end{aligned} \qquad \text{Eq. 2.81}$$

That is, natural (Neumann) boundary condition at the warm face and forced (Dirichlet) boundary condition at the cold face. Also initial conditions at t=0, obtained by applying the steady state condition to the equation, which results in an elliptic equation.

2.4.4 Coolant tubes

Moreover, the treatment given to the convective heat transfer in the coolant tubes comes from considering them planar and to occupy only one node. In this way, heat transfer can be modelled strictly from a one-dimensional approach, by weighting the conductive and convective contributions to heat transfer with a surface coefficient, which is equal to the relative surface of the coolant tubes to the total surface of the module section (Figure 2-10). Thus, by adding the convective terms, a new heat transfer equation is obtained (Eq. 2.82),

$$\rho(T,x)c(T,x)\frac{\partial T}{\partial t} = \frac{\partial}{\partial x}\left(f_{cool}\cdot h\cdot(T-T_{cool}) + (1-f_{cool})\cdot \kappa_T(T,x)\frac{\partial T}{\partial x}\right) + Q_n(x,t)$$

$$f_{cool} = \frac{S_{cool}}{S_{tot}}$$

Eq. 2.82

where f_{cool} is a discrete function, taking values only at the specified coolant positions, in the "planar coolant tubes" approach (Eq. 2.83),

$$f_{cool}(x) = \sum_{i}^{\substack{coolant\\positions}} \delta_i(x)\frac{S_{cool,i}}{S_{tot}} \qquad \text{Eq. 2.83}$$

with $\delta_i(x)$ the Dirac delta function at the coolant position i.

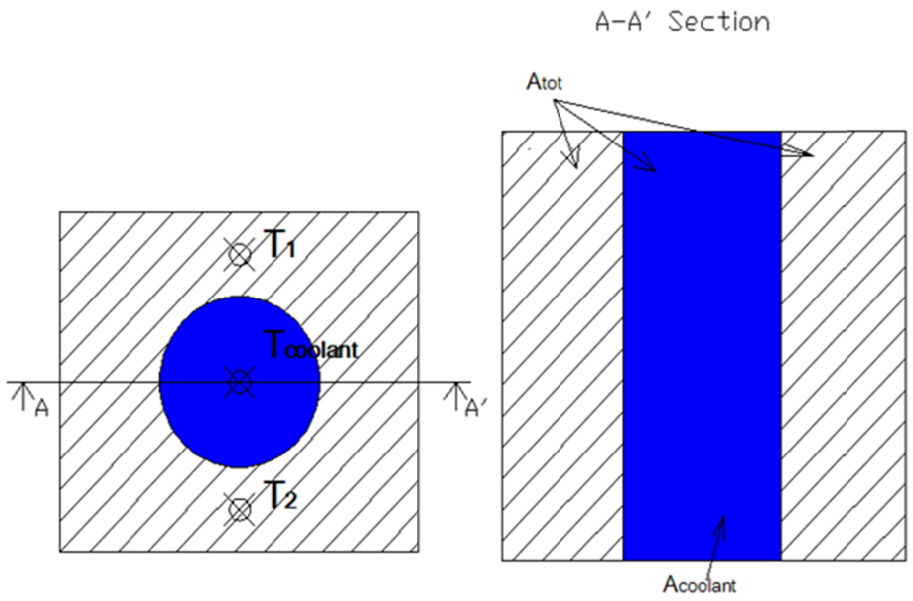

Figure 2-10: Modelisation of coolant channels

2.4.5 Gaps

There are also welds and junctions in the shielding, where the heat transfer problem must be modelled by considering the presence of a gap where conduction is modified by taking a compound thermal conductivity, as shown in Eq. 2.84.[Holm97]

$$k_{T,GAP} = \frac{1}{\frac{\Delta x_{GAP}}{k_{T,A}\,S} + \frac{1}{h_c S} + \frac{\Delta x_{GAP}}{k_{T,B}\,S}} \qquad \text{Eq. 2.84}$$

Two gaps are considered in the wall model implemented in AINA code: the junction between the First Wall module and the blanket module, and the junction between the blanket module and the vacuum vessel.

2.5 Numerical models in AINA code

2.5.1 Introduction

In the following, the numerical models employed in the AINA 3.0 code are explained. The numerical algorithms were selected for the specific needs of AINA code. These are basically the calculation of the initial equilibrium state of plasma and wall, and the simulation of the transient evolution of the plasma-wall system. First, the flux diagram of the code is described. Then, the numerical methods, the error estimation and control, and the stability, convergence and accuracy analysis are exposed. The flux diagram of AINA simulation is shown in Figure 2-11.

Basically, there are two systems of differential equations that are coupled through their boundary conditions. First, a system of nonlinear ODEs that are used for the calculation of the plasma 0D balance. Second, a set of PDEs that are used for the calculation of the 1D thermal balances, one for each calculation region.

The initial equilibrium problem is solved by making zero the time derivatives. For the plasma, the solution is given for certain values of input parameters that are selected to match those of the specific ITER reference scenario that will be used. The remaining variables of the 0D model are then determined by solving iteratively a system of nonlinear equations.

There are some degrees of freedom in the 0D model that allow the fitting of the results of the reference scenario calculated with a 1.5D model. These degrees of freedom are the density and temperature profiles, the sources of fuel and impurities, plus an additional unknown for the distribution of external heating between ions and electrons, which allows the calculation of the external heating composition. By varying them, the results from the 0D model can be fitted to the reference scenario.

The wall heat transfer equilibrium problem is calculated from a similar approach. The time derivative is set to zero, and the resulting elliptic problem is solved.

Wall heat transfer model takes as a boundary condition the heat flow coming from the plasma. On the other hand, the impurity transport model adjusts a coefficient to balance the impurity flow with the expected impurity equilibrium concentration in plasma. This value is then kept constant during the evolution of a transient.

The problem of the evolution of a transient is solved as an initial value problem, and the steady state is the initial condition.

Actually, two initial value problems are solved, one for plasma and one for the wall, both with adaptive time step to bound the error. The two problems are coupled at the beginning of each sub-interval. Plasma system takes the value of the wall impurity as an input. Wall system takes the value of the plasma energy flow as a boundary condition. Neutron volumetric deposition takes also input from plasma data.

Therefore, there is an additional numerical error in both systems induced by the fact that, within a sub-interval, the values of the coupling functions are considered constant.

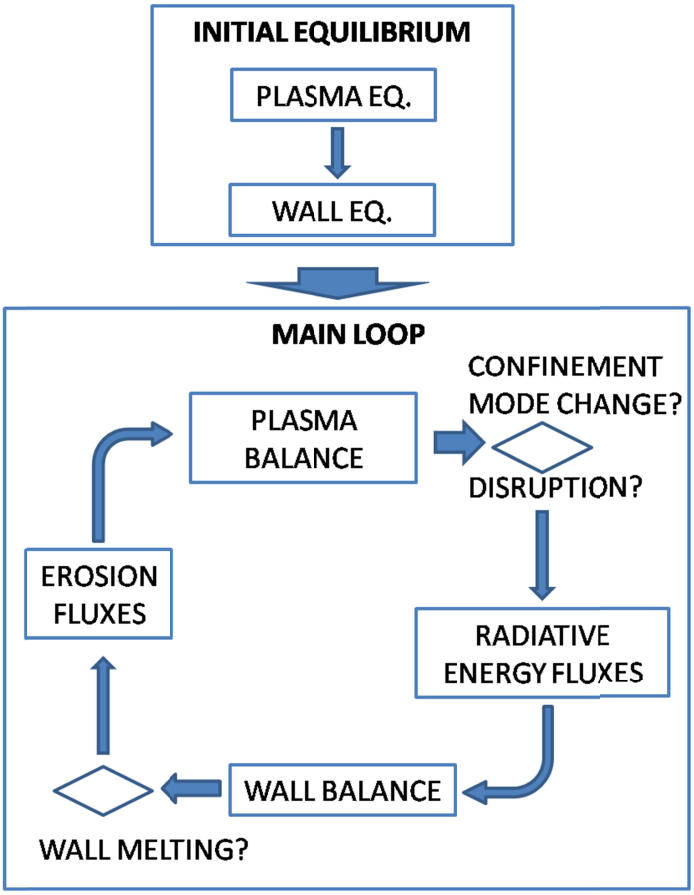

Figure 2-11: AINA 3.0 CORE calculations flux diagram

2.5.2 Numerical analysis

2.5.2.1 Plasma model numerical analysis

2.5.2.1.1 Initial Equilibrium

In order to solve the steady state equilibrium of the plasma model, the time derivatives are set to zero, and a non-linear system of equations results (Eq. 2.85).

$$\mathrm{S}_\alpha = \frac{1}{4}\int_V n_H^2 \langle \sigma v \rangle_{DT}\, dV \qquad \text{Eq. 2.85}$$

$$P_{FUS} = \mathrm{S}_\alpha E_{FUS}$$

$$S_H - 2S_\alpha - \frac{n_H}{\tau_{p,H}} = 0$$

$$S_\alpha - \frac{n_\alpha}{\tau_{p,\alpha}} = 0$$

$$S_{Z,j} - \frac{n_{Z,j}}{\tau_{p,Z}} = 0$$

$$f_{ext}P_{ext} + f_\alpha P_\alpha - P_{ie} - \frac{3}{2}\frac{n_i T_i}{\tau_{E,i}} = 0$$

$$(1-f_{ext})P_{ext} + (1-f_\alpha)P_\alpha + P_\Omega + P_{ie} - P_{br} - P_{cy} - P_{li} - \frac{3}{2}\frac{n_e T_e}{\tau_{E,e}} = 0$$

2.5.2.1.2 Transient

The initial value problem solves the 0D equilibrium equations (See subsection 2.2.3). The initial value algorithm selected is an adaptive Euler method,[Pres07] as explained in subsection 2.5.2.2.4.

2.5.2.2 Wall model numerical analysis

2.5.2.2.1 Discretised equations

The 1D wall model is discretised by using a finite difference nodalisation of the parabolic heat conduction equation. For each poloidal region of the First Wall, the equations that allow the calculation of the temperature profile are structured as shown below.

First of all, it is assumed that the first node gets all the EM and convective energy from plasma (Eq. 2.86). Heat transfer by radiation among different modules is also taken into account.

$$\rho_1 \cdot C_{p,1} \cdot \frac{dT_1}{dt} = \frac{P_{rad,1} - k_T \frac{T_1 - T_2}{\Delta x_1}}{\Delta x_1} + Q_{n,1} \qquad \text{Eq. 2.86}$$

Heating produced by neutrons, $Q_{n,i}$ depends on the region they target and on the plasma evolution. The heating power at the first node, P_{rad}, is calculated with Eq. 2.87,

$$P_{rad} = \dot{q}_h - \dot{q}_{rt} - \dot{q}_{erosion} \qquad \text{Eq. 2.87}$$

where the heat fluxes emitted from the wall, due to impurity flux leaving the wall and to radiation reflection are shown in .

$$\dot{q}_{rt} = \sum_{j=1}^{regions} f_{ij} \cdot \varepsilon_i \cdot \sigma_{SB} \cdot \left(T_j^4 - T_i^4\right) \qquad \text{Eq. 2.88}$$

$$\dot{q}_{erosion} = \dot{\delta} \cdot \rho \cdot L_v$$

The symbol $\dot{\delta}$ is explained in Eq. 2.78.

For the next nodes, the equation ruling the thermal behaviour is shown in Eq. 2.89.

$$\rho_i \cdot C_{p,i} \cdot \frac{dT_i}{dt} = \frac{k_{T,i-1} \frac{T_{i-1} - T_i}{\Delta x_{i-1}} - k_{T,i} \frac{T_i - T_{i+1}}{\Delta x_i}}{0.5 \cdot \left(\Delta x_{i-1} + \Delta x_i\right)} + Q_{n,i}$$

Eq. 2.89

While in the last node we have to use Eq. 2.90.

$$\rho_{LAST} \cdot C_{p,LAST} \cdot \frac{dT_{LAST}}{dt} = 0 \qquad \text{Eq. 2.90}$$

The time derivative is zero, because the temperature in the last node is fixed (Dirichlet boundary condition).

2.5.2.2.2 Coolant Channels

There is a grid of coolant channels in the shielding. As previously stated, the only allowable design in the current version of AINA code is arranging them parallel to the wall surface. In that way, a subset of coolant tubes at the same depth is considered as occupying one node, in planar approximation.

To solve the heat transfer problem for this node, both conduction and convection with adjacent nodes are considered, in their respective domain areas. To make the calculations, a channel fraction and a wall fraction are considered when discretising the equation at the coolant node, as showed below in Eq. 2.91, Eq. 2.92 and Eq. 2.93:

For the previous node:

$$\rho_{i-1}\cdot C_{p,i-1}\cdot\frac{dT_{i-1}}{dt}=\frac{k_{T,i-1}\dfrac{T_{i-2}-T_{i-1}}{\Delta x_{i-2}}-f_s\cdot h\cdot\left(T_{i-1}-T_{cool}\right)-\left(1-f_s\right)\cdot k_{T,i}\dfrac{T_{i-1}-T_i}{\Delta x_{i-1}}}{0.5\cdot\left(\Delta x_{i-2}+\Delta x_{i-1}\right)}+Q_{n,i-1}$$

$$with\ \ f_s=\frac{S_{coolant}}{S_{total}}$$

For the coolant node: Eq. 2.91

$$\rho_i\cdot C_{p,i}\cdot\frac{dT_i}{dt}=\frac{\left(1-f_s\right)\cdot\left(k_{T,i}\dfrac{T_{i-1}-T_i}{\Delta x_{i-1}}-k_{T,i+1}\dfrac{T_i-T_{i+1}}{\Delta x_i}\right)}{0.5\cdot\left(\Delta x_i+\Delta x_{i+1}\right)}+Q_{n,i}$$ Eq. 2.92

For the next node:

$$\rho_{i+1}\cdot C_{p,i+1}\cdot\frac{dT_{i+1}}{dt}=\frac{f_s\cdot h\cdot\left(T_{cool}-T_{i+1}\right)+\left(1-f_s\right)\cdot k_{T,i+1}\dfrac{T_i-T_{i+1}}{\Delta x_i}-k_{T,i+2}\dfrac{T_{i+1}-T_{i+2}}{\Delta x_{i+1}}}{0.5\cdot\left(\Delta x_i+\Delta x_{i+1}\right)}+Q_{n,i+1}$$

Eq. 2.93

There exists also the possibility of the coolant channels losing all the coolant fluid, for example in a LOCA accident. In such case, radiation heat transfer is considered to be dominant in the empty tube, as shown in Eq. 2.94, Eq. 2.95 and Eq. 2.96:

For the previous node:

$$\rho_{i-1}\cdot C_{p,i-1}\cdot\frac{dT_{i-1}}{dt}=\frac{k_{T,i-1}\dfrac{T_{i-2}-T_{i-1}}{\Delta x_{i-2}}-\left(1-f_s\right)\cdot k_{T,i}\dfrac{T_{i-1}-T_i}{\Delta x_{i-1}}}{0.5\cdot\left(\Delta x_{i-2}+\Delta x_{i-1}\right)}- \qquad \text{Eq. 2.94}$$

$$-\frac{f_s\cdot\varepsilon_{i-1}\cdot\sigma_{SB}\cdot f_{i-1,i+1}\cdot\left(\left(T_{i-1}+T_0\right)^4-\left(T_{i+1}+T_0\right)^4\right)}{0.5\cdot\left(\Delta x_{i-2}+\Delta x_{i-1}\right)}+Q_{n,i-1}$$

For the coolant node:

$$\rho_i\cdot C_{p,i}\cdot\frac{dT_i}{dt}=\frac{\left(1-f_s\right)\cdot\left(k_{T,i}\dfrac{T_{i-1}-T_i}{\Delta x_{i-1}}-k_{T,i+1}\dfrac{T_i-T_{i+1}}{\Delta x_i}\right)}{0.5\cdot\left(\Delta x_i+\Delta x_{i+1}\right)}+Q_{n,i} \qquad \text{Eq. 2.95}$$

For the next node:

$$\rho_{i+1}\cdot C_{p,i+1}\cdot\frac{dT_{i+1}}{dt}=\frac{\left(1-f_s\right)\cdot k_{T,i+1}\dfrac{T_i-T_{i+1}}{\Delta x_i}-k_{T,i+2}\dfrac{T_{i+1}-T_{i+2}}{\Delta x_{i+1}}}{0.5\cdot\left(\Delta x_i+\Delta x_{i+1}\right)}+ \qquad \text{Eq. 2.96}$$

$$+\frac{f_s\cdot\sigma_{SB}\cdot f_{i+1,i-1}\cdot\left(\left(T_{i+1}+T_0\right)^4-\left(T_{i-1}+T_0\right)^4\right)}{0.5\cdot\left(\Delta x_i+\Delta x_{i+1}\right)}+Q_{n,i+1}$$

2.5.2.2.3 Initial Equilibrium

The numerical algorithm is based on the Method Of Lines (MOL),[SaOb15] which in this case consists of a finite difference discretisation in the spatial (radial) dimension and an initial value algorithm which solves the resulting initial value problem.

2.5.2.2.4 Transient

The numerical algorithm is the same already described for the calculation of the initial equilibrium. The difference is that, for the initial equilibrium calculation, a pseudo-transient calculation is done, whereas for this case, the boundary conditions are actualised with values obtained from the plasma transient calculation.

2.5.3 Error estimation and control

The method employed for solving the initial value problem is an Euler method with error correction, which estimates the numerical error with the local truncation error, $O(h^2)$. For a finite interval, it can be shown that the global truncation error is $O(h)$.

An estimator of the truncation error is calculated by means of the values of the derivative in t and t+h. After that, the truncation error is added to the calculated value in t, in order to improve the solution. If the estimated error is greater than a specified bound, then the time step will be decreased, and the calculations will be repeated, until the solution is found or until time step goes below the minimum value.

2.5.3.1 Stability analysis

In order to ensure stability of the numerical method for heat conduction in the wall, a criterion has been established[Pata80] following the finite volume analysis of the heat conduction equation (Eq. 2.97).

The finite volume analysis is as follows:

$$\int_w^e \int_t^{t+\Delta t} \rho\, c \frac{\partial T}{\partial t} dt\, dx = \int_t^{t+\Delta t} \int_w^e \left[\frac{\partial}{\partial x}\left(k \frac{\partial T}{\partial x} - h\left(T - T_{cool}\right)\right) + S \right] dx dt$$

(*fully explicit discretization*)

$$\frac{\Delta x}{\Delta t} \rho_P^{t+\Delta t} c_P^{t+\Delta t} T_P^{t+\Delta t} = \frac{\Delta x}{\Delta t} \rho_P^t c_P^t T_P^t + k_e \frac{T_E^t - T_P^t}{(\delta x)_e} - k_w \frac{T_W^t - T_P^t}{(\delta x)_w} + \bar{S}\Delta x - h_e\left(T_e^t - T_{cool}\right) + h_w\left(T_{cool}\right.$$

$$\frac{\Delta x}{\Delta t} \rho_P^{t+\Delta t} c_P^{t+\Delta t} T_P^{t+\Delta t} = \frac{\Delta x}{\Delta t} \rho_P^t c_P^t T_P^t + k_e \frac{T_E^t - T_P^t}{(\delta x)_e} - k_w \frac{T_W^t - T_P^t}{(\delta x)_w} + \bar{S}\Delta x + 2 \cdot h \cdot \left(T_{cool} - T_P^t\right)$$

defining the following coefficient:

$$a_P^0 = \frac{\Delta x}{\Delta t} \rho_P^t c_P^t - \frac{k_e}{(\delta x)_e} - \frac{k_w}{(\delta x)_w} - 2 \cdot h$$

and demanding:

$$a_P^0 > 0$$

Eq. 2.97

Finally, we obtain an upper bound for the time step (Eq. 2.98).

$$\Delta t_i^n < \frac{\Delta x_i^n \cdot \rho_{p_i}^{\ n} \cdot c_{p_i}^{\ n}}{\frac{k_{i+1}^n}{(\delta x)_{i+1}^n} + \frac{k_{i-1}^n}{(\delta x)_{i-1}^n} + h_i^n}$$

Eq. 2.98

with:

$$\Delta x_i^n = \frac{1}{2}\left((\delta x)_{i+1}^n + (\delta x)_{i-1}^n\right)$$

2.5.3.2 Convergence analysis

A small code has been developed for testing purposes, which calculates a simple wall model. The main simplifications with respect to the ITER wall model in AINA code were:

- Simplified design. Three coolant positions have been established for the wall, symmetrically located along the depth.
- Uniform radial step.
- Only steel is considered as material

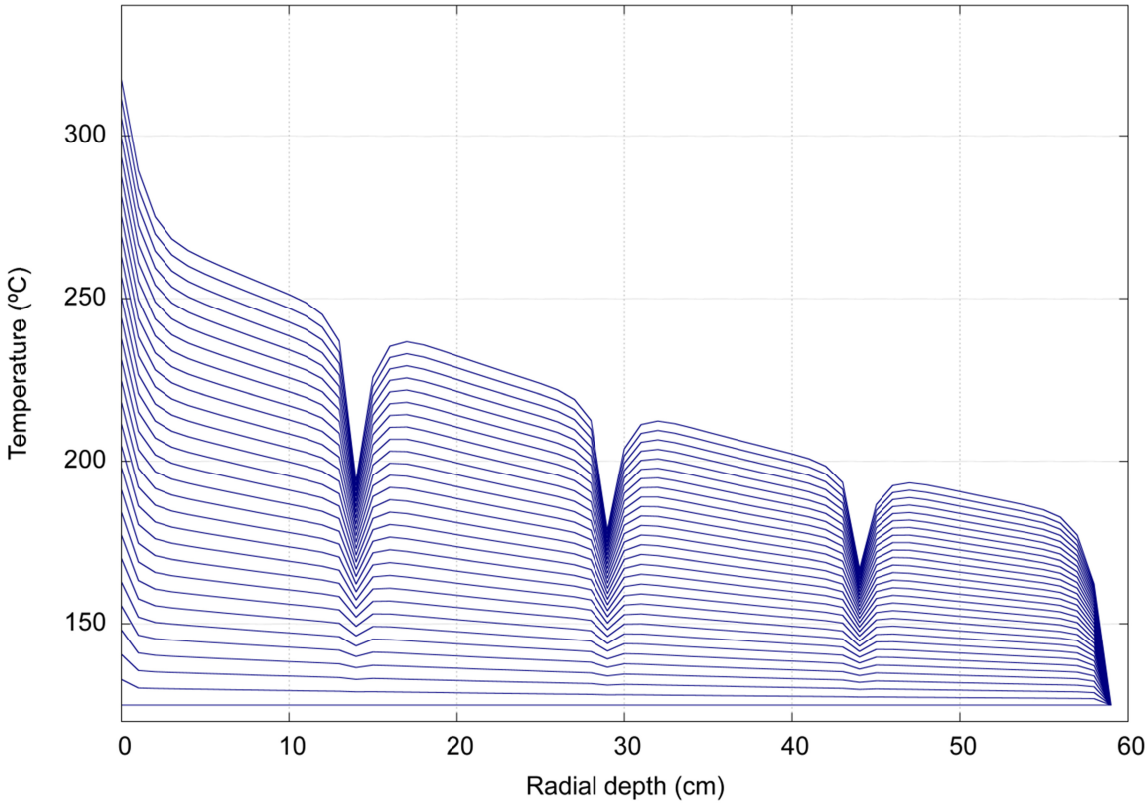

Figure 2-12: Time evolution of the radial temperature profile in simple test code, temperature grows with time

In Figure 2-12 , the time evolution of the radial temperature profile can be seen. The left side would represent the plasma face of the wall, whereas the right side would be the cold face.

In order to evaluate the convergence of the numerical method, the integral of the radial temperature profile at the end of a transient has been calculated by varying the mesh density. As can be seen in Figure 2-13, the integral converges to a finite value as the number of steps grows.

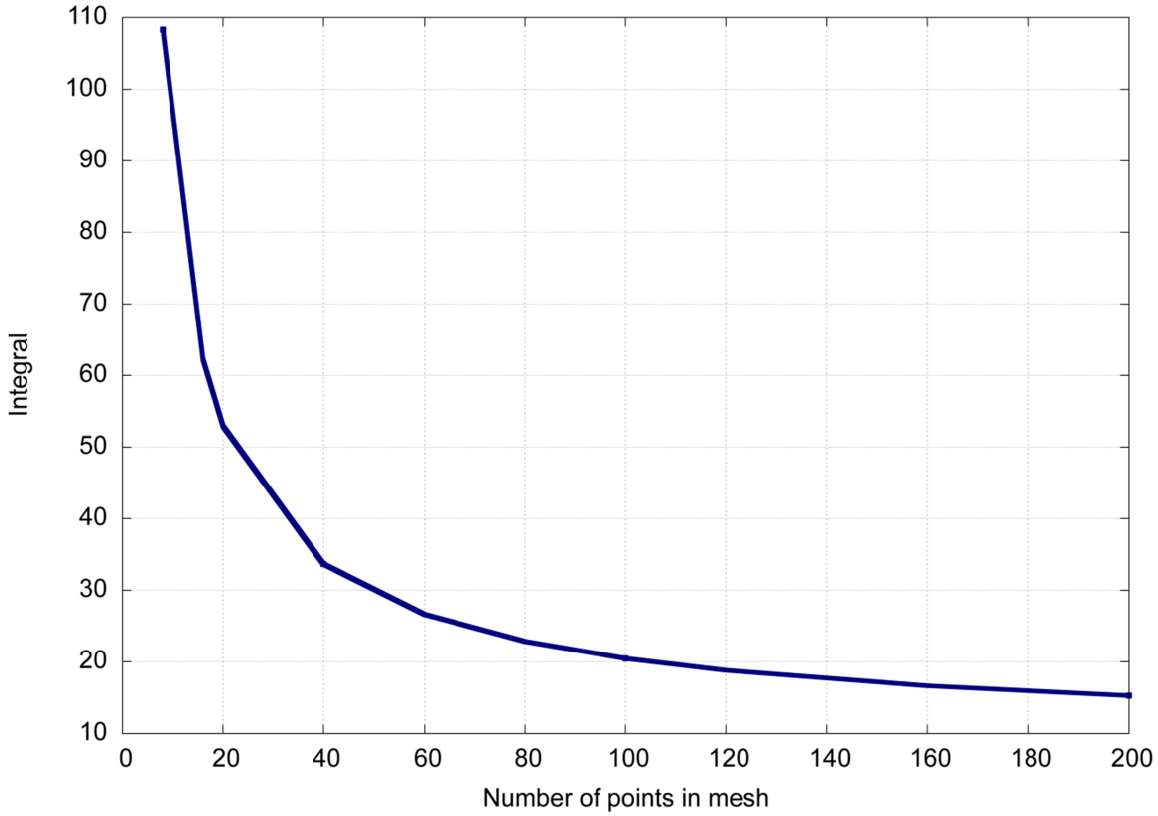

Figure 2-13: Evolution of an estimator of error against the grid density

2.5.3.3 Coupling error between plasma and wall models

As it was explained at the beginning of this subsection, numerical calculations are carried out in fixed length sub-intervals. Inside each sub-interval, the time step is varied to control the numerical error.

There is a coupling between the algorithms solving differential equations for the wall thermal model and for the plasma balance model. This coupling is carried out through the boundary conditions of each system. The plasma model updates the value for the impurity flux entering into plasma due to wall erosion. The wall model updates the thermal fluxes coming from the plasma.

These boundary conditions are updated only at the beginning of each sub-interval and for the rest of the time are kept constant. This fact induces an additional numerical error in both plasma and wall subsystems.

Plasma is very sensitive to small variations in the impurity fraction but, the wall temperature varies very slowly compared with the plasma temperature. The two error sources are analysed separately.

In the case of the error in the wall surface temperature due to the ignored variation in the heat flux from plasma, it is bounded by assuming the worst case is produced when the variation in heat flux to divertor, due to an H-L transition, is ignored

Assuming that the effect induced by an H-L transition can be modelled with a δ-Dirac function, and that the final flux is twice the original flux, the following values are obtained for the flux that is used in the subinterval, and for the flux that is being ignored (Eq. 2.99).

$$\rho_1 c_{p,1} \frac{\Delta T_1}{\Delta t} = \frac{P_{rad} - k_T \frac{T_1 - T_2}{\Delta x_1}}{\Delta x_1} + Q_{n,1}$$
$$\rho_1 c_{p,1} \frac{\Delta \tilde{T}_1}{\Delta t} = \frac{2P_{rad} - k_T \frac{T_1 - T_2}{\Delta x_1}}{\Delta x_1} + Q_{n,1} \quad \text{Eq. 2.99}$$

Supposing that the density, specific heat and thermal conductivity of the material vary slowly when compared with the material temperature, the committed error would be as shown in Eq. 2.100 for the initial time step.

$$e = \left\| \Delta T_1 - \Delta \tilde{T}_1 \right\| = \frac{P_{rad} \Delta t}{\rho_1 c_{p,1} \Delta x_1} \quad \text{Eq. 2.100}$$

For subsequent time steps, the temperature gradient at the wall surface would grow. Therefore, the calculated value would be an upper bound for the entire sub-interval (Eq. 2.101).

$$e_{subinterval} \leq \frac{P_{rad}}{\rho_1 c_{p,1}} \sum_{i=1}^{N} \frac{\Delta t_i}{\Delta x_{1,i}} \quad \text{Eq. 2.101}$$

Because of the stability condition of the wall numerical model, there is a functional relation between dt and dx. Due to the wall temperature gradient reaching its maximum at the wall surface, it is reasonable to suppose that the lower value of dx is just there. Therefore, it can be assumed $dt=f(dx_1)$, or $dx_1=f^{-1}(dt)$. This way, it is possible to find a relation between the maximum error in a sub-interval and the time step being used.

2.6 Summary

The following achievements were obtained in this work from the previous version of AINA code that was found at the beginning of this thesis work.[IDEU08]

- A new C++ code was developed, initially with the same functionalities as the previous Fortran code. Only the graphical interface was re-used in this work.
- The code was developed with an OOP architecture, using DbC to control error propagation, and with three distinct programming layers:
    - Structural code
    - Numerical models
    - Physics and engineering models

  With the purpose of building a reliable, maintainable and scalable code.
- Development was done using an integrated development cycle including version control with Git, unit testing, bug tracking, project documentation, code documentation, Scrum framework and debugging with reliability growing measurement.
- The following models were developed for AINA code in this thesis:
- Numerical models for calculation of steady state and transient, for plasma dynamics and for wall thermal equilibrium. The numerical problems were analysed, and the solution was checked for stability and convergence. Coupling errors between different calculations were also analysed.
- Generalised radial profiles and volume integrals.
- Plasma erosion models based on sublimation, sputtering and chemical erosion were further developed from the initial version at the beginning,[IDEU08] to couple them with flues coming from plasma and to include SOL model.
- All the terms in balance equations are now the result of volume integrals and not just calculated as scalings that depend on the specific radial profile used.

- Individual equations for particle balance of each impurity are now used in AINA code instead of an equation for all impurity ions.
- New algorithms for ohmic power and for synchrotron power were included in AINA code.
- The calculation of the wall thermal equilibrium is now done in three steps. First, a structure is defined internally with geometry and material composition of each region of wall. Second, a mesh is defined inside each region, attending to numerical considerations of stability and convergence, and also to minimize computational cost. Third, the numerical problem is solved, either for initial steady state equilibrium or for transient, applying initial and boundary conditions. A major contribution of this thesis is the calculation of steady state equilibrium, both for plasma and for wall. In the previous version, initial temperatures of wall were configured externally after calculating them by performing a transient calculation until finding a steady state.
- Calculation of the plasma operating window. Now, AINA code can calculate the plasma operating window and thus establish the range of variation for parameters previous to performing a parametric analysis. It is also useful for validation purposes and to extract further insight from safety analysis.
- External macros to automate simulations with AINA code. At the beginning of this thesis work, simulations with AINA code were performed individually. AINA users had to configure each simulation in the graphical interface and run it, usually a lengthy process of more than half an hour. If a parametric study was planned, the number of simulations had to be restricted according to the available time of people working on it. Besides, post processing of data was also lengthy. An Excel macro was developed to automate multiple simulations and to store results and main statistics. Now, simulations can run for days without supervision, and most of post-processing is done without need of a group of AINA users working on it. In fact, with a modern desktop computer and this automation system it is possible to perform thousands of AINA simulations in a few days,

throughout the plasma operating window, a work completely impossible in the past.

During work at IFERC in 2014-2015 many improvements were added to AINA code, including:

- Plasma geometry. New simple model based on two elongations and two triangularities, resulting in a poloidal section with four elliptical segments. The external surface is calculated with Pappus theorem, and the perimeter is calculated with an approximate formula.[Rama14]
- Thermal model for WCPB breeding blanket, based on the 1D thermal model used previously for ITER, but now using an externally calculated radial profile for volumetric power deposition.
- Upgrading of erosion model, calculating sputtering of tungsten taking into account different species, thermalised or from plasma core, with maxwellian distributions of energy and considering self-sputtering.
- Integrated pedestal-SOL model, based on scalings.
- Optimisation algorithm that replaces parameter scan. It is based on basing-hopping algorithm (global non-linear optimisation).

Chapter 3: Revisiting the analysis of passive plasma shutdown during an ex-vessel loss of coolant accident in ITER blanket

3.1 Introduction

Thermohydraulic accidents of ITER cooling systems will have the potential to originate serious safety events. There are three possible types: LOCA (loss of coolant accident), LOFA (loss of flow accident) and LOVA (loss of vacuum accident).

In the case of a LOCA, the event sequence depends on where the loss of coolant takes place. If it occurs inside the vacuum vessel, the plasma discharge will end immediately. But if it takes place outside the vacuum vessel, the plasma discharge will continue, and the wall will heat up. If an aggravating failure in the active shutdown system is considered in the accident sequence, the temperature could rise up and damage the wall.

However, the plasma facing components of ITER First Wall will be made with beryllium. This fact allows an alternative mechanism for passive termination of the plasma discharge. It is based on the evaporation of beryllium when the wall heats up, inducing an impurity flux into plasma that would increase radiative losses and finally shut down the plasma.

Passive plasma shutdown by evaporation of Be at high temperature has been examined in the past with conservative plasma physics models,[Aman96, HBNS01, UPWB96] based on simple 0D models for plasma balance equations and 1D models for wall heat transfer. Results showed that, after the heating up of First Wall due to the loss of all coolant, the beryllium evaporation in the wall surface would increase impurity fraction in core plasma and finally would induce a passive shut down of the discharge.

Passive plasma shutdown will be one of the safety features in magnetic fusion reactors, however, the scenario strongly depends on plasma physics model, PFC temperature transient and impurity concentration.

Estimations for the final maximum temperature were under the beryllium melting point, and therefore the conclusion was that the First Wall would remain intact. However, the results rely very much on the conservative assumptions taken for plasma physics and in-vessel components.

The conclusions (that the plasma can be passively shutdown by beryllium evaporation) are used for the study of the accident sequence derived from a hypothetical event, namely: "Ex-vessel rupture of FW/Blanket primary cooling circuit, with failure of fusion power shutdown system", as explained in the "Accident Analysis Specifications" ITER document.[ReTT07]

This accident sequence[Ayma01b] is an example of beyond design basis accidents, which are analysed to show the absence of "cliff effects" in the safety analysis. It is used to show the intrinsic safety features of magnetic fusion. Even in the case of an improbable major ex-vessel LOCA event, the plasma would passively shut down due to beryllium evaporation without major damages for the device.

During this thesis, this analysis has been done two times. The first one was in 2008, when a new erosion model was implemented in AINA 1.0, giving birth to AINA 1.2 code. With this code, and in the frame of a collaboration between FEEL-UPC and ITER-Safety, the passive plasma termination for beryllium evaporation was studied once again.[RiDi11]

The conclusions showed that it was difficult to state that beryllium wouldn't melt at least in some points of the vacuum vessel before plasma shutdown, due to the uncertainties in the temperature distribution over the wall surface, and in the plasma behaviour, particularly in relation to the impurity particle transport phenomena.

Following the development of the AINA 3.0 code, the study was repeated, and the conclusions were compared with those of the 2008 study with AINA 1.2, and with those of previous studies.[RiDF15]

In this chapter, the analysis of passive safety during an ex-vessel loss of coolant accident (LOCA) in the First Wall/shield blanket of ITER is presented. The analysis of plasma-wall transients is based on results from AINA code simulations. Results have been compared with those of previous studies. Besides, a sensitivity study has been done over parameters of the model with relevant uncertainties associated withbased on their values.

3.2 Models relevant for this study

3.2.1 Ex-vessel LOCA model in AINA

The development of LOCA accident is modelled in AINA by specifying the variation in temperature and film coefficient in the coolant channels.

LOCA events can be configured in AINA in time, poloidal position and surface extension. Independent LOCA events can be configured for every calculation region of the vacuum vessel (blanket modules and divertor) simultaneously, and they can be activated independently at any moment of the transient simulation.

The toroidal extension can also be specified by selecting the fraction of calculation region area affected by the LOCA event.

When the fraction of toroidal area is lower than one, the calculation is done in the following way:

- First, the temperature equilibrium for the area affected by LOCA is calculated.
- Second, the temperature equilibrium for the area not affected by LOCA is calculated.
- The erosion fluxes corresponding to the different surface temperatures are calculated and then averaged together using the factor of area affected by LOCA.
- Finally, for each calculation region, the code simulates the decreasing flow in the coolant channels during a LOCA accident by varying the convection coefficient with time after the LOCA starts.

Related to the simulation of the cooling function, the model used is one-dimensional (see Eq. 2.82) but it takes into account that the cooling channels do not take up all the transversal section of the blanket.

It uses a ratio factor between the coolant transversal (taking toroidal and poloidal directions, which is considered in this model normal to the gradient of temperature) section and the total transversal section at a specific radial position of the blanket. Figure 2-10 and Eq. 2.82 show an example of discretisation of coolant channels in the discrete heat transfer model.

If the LOCA accident flag is activated for a calculation region, a multiplier is applied over the corresponding convection coefficient. This multiplier takes values between 1 and 0.

Thus, the value of the convective coefficient is reduced during the LOCA, as shown in Eq. 4.2. When the multiplier is equal to zero, representing that the calculation region has run out of coolant, the code applies radiative heat transfer equations instead of the convective ones.

$$h(t) = h_0 \cdot c_h(t),\ c_h(t) \in [0,1] \qquad \text{Eq. 3.1}$$

If a channel loses all its coolant, heat transfer is done by radiation through the walls of the cooling channel. By default, the code assumes that the coolant temperature is always constant. However, it can be also configured.

3.2.2 View factor

The view factor FA→B is defined as the fraction over the total electromagnetic radiation leaving surface A that reaches surface B, considering no external influences over radiation. The sum of all view factors with origin in a specific surface must be one.

For AINA calculations, it is necessary to determine the view factors of a blanket module surface with the rest of in-vessel components in order to calculate the reflection of EM power, which is especially important in the case of synchrotron radiation power losses.

For this specific purpose, an auxiliary code has been developed. Any toroidal geometry can be configured through a poloidal section composed by segments, plus a toroidal radius, plus the toroidal length of every blanket module, which can fit an integer number of modules in toroidal direction. Therefore, toroidal symmetry is considered. Characteristics of code and calculations are explained in Annex 4.

3.2.3 Impurity transport in plasma

There are many uncertainties about the impurity transport in plasma. It is generally admitted[STA00] that most of the impurities enter the plasma as neutrals and ionize inside. The relatively simple Engelhardt model[EBBC82, EnFe78] gives an explanation for the penetration of impurities in plasma core from a limiter. However, in the case of divertor the model is more complex and dependant on design and operating conditions.

The model used in AINA, as explained in Eq. 2.79, consists of two screening factors considered separately for First Wall and divertor, plus a common delay time in the order of the energy confinement time, accounting for the transport time.

Screening factors are calculated to fit the impurity values in plasma core for the ITER reference scenario once erosion fluxes are calculated. These factors remain

constant during transient calculation, because they are not related to plasma models in AINA code. This is a weak point of transient calculations and should be further studied in the future.

3.2.4 Evaporation model

Evaporation model in AINA accounts for the sublimation process that happens when beryllium heats up during LOCA transient. It comprises the Knudsen equation, as described in Eq. 2.62 and the radiation enhanced sublimation (RES) model,[DBKS05] described by Eq. 2.77.

The effect of adding Beryllium RES to evaporation has been checked. It can be seen that, in the vicinity of 700ºC, the whole evaporation process begins to be dominated by thermal sublimation, and beyond 1000ºC, the thermal sublimation flux is 50 times greater than that generated by RES (See Figure 3-1).

It is concluded that Beryllium RES effect during LOCA transient can be neglected, because the evaporation process is controlled by thermal sublimation.

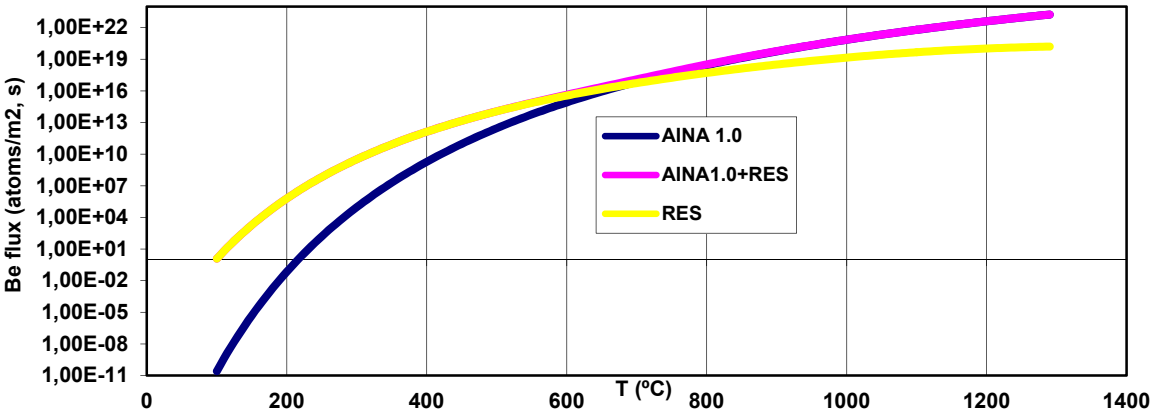

Figure 3-1: Comparison of adding Beryllium RES effect (considering physical sputtering yield of 2% and particle flux of 1e20at/m2 s) to sublimation flux. The effect of thermal sublimation becomes dominant at about 700ºC. Logarithmic coordinates in y axis.

3.3 Numerical results

The study starts with a simulation of the safety event consisting of an ex-vessel LOCA transient affecting 33% of First Wall surface, during the 500MW inductive ITER reference scenario.

Analysis with AINA 3.0 shows that fusion reaction performance deteriorates quickly after 76 seconds due to the increase in impurity fraction. The discharge ends passively after 109 seconds due to a disruption triggered by density limit (Greenwald). Beryllium evaporation rate increases abruptly after 62 seconds, when the temperature at the beryllium surface exceeds 800ºC. The highest surface temperature after ending the discharge is 1140ºC, and the temperatures at the copper heat sink lie in the interval from 887ºC to 983ºC. Neither the steel coolant tube nor the copper heat sink will melt at those temperatures. Considering the results conservatively, the time scale for an externally triggered plasma shutdown is about 47 seconds. Therefore, the results show the passive safety of the system without melting the First Wall.

From this accident scenario, a sensitivity analysis is done by scanning ranges of values for the parameters of interest. The objective is to explore the parametric space in order to discard the existence of possible cliff effects in the vicinity of the reference scenario that could change the conclusions. The parameters considered were fusion power, toroidal surface fraction affected by LOCA, poloidal position affected by LOCA, beryllium fraction in plasma at initial equilibrium, and value of time delay for the impurity transport.

3.3.1 Fusion power

Comparison between results of the three ITER inductive reference scenarios is shown in Table 3-1 and Figure 3-2.

Table 3-1: Comparison of results for the three inductive ITER reference scenarios

Fusion power (MW)	500	400	700
Fusion performance deteriorate (s)	76	98.5	34
Discharge ends passively (s)	109	133	80.5
Steep increase in beryllium evaporation (s)	62	82	42
Highest FW temperature at the end of discharge (ºC)	1140	1106	1203

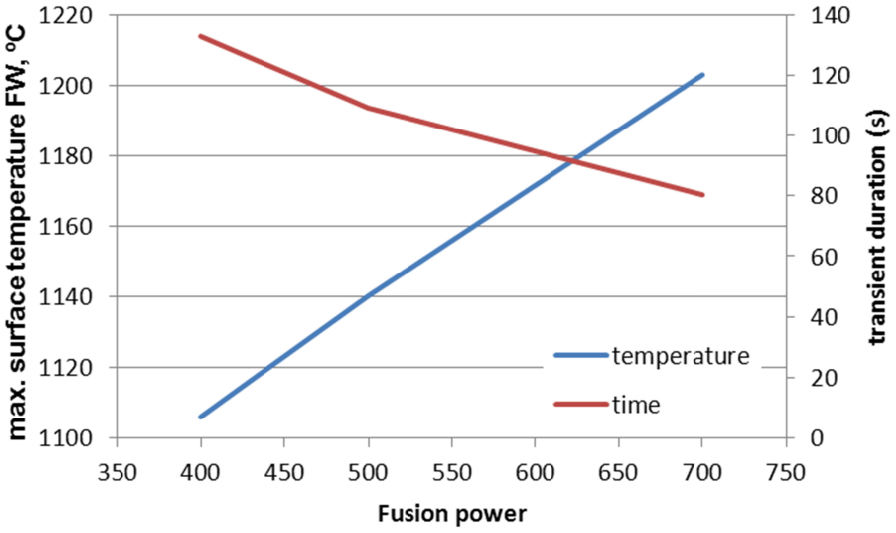

Figure 3-2: Influence of initial fusion power in final temperature (ºC) and transient duration (s)

3.3.2 Toroidal surface affected by LOCA transient

One, two or three cooling circuits of the First Wall can be affected by an ex-Vessel LOCA transient. To quantify the influence of the surface affected by a LOCA transient, a series of simulations were done varying this parameter. The results are shown in Figure 3-3. It can be seen that both temperature and shutdown time grow for lower area fraction affected by LOCA transient.

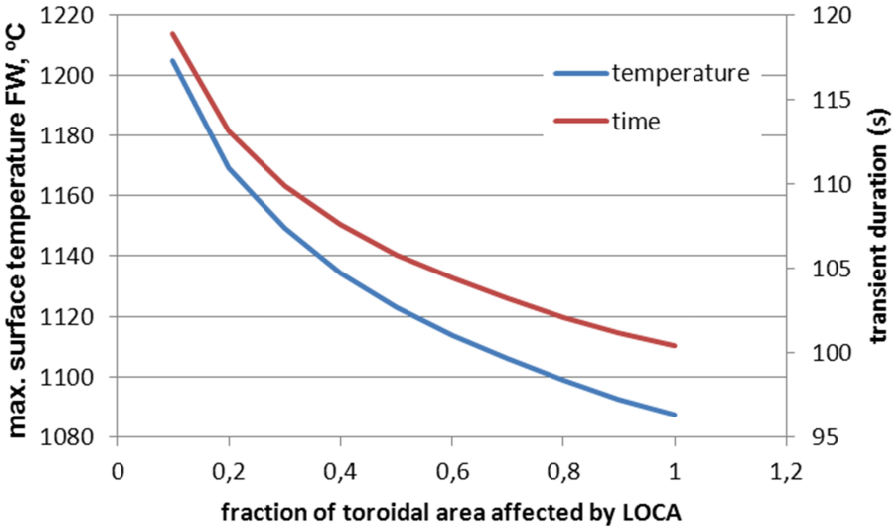

Figure 3-3: Influence of the Surface fraction affected by LOCA, in final temperature (ºC) and transient duration (s)

3.3.3 Poloidal position affected by LOCA transient

Influence of poloidal position has also been analysed. Individual poloidal positions occupying 33% of toroidal surface were considered to analyse the LOCA transient. The results are shown in Figure 3-4. Different factors affect duration, therefore the lines are not smooth. However, a clear maximum appears, providing useful information for the analysis.

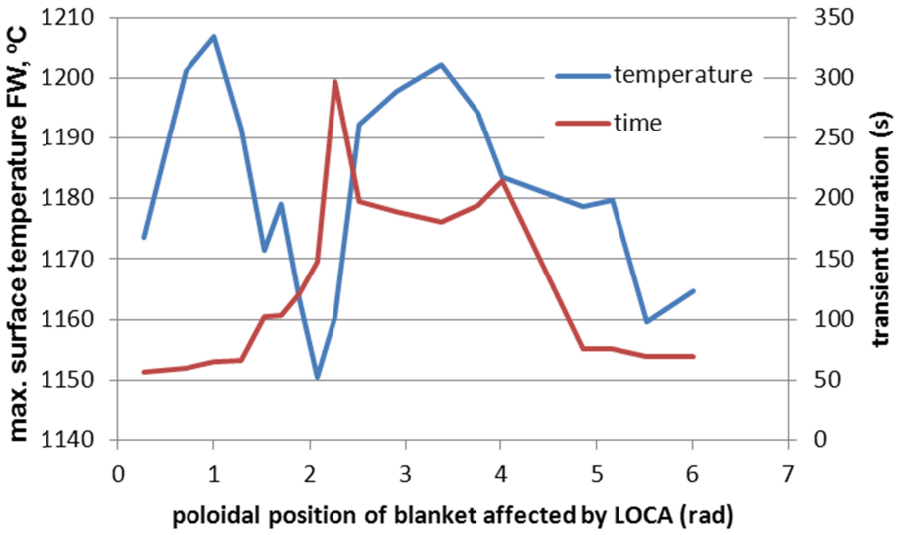

Figure 3-4: Influence of the poloidal position affected by LOCA, in final temperature (ºC) and transient duration (s)

3.3.4 Initial beryllium fraction in plasma

In ITER inductive reference scenarios, beryllium fraction in plasma is assumed to be 2%. The parametric analysis varies this percentage between 0.5% and 3%. Results are shown in Figure 3-5.

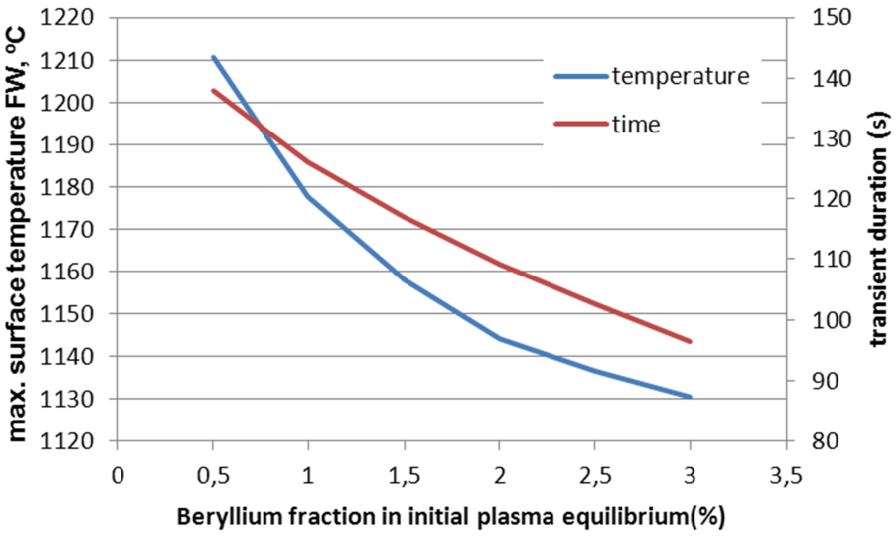

Figure 3-5: Influence of initial beryllium fraction in plasma, in final temperature (ºC) and transient duration (s)

3.3.5 Value of time delay for impurity transport to plasma core

The impurity transport time is assumed to be of the same order as the energy confinement time. However, multipliers from 0 (instantaneous transport) to 3 are used in this analysis. Results are shown in Figure 3-6.

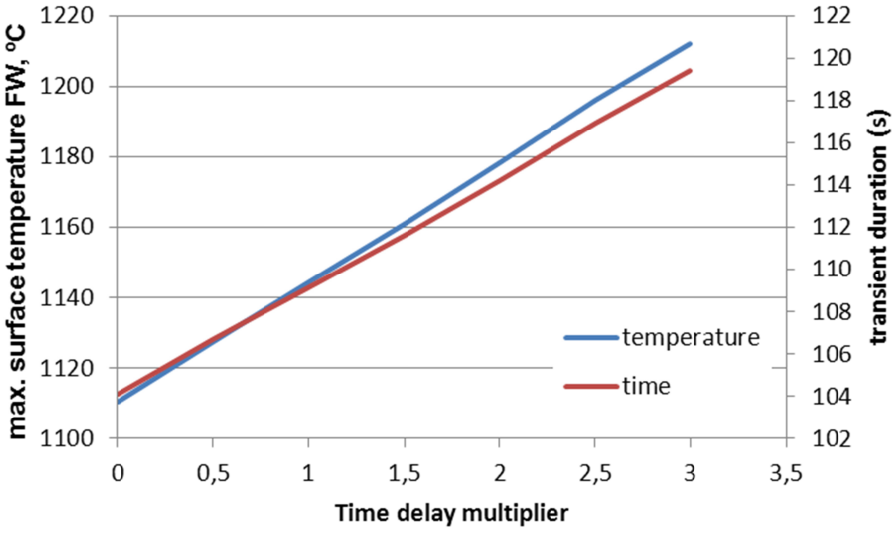

Figure 3-6: Influence of impurity transport delay time multiplier (from 0 to 3) over the final Wall temperature (ºC).

3.4 Discussion

The results of the sensitivity analysis show that high fusion power, low toroidal area fraction, low initial beryllium fraction in plasma and high time delay multiplier produce increases in maximum final temperature of First Wall after a LOCA transient. Poloidal position does not show a defined trend, but a maximum value can also be defined.

Therefore, a new scenario has been studied with the following values for the previous parameters: 700 MW of fusion power, 10% of toroidal area fraction, 0.5% of Be in plasma equilibrium, a value of 2 for time delay multiplier and poloidal position coincident with the maximum found in the sensitivity analysis.

During the transient, beryllium PFCs reach the melting point after 123 seconds. At that moment, fusion power is still 665 MW.

3.5 Conclusions

The study of this ITER safety case with AINA 3.0 code points to the possibility of a passive safety mechanism for the shutdown of plasma discharge by evaporation of beryllium at the surface of the First Wall. This result was shown before for ITER EDA design.

However, to examine the possible existence of a cliff effect affecting the results of the study, a sensitivity analysis was performed considering some important parameters.

From the results of this parameter scan, a new scenario has been selected and studied. The results of the study of this new scenario show that the First Wall integrity would be compromised because beryllium surface would melt before the end of plasma discharge.

Moreover, the analysis of the radial temperature profile in the blanket module affected by loss of coolant show that also the heat sink would melt. At that point, the structural integrity of the coolant tubes could be compromised. This result points to the possibility of an accident with the potential to mobilize the in-vessel radioactive inventory.

The usefulness of AINA code is shown here, because it is possible to perform a parametric analysis in a wide range of parameters to find the potentially most dangerous plasma-wall transients from the point of view of safety, that can be analysed in detail later with a thermohydraulics code.

Initial results support previous studies in that plasma shutdown happens before significant melting occurs in first wall. However, after a parametric survey a new scenario was identified with the potential not only to melt beryllium but also the copper heat sink. If the coolant tubes were compromised in this scenario, the in-vessel radioactive inventory could be mobilised.

Results show that, even though the passive safety mechanism would work in shutting down the plasma. Therefore, a cliff effect in this scenario that could lead to a partial melting of the beryllium wall cannot be discarded.

Anyway, this is not a safety problem as long as there is no release of radioactive inventory, which would happen in the case of massive melting of First Wall. These results does not alter the development of the accident sequence described in GSSR, [Ayma01b] and as long as a subsequent in-vessel LOCA is assumed at the end of the plasma discharge, the partial melting of beryllium tiles should be taken into account only if it increases the mobilised radioactive inventory.

Therefore, a conclusion of this study could be that even if the passive plasma shutdown could imply a partial melting of beryllium tiles, the initial assumption that plasma discharge would be inherently safe is still valid.

Chapter 4: ITER Safety Studies: The effect of two simultaneous perturbations during a Loss of Plasma Control Transient

4.1 Introduction

In this chapter, a transient with two simultaneous perturbations acting over plasma is shown to have a possibly more severe effect than those of the perturbations considered separately. The study has been done with AINA code. The consequences of these transients are shown over a n-T diagram. A method to assess the characteristics of the transients over a nT diagram has been developed.[RiDi13] [RiDi14]

The rationale of this study is that, once the occurrence of a loss of plasma transient has been assumed, and due to the uncertainties in plasma physics, it does not seem so unlikely to assume the possibility of finding a new confinement mode during the transient.

The cases selected are intended to answer the question "what would happen if an unexpected change in plasma confinement conditions takes place during a loss of plasma control transient due to a simultaneous malfunction of heating, or fuelling systems?"

The results of this chapter show the effect of two simultaneous perturbations (combinations of overfuelling, overheating and increase in confinement time) over a plasma transient, and compare it with the isolated effects of each perturbation. It is shown that the combined effect can be more severe, and a method is outlined to locate the most dangerous transients over a nT diagram.

4.2 Calculation of the Plasma Operating Window with AINA code

Physics and technological constraints impose limits on the operating space of a tokamak. In the case of plasma, there are constraints that define a region where plasma operation is stable. Besides, there are technological limits imposed by the design and the technology, determining the values of other external variables, like the toroidal magnetic field, the fuelling, heating or pumping systems, or the limits of operation of in-vessel materials.

If we define the ITER plasma operational window as the region where the H-mode is stable, then it can be bounded by plasma operation limits, such as plasma pressure (beta limit), density limits, the threshold power of H-L confinement mode transition, and the current limit.

The fact that outside of this region the plasma is not stable or has degraded confinement establishes limits to the maximum fusion power achievable, being one of the inherent features of magnetic fusion safety.

A usual way to represent plasma operating window in 0D analysis is through Plasma Operation Contours[WaSL82] (POpCon) plots.

In these plots it is possible to represent in a plane, for example the (n,T) plane, the limits that define the plasma operation space as a closed region. Limits that can be used include the beta limit, an upper density limit (Greenwald), a lower density limit (locked modes), H-L transition, current limit, or also a restriction in maximum power over divertor targets.[John11]

Constant-value contours of different plasma or reactor parameters can also be represented to give insight on plasma behavior inside the region. Useful parameters to fix are fusion power, or capital Q.

The plasma operating window, calculated by AINA code, is composed of points where plasma equilibrium calculations give a valid solution. This is useful in safety analysis when doing a parametric survey, because from the beginning the limits for the analysis are clear.

In fact, plasma window calculation in AINA code is a full parametric survey of plasma equilibria. First, a grid is defined, with a configured resolution. Then, equilibria are calculated and all their parameters stored. With this data, it is possible to trace iso-contours of any variable produced by AINA code, either from plasma variables set from wall temperatures, or erosion rates from the plasma wall interaction model.

Plasma transients for specific perturbations can also be analysed in this way, and output data can be processed to extract maxima, minima or average values. However, this method is not practical for transients, and optimisation is preferred.

4.3 Numerical results

In order to show the effects of two combined perturbations over a plasma equilibrium, relatively simple cases have been selected. The first one is a combination of overfuelling and overheating.

Starting from the position of the 500 MW inductive ITER reference scenario[PoSM06] operating point, at 8.1 keV, 1.1x1020 m-3 and Q=10, different combinations of overheating and overfuelling have been explored.

In Figure 4-1, the results of the analyses are shown over the plasma operating window. The different transients are plotted over the n,T diagram, starting from the equilibrium point and ending in a disruption or in a new steady state.

For the analyses performed, all the points located outside of the operating window correspond to disruptions, whereas the ones located inside the window correspond to new steady states.

It can be seen that, inside the operating window, and for each overheating level, the ending points of the transients are grouped in concentric curves with the approximate appearance of parallel straight lines.

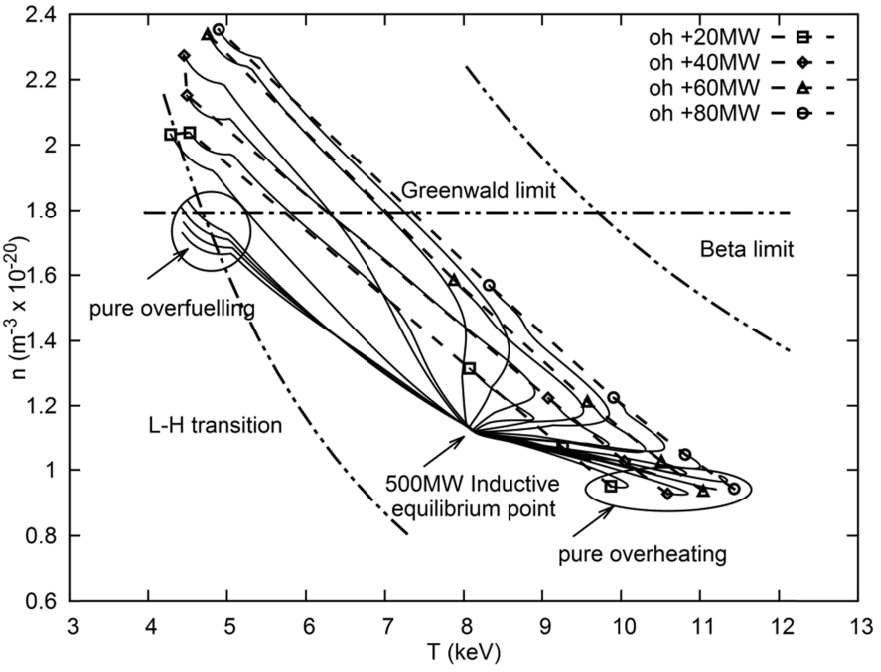

Figure 4-1: Evolution of plasma transients resulting from the combination of different overfuelling and overheating perturbations, represented in the plasma operating window.

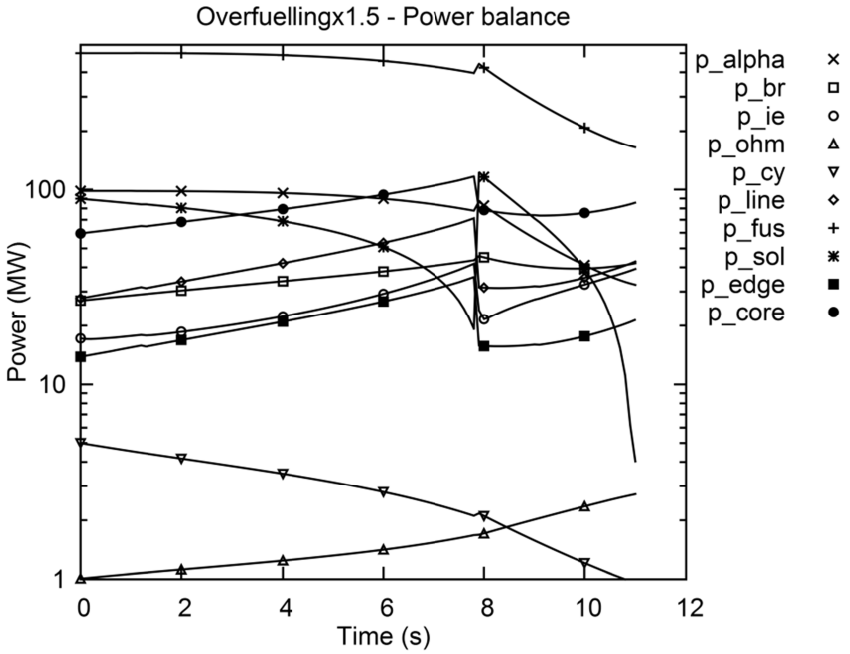

Figure 4-2: Evolution of the power balance equation terms during an overfuelling x 1.5 transient

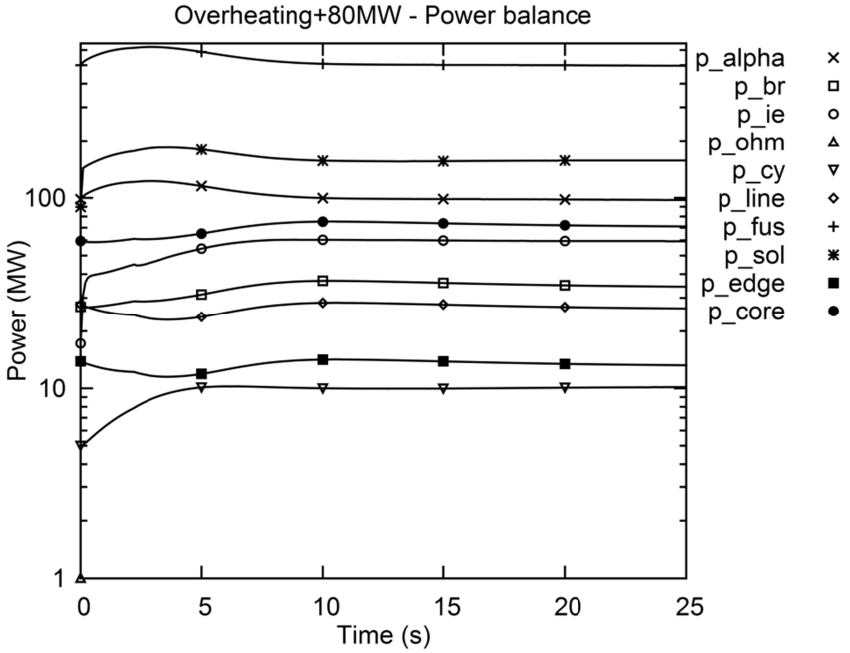

Figure 4-3: Evolution of the power balance equation terms during an overheating + 80MW transient

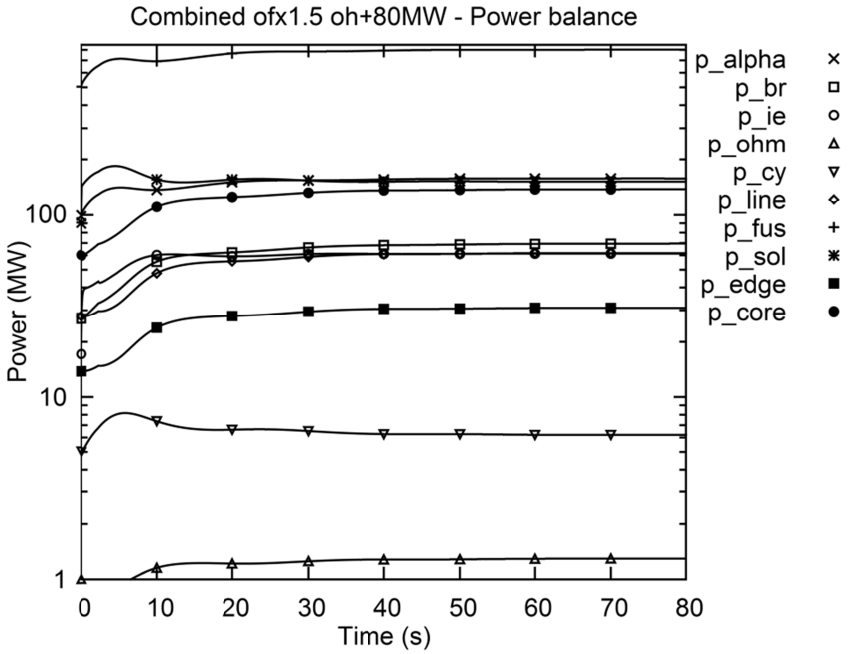

Figure 4-4: Evolution of the power balance equation terms during a combined overfuelling x 1.5 and overheating + 80MW transient

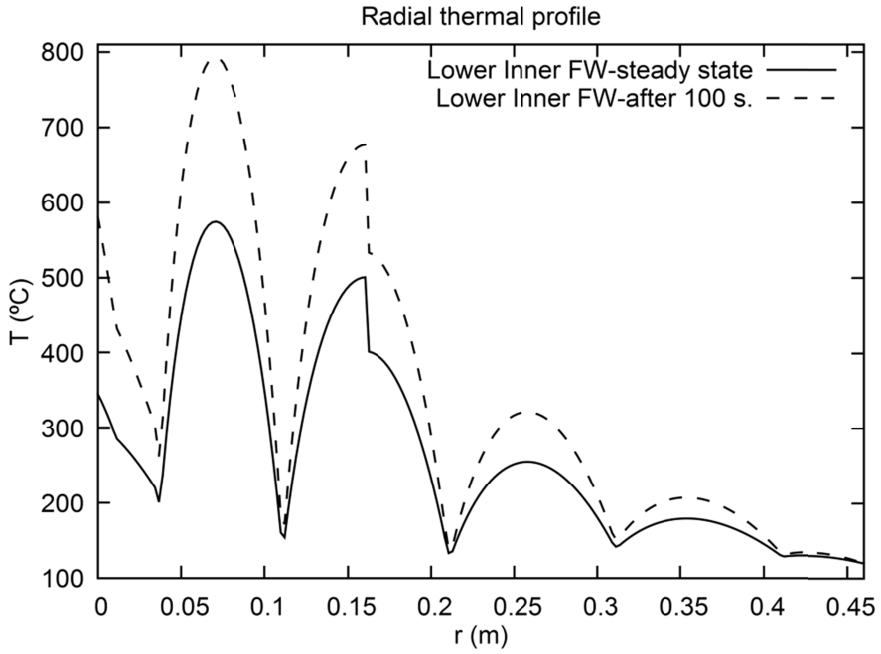

Figure 4-5: Radial thermal profile at the lower inner FW calculation region. Comparison between the initial steady state and after 100 s. of the combined overfuellingx1.5 overheating+80MW transient

To show an unfavourable case of the combined effect of both overfuelling and overheating, the case corresponding to an overfuelling x1.5 and an overheating of

80MW have been studied, for the combined and for the individual cases (Figure 4-2, Figure 4-3, Figure 4-4 and Figure 4-5).

The second selected case is a simultaneous overheating and increase in confinement time. Different combinations of the two perturbations have been explored starting from the scenario operating point, at 8.1 keV, 1.1e20m-3 and Q=10.

In Figure 4-6, the results of the analyses are shown over the plasma operating window. The different transients are plotted over the n,T diagram, starting from the equilibrium point and ending in a disruption or in a new steady state.

For the analyses performed, all the points located outside of the operating window correspond to disruptions or to L-mode equilibria whereas the ones located inside the window correspond to new H-mode steady states.

For this case, it can be seen that increasing the confinement time and decreasing the external heating, the fusion power increases. The most unfavourable case produces up to 1,421MW of fusion power in steady-state.

The third case is a simultaneous overfuelling and increase in confinement time. Different combinations of the two perturbations have also been explored.

In this case (Figure 4-7), a curve of zero-Psol disruption is clearly visible on the left, and the curve of beta limit on the right. A safety margin is used in the code over the Greenwald limit (x2), but in the figure the usual limit is plotted. Because of that, there are results of the simulations that apparently lie beyond the Greenwald limit.

The overfuelling case seems to be especially dangerous from the point of view of wall integrity, as it shows the ability to reach the upper right corner of the plasma operating window, where the fusion power reaches a maximum.

The most unfavourable case found in this study (under the ordinary Greenwald limit) corresponds to an overfuelling x1.1 and an increase in energy confinement time x1.4, which induces a new steady state that generates 1,421MW of fusion power. This case has been studied in detail, and the effects on plasma and wall thermal equilibria are shown below (Figure 4-8, Figure 4-9, Figure 4-10 and Figure 4-11).

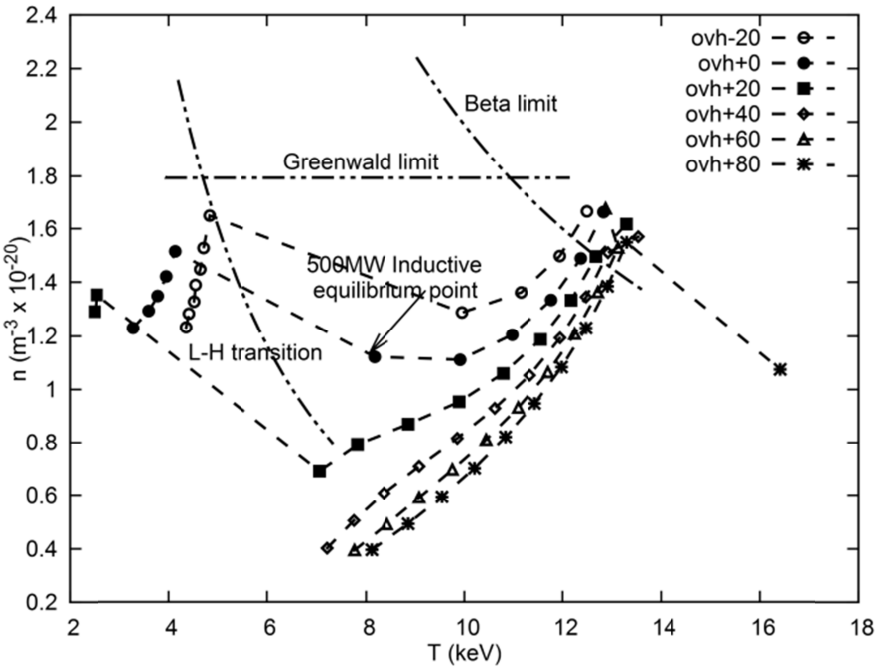

Figure 4-6: Final state (after 100 s. or disruption) of plasma transients resulting from the combination of different overheating and confinement time variation (multiplier over confinement time) perturbations, represented in the plasma operating window.

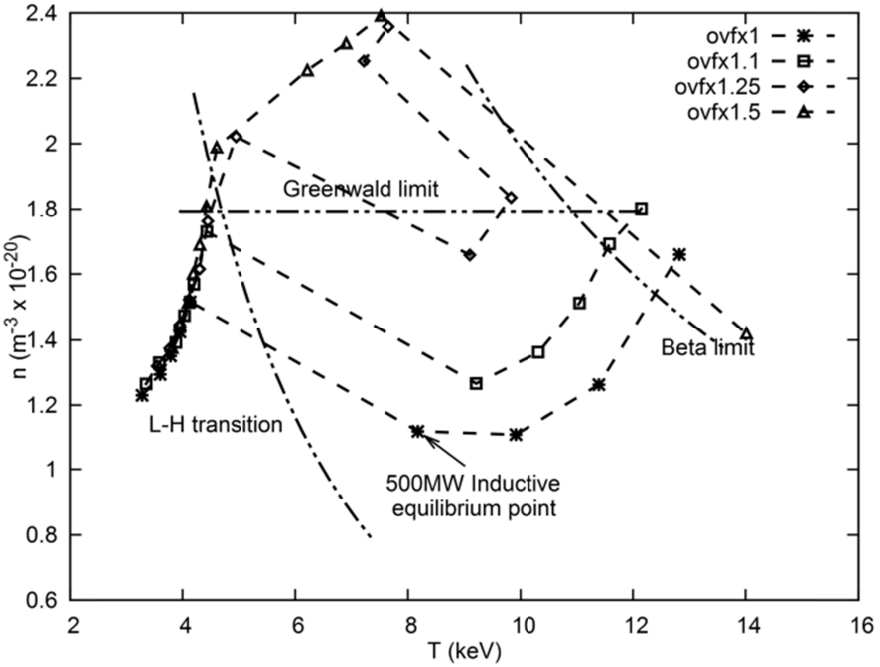

Figure 4-7: Final state (after 100 s. or disruption) of plasma transients resulting from the combination of different overfuelling and confinement time variation (multiplier over confinement time) perturbations, represented in the plasma operating window.

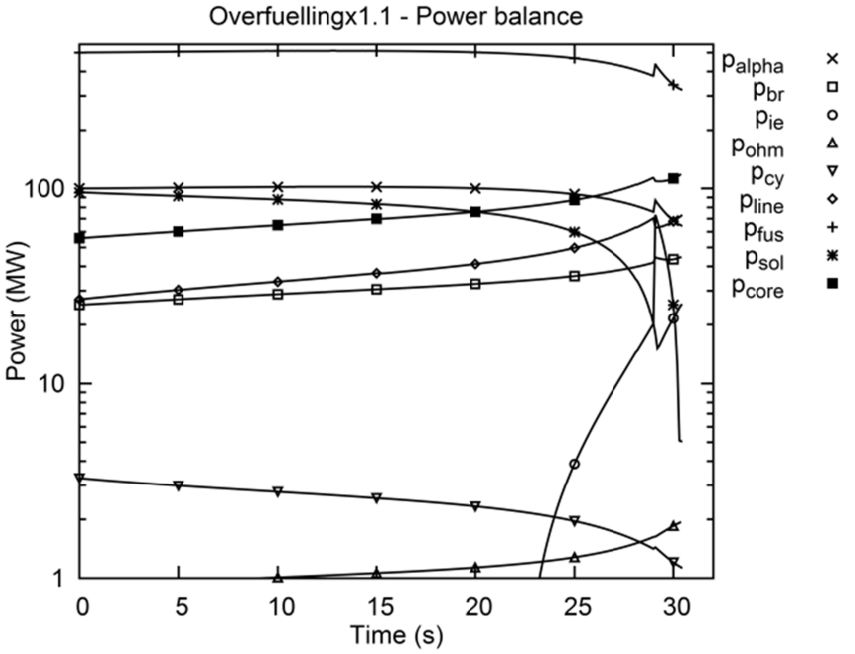

Figure 4-8: Evolution of the power balance equation terms during an overfuelling x1.1 transient

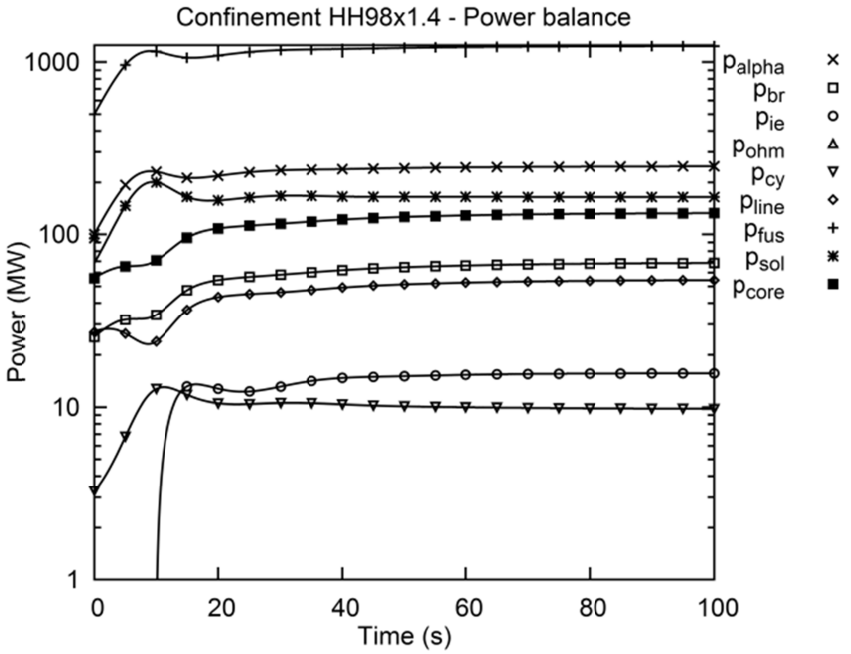

Figure 4-9: Evolution of the power balance equation terms during an increase in confinement timex1.4 transient

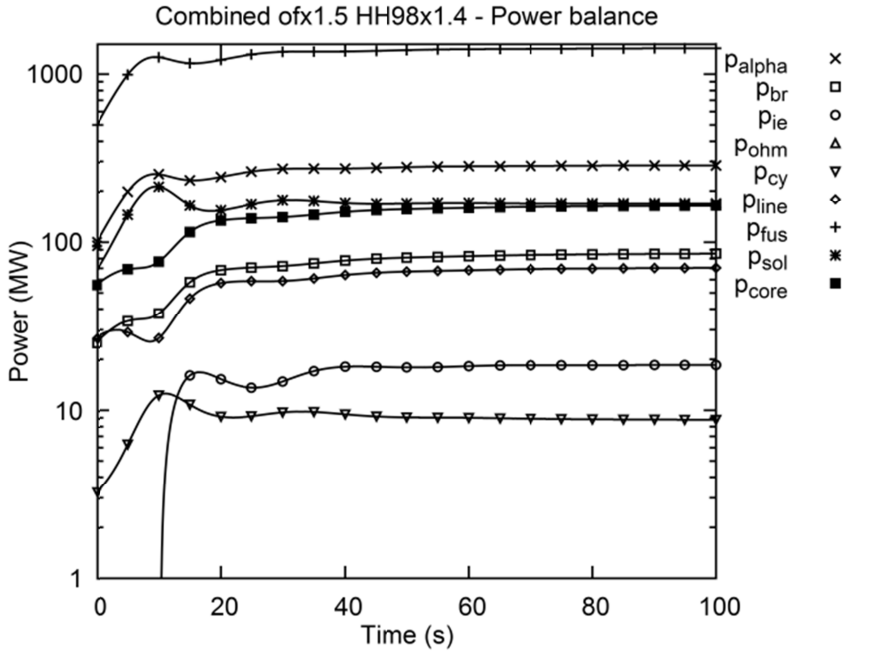

Figure 4-10: Evolution of the power balance equation terms during a combined overfuelling x 1.1 and confinement timex1.4 transient

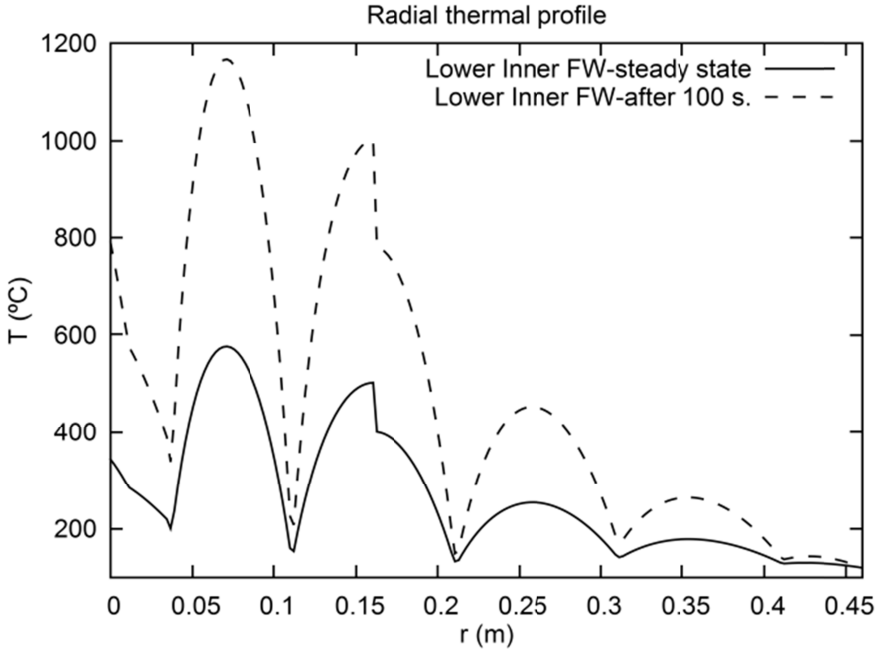

Figure 4-11: Radial thermal profile at the lower inner FW calculation region. Comparison between the initial steady state and after 100 s. of the combined overfuellingx1.1 confinement timex1.4 transient

4.4 Discussion

In the case of overfuelling+overheating transients, by plotting the evolution of the transients calculated with AINA code in a nT diagram, it can be seen that the location of the final points shows a regularity that can be used to extract insight.

This regularity takes the form of concentric curves, almost straight lines, for constant overheating and varying degree of overfuelling.

From these curves, it is possible to predict the approximate location of the new steady state with origin in these two simultaneous perturbations.

It is also possible to mark out the areas where these new transients will be located and the areas where they cannot happen.

The prediction of the steady states of maximum power is not so trivial when using the nT diagram. This is because AINA plasma model is multispecies and has different temperatures for ions and electrons.

During a plasma transient, mostly during a transient affecting the external heating, both temperatures tend to separate, and this has the effect of displacing the constant fusion power contours, and also the constant Q ones.

However, as nT product yields an estimate of the plasma thermal energy, in the straight lines we can find a maximum of the form:

$$\begin{gathered} n \approx a - bT \rightarrow nT \approx aT - bT^2 \\ max(nT) \rightarrow \frac{d(nT)}{dt} = 0 = a - 2\mathrm{bT} \\ T \approx \frac{a}{2\mathrm{b}} n \approx \frac{a}{2} \end{gathered} \qquad \text{Eq. 4.1}$$

If ionic and electronic densities and temperatures are not so different, we can correlate fusion power with the nT product, and thus the maximum of fusion power for each curve would fall near the point calculated in Eq. 4.1.

For each curve, and attending to the definition of the fusion gain, the maximum in Q would be located at the same point as the maximum in fusion power.

Following the previous considerations, the transient that was taken as an example would result in a new steady state that would fall near the maximum in fusion power for the +80MW curve, as can be seen in the Figure 4-1.

In Figure 4-2, Figure 4-3 and Figure 4-4, the evolution of the different power terms of the plasma thermal energy equation are represented, for the pure overfuellingx1.5, pure overheating+80MW and for the combined transient.

It can be seen that the fusion power for the combined transient is higher than that of the overheating transient. The overfuelling transient ends in a disruption after 11 seconds.

Figure 4-5 shows, as an example, the comparison of radial thermal profiles for the lower inner FW calculation region, for the initial reference steady state and after 100s. For the combined overfuelling.x1.5,overheating.+80MW transient.

Even considering the simplicity of the wall design implemented in the code, it can be seen how the new steady state can affect the wall integrity, not only due to the occurrence of melting, but also because of material heated over its nominal working temperature.

For the second and third cases where increase in confinement time is considered, the curves that result from making constant one of the perturbations are clearly not straight lines. However, they are continuous and bijective inside the operating window. Therefore, from the values obtained, a two-dimensional function can be approached that maps the values of perturbations to the final (n,T) steady-state point. And conversely, this function would allow obtaining the value of a perturbation that moves a plasma from its initial equilibrium to a specified final state.

Thus, if a maximum fusion power inside the operating window is known (or maximum in EM radiation, or in power to the divertor), it can be mapped to the initial perturbation values that could induce a new steady-state at that point.

This solution is slightly more complex than in the previously studied case,[RiDi13] but the methodology is still the same. In the previous case, the final points of the initial perturbations were mapped to straight lines, and then the tangency with the constant fusion power curves was found, and thus the maximum fusion power was correlated to an initial two-dimensional perturbation.

In Figure 4-8, Figure 4-9 and Figure 4-10, the evolution of the different power terms of the plasma thermal energy equation are represented, for the pure overfuellingx1.1, for the pure increase in confinement timex1.4 and for the combined transient.

It can be seen that the fusion power for the combined transient is higher than for the overheating transient. The overfuelling transient ends in a disruption after 30 seconds.

Figure 4-11 shows, as an example, the comparison of radial thermal profiles for the lower inner FW calculation region, for the initial reference steady state and after 100s. for the combined overfuelling.x1.1, increase in confinement timex1.4 transient.

Even considering the simplicity of the wall design implemented in the code, it can be seen how the new steady state can affect the wall integrity, not only due to the occurrence of melting, but also because of material heated over its nominal working temperature.

4.5 Conclusions

In previous studies,[DDRL09] the influence on plasma of isolated perturbations, like overfuelling, overheating or increase in confinement time, was analysed. Separate scans for each perturbation were performed to find the most dangerous transients from the point of view of wall thermal integrity.

A conventional preliminary analysis of the magnitude of the studied perturbations would show which transients can create the most severe thermal effects in the wall for each perturbation considered separately.

However, a similar analysis, applied to the study of the effect of two simultaneous perturbations, would need a greater computational effort.

In this work, the effects of two simultaneous perturbations (combinations of overfuelling, overheating and increase in confinement time) have been analysed with AINA code, for the plasma of the ITER 500MW inductive reference scenario[PoSM06]

The evolution of the transients was plotted over a (nT) diagram, and patterns in the location of the final steady states were detected. These patterns allowed for the outlining of a new method to predict the location of the most dangerous transients from the point of view of wall integrity.

As an example, results from the most severe transient detected are shown, to illustrate how the combined effect of both perturbations can have a synergetic effect and generate a steady state with more severe impact on the wall thermal conditions.

The occurrence of a simultaneous two-dimensional perturbation can seem highly unlikely, but it is more probable if we consider that the change in confinement mode could be induced by the initial perturbation itself. However, there is a high uncertainty about the functional dependence of plasma confinement, and therefore it is highly risky even to suppose a constant multiplier over HH98 during the course of the transient.

Other possible variation happens when the confinement perturbation does not start simultaneously with the other perturbation. In such case, the final state would also be altered. However, as there are so many uncertainties about the functional dependence of the confinement, this change probably would not contribute to any useful information.

What is important about these results is that they show that the methodology of the previous analyses could probably be modified to obtain improved results from the point of view of safety.

With all caveats regarding to the simplifications assumed in AINA code models, it is shown that, in the improbable case of overfuelling or overheating events, it cannot be

discarded that a simultaneous change in confinement could happen, which can significantly worsen the conditions of the transient.

Specifically, in the case of constant, moderate overfuelling (up to x1.5), or overheating (up to x3.0) events, if we add the occurrence of a constant, moderate increase in confinement time (up to x1.5), and we leave the plasma without control during as much as 100 s., then it is possible (though unlikely) that the plasma reaches the maximum fusion power inside the operating window.

The prediction method developed for the location of the final equilibrium point of an overfuelling+overheating transient was modified for the cases including a confinement time perturbation, based on the approach of a 2D function that maps the initial perturbation magnitude to the final equilibrium point.

As an example, results from the most severe transient detected are shown, to illustrate how the combined effect of both perturbations can have a synergetic effect and generate a steady state with a more severe impact on the wall thermal conditions.

This study was not demanded by ITER, but served to the purpose of exploring new methodologies for finding answers in relation to the study of plasma transients.

If we consider that during a transient the plasma evolves in quasi-static equilibrium, then it is possible to predict in a relatively simple way the characteristics of the transient just knowing the initial state and the characteristics of the perturbations.

Even if the application of this study is rather limited, it served the purpose of exploring a new methodology of work and of getting insight on the behavior of a 0D plasma transient inside the operation window.

Results also showed that even after having taken into account the simple models used and the uncertainties in plasma physics and design data, the results show that the methodology used in previous analyses could probably be improved from the point of view of safety.

Chapter 5: Safety Studies of Plasma-Wall Events with AINA code for Japanese DEMO

5.1 Introduction

In the frame of Japan-EU collaborative work for development of AINA code in 2014-2015, a version of AINA code has been developed for a Japanese DEMO design. This design includes a water cooled pebble bed blanket, water cooled divertor with copper heat sink at target area, and all-tungsten First Wall.

It was decided that some of the postulated initiating events found in the hazard analysis done for this DEMO design,[Naka13] needed to be investigated with AINA code. Specifically, ex-vessel loss of coolant for blanket, or divertor, and abnormal plasma overpower events.

Code development focused on the following points:

- A 1D thermal diffusion model for WCPB breeding blanket was developed. DEMO design data was used to create the configuration for AINA simulations.

- Plasma core models were upgraded when necessary for the purposes of benchmarking with TPC systems code.

- An integrated pedestal-SOL model, based on Pacher scalings,[AHGG03, GHGA07, PKPJ07] was implemented in AINA code, with capability of prediction of divertor regime during plasma-wall transients.

- Erosion model was modified to include poloidal wall loading of particle fluxes, calculated with SONIC code.[HASN14]

- A 1D thermal diffusion model for DEMO divertor design was implemented in AINA based on design data.

Extensive benchmarking was done based on two sources:

- Benchmarking of plasma equilibrium was done with results of TPC systems code.[Naka13]

- Benchmarking of wall thermal equilibrium was done with results from coupled neutronics and thermohydraulics analysis done by JAEA Fusion Reactor Design Group[STUT15] and UPC-FEEL group.[Fabb14]

- Comparison of pedestal results was done with results of HELIOS code.[John11]

Preliminary safety studies included Loss Of Plasma Control (LOPC) transients and ex-vessel Loss Of Coolant Accident (ex-vessel LOCA) for both divertor and blanket.[RNST14]

In this chapter, the work done in AINA code during 2014 and 2015 at IFERC is presented. The main motivation of this work was to adapt the code and to perform safety studies for a Japanese DEMO design. In relation to to AINA code, the work has supposed major changes in plasma models.

5.2 Models relevant for this study

These models are explained in detail in Chapter 2. However, they are commented on here in the context of their development for the Japanese version of AINA-DEMO.

5.2.1 Thermal model for WCPB breeding blanket

The thermal model for WCPB breeding blanket modules is based on the 1D thermal model used previously for ITER,[Fabb14, STUT15] but now an externally calculated radial profile for volumetric power deposition is used. This radial profile was calculated for the reference scenario, and during transients it is weighted using the variation in fusion power.

The new model allows different combinations of materials and thermal gaps. A model for heat transfer by radiation between cooling channel walls in case of coolant drainage (Loss of coolant accidents, etc.) is also implemented. The resulting configuration can be described as follows:

First Wall 1D model is configured with tungsten layers for the plasma facing components (PFCs), and low activation F82H steel for the structure and coolant channels.

Breeding blanket uses F82H steel for the structural layers, and average properties of helium and of the mixed breeder for the breeding area.

5.2.2 Thermal model for divertor.

The thermal model of divertor is the same as for ITER. Regarding the volumetric power deposition, an inverse exponential law is used, for there is no breeder area in this divertor design. The configuration resulting from design data includes a layer of tungsten for the PFCs, layers of copper and copper alloy for the heat sink and coolant tubes in target area, and layers of F82H steel for structure and also for coolant tubes outside the target region.

5.2.3 Upgrading of erosion model

Erosion model calculates sputtering of tungsten, taking into account different ion species present in plasma core, plus impurities injected in scrape off layer. Both ions and neutrals are considered in targets, while only neutrals are considered in First Wall.

The particle flux coming to surface from plasma is modelled on the basis of a poloidal wall loading calculated with SONIC code.[HASN14] During a plasma transient, this poloidal wall loading is weighted with the variation of plasma core temperature and density, in the case of First Wall, and with the variation of SOL power, density and

temperature in the case of divertor. The energies of particles at the wall used for calculating erosion undergo a further transformation when a maxwellian distribution is applied to them, so erosion calculation can account for the high energy particles from the distribution tail that can produce erosion even at low average energies.

Self-sputtering is taken into account only in divertor, and two sources are considered, one from main plasma, with the same temperature as the rest of ions, and the other composed by thermalised neutrals coming from recent sputtering processes.

Impurity transport uses a model based on two screening coefficients, one for divertor and one for First Wall. A delay time in the order of energy confinement time accounts for the transport time of impurities.

Due to changes in confinement time, delay time also changes. To model impurity flux in these circumstances, an intermediate discrete buffer is used. However, the result can produce peaks in impurity flux into plasma. To avoid this, the impurity flux is smoothened by applying a normal distribution to the delay time of particles eroded at a discrete timestep. This way, the impurity flux into core plasma becomes continuous.

5.2.4 Upgrading of plasma core models

A new simple model for plasma geometry has been developed, based on two elongations and two triangularities, used to build four elliptical segments that compose the poloidal section. The toroidal volume is calculated in a simple way with Eq. 2.1

The external surface is calculated from the poloidal perimeter by applying Pappus theorem to each of the four elliptical segments, and the elliptical segments that compose the perimeter are calculated using the approximate formula from Ramanujan.[RNST14]

The final volume and surface are multiplied by coefficients that fit ITER data. The rate of error is under 10%.

5.2.5 Integrated pedestal-SOL model

In previous studies, only parabolic radial profiles were used for plasma core calculations. Besides, divertor model consisted in a very rough interpolation.[Ayma01b]

In this work, an integrated pedestal and SOL model has been implemented in AINA code based on SOL scalings[AHGG03, GHGA07, PKPJ07] and pedestal scalings.[John11]

By using the neutral pressure normalised to 1 at incipient detachment, as described by Pacher, [AHGG03, GHGA07, PKPJ07] to define the divertor regime, it is possible to calculate

the initial equilibrium and the transient evolution of the SOL-core plasma coupled model.

At every initial equilibrium of plasma, target power flux can be specified at a design value, that in present calculations was 10 MW/m^2. This target power flux, together with values at the interface pedestal-SOL, define a regime represented by the μ parameter.[AHGG03]

During a plasma transient, as core plasma conditions change, also divertor conditions and target power flux evolve, causing a change in target thermal equilibrium.

5.3 Safety analysis: numerical results

5.3.1 Introduction to LOPC transient studies

In the past, the loss of plasma control transients were studied for ITER with an approach based on parameter scans.[HBNS01] In this approach, a scan is done of plasma equilibrium input parameters and of the magnitude of plasma perturbations to determine the maximum fusion power during subsequent plasma transients.

The resulting figures allow estimating trends and possible relative maxima in fusion power. Thus, once decided which transient will be taken as a reference most severe transient in terms of fusion power, the effect over wall thermal profile, specifically at divertor target, is studied.

In this study, two main changes are introduced for the study of LOPC transients: first, now the objective variable to determine the severity of a transient is not the maximum fusion power but the melting time at some position of poloidal section.

The second change is related to the method for finding the most severe transients. The parameter scan does not cover the full range of variation of the target heat flux in the plasma operating window. Therefore, a new method based on global optimisation constrained by the plasma operating window has been used here.

For completeness, and to check results with previous studies, a sensitivity analysis was also done.

5.3.2 LOPC and Ex-Vessel LOCA for blanket

In the case of plasma overpower events, two cases of overfuelling are presented:

1.- Study of overfuelling x1.25, which produced a new steady state of 1702MW of fusion power.

2.- Study of overfuelling x1.35, which produced a new steady state of 1840MW of fusion power.

The resulting radial temperature profiles in the outer equatorial blanket can be seen in Figure 5-1.

For the ex-vessel LOCA accident, the case presented considers 33% of wall surface affected. Based on MELCOR simulation, the coolant circuit is supposed to maintain the cooling function during the first two seconds. After that, during 10 seconds it is considered that a certain cooling capacity is maintained. After 10 seconds, it is considered that the cooling function is completely lost.[NITS14] The results show in

Figure 5-2 that after 217 seconds, structural steel melts at the outer equatorial blanket module, after reaching 1370ºC.

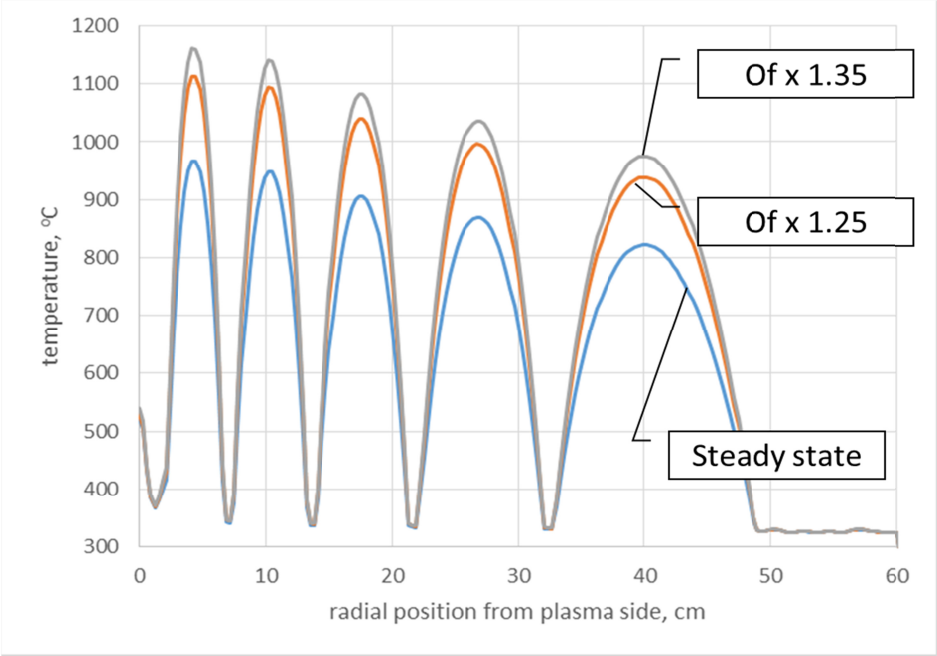

Figure 5-1: Radial thermal profile at outer equatorial position, 200 s after the beginning of the plasma transient

Figure 5-2: Radial thermal profile at outer equatorial position, during an ex-vessel LOCA accident

5.3.3 Parameter scan

The parameters considered in this study were the initial fusion power, the initial ion temperature and the pedestal fraction (over the central value) for the plasma density radial profile.

The perturbations studied were a sudden (step) increase in fuelling (overfuelling), a sudden increase in external heating (overheating) and a sudden increase in confinement time, accounting for unexpected changes in plasma physics to cover uncertainties in knowledge of plasma transport.

Figure 5-3 and Figure 5-4 show the results of this parameter scan using maximum fusion power and maximum target heat flux as objective variables. It can be seen that there is a clear divergence between both analyses, and thus the resulting reference transients would be different in many cases.

5.3.4 Determination and study of reference plasma-wall transients

The previous scans are useful to get insight into the behavior of plasma, but to determine the reference transients, global optimisation was used for each of the three considered perturbations, and also for a case that considers a combination of all of them. The results are shown in Table 5-1, together with the duration of transient and the final consequences for divertor.

Figure 5-5 shows the final radial temperature profile at outer divertor target for the reference plasma transients.

5.3.5 Study of ex-vessel LOCA of divertor

As in the case of the blanket,[RNST14] an Ex-vessel LOCA transient affecting divertor has been studied. The case presented considers 25% of wall surface affected, corresponding to one of four coolant circuits. The coolant circuit is supposed to lose the cooling function from the beginning of the LOCA transient. The results show in Figure 4 that after 10.9 seconds and after reaching 1083C, the copper heat sink melts at the outer target.

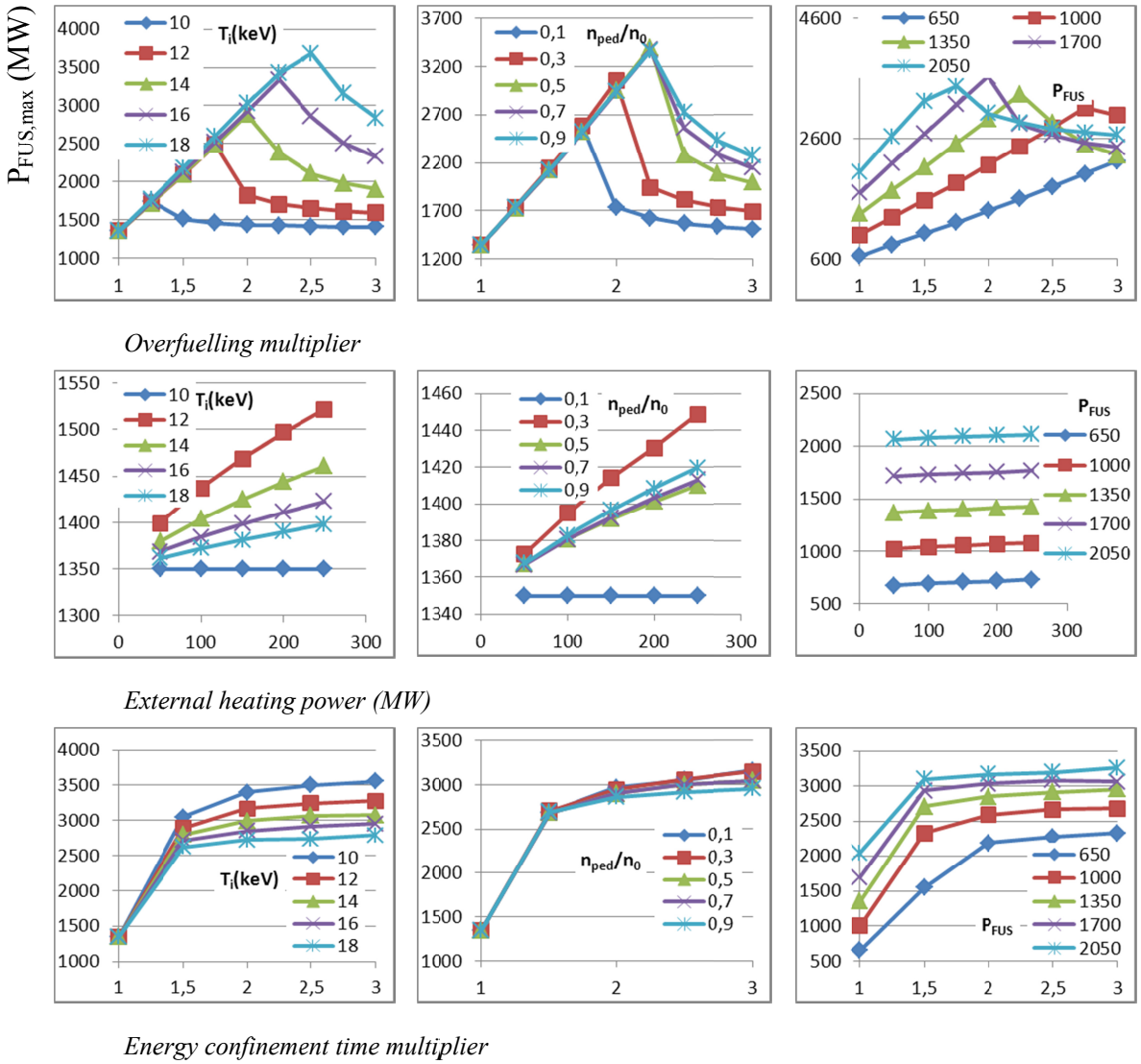

Figure 5-3: Results of parameter scan using the maximum transient fusion power (y axis) as objective variable. Each perturbation is arranged in a different row (x axis), and each plasma parameter in a different column.

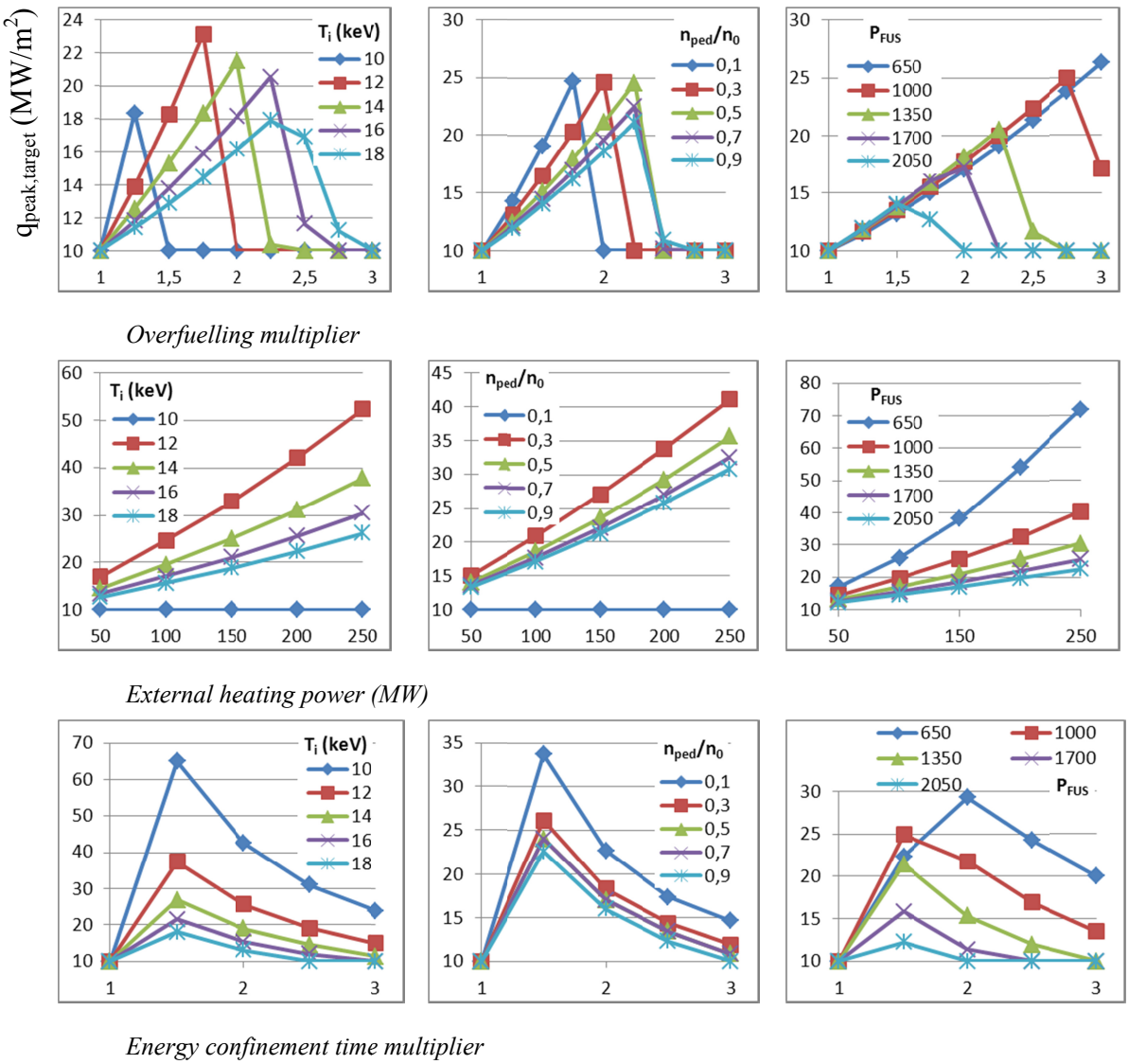

Figure 5-4: Results of parameter scan using the maximum heat flux over target (y axis) as objective variable. Each perturbation is arranged in a different row (x axis), and each plasma parameter in a different column (see legend).

Category	$Q_{target,peak}$ (MW/m^2)	Initial plasma equilibrium			Perturbative parameters			Transient duration/final surface temperature /divertor status
		P_{FUS} (MW)	T_i (keV)	$f_{ped,n}$[2]	xOF[3]	+OH[4]	$x\tau_E$[5]	
Overfuelling	24.41	1478	15.11	0.89	2.11	0	1	162.1s/2500°C/stabilised, but F82H melts in blanket
Overheating	40.18	1181.6	11.21	0.824	1	150	1	4.2s/3500°C /melting
Confinement time	107.31	1000	10	0.3	1	0	1.5	8.1s/3500°C /melting
Combined	56.45	870.8	11.49	0.548	2.09	206.38	2.053	2.0s/3500°C /melting

Table 5-1: Results from optimisation: most severe transients for each plasma perturbation

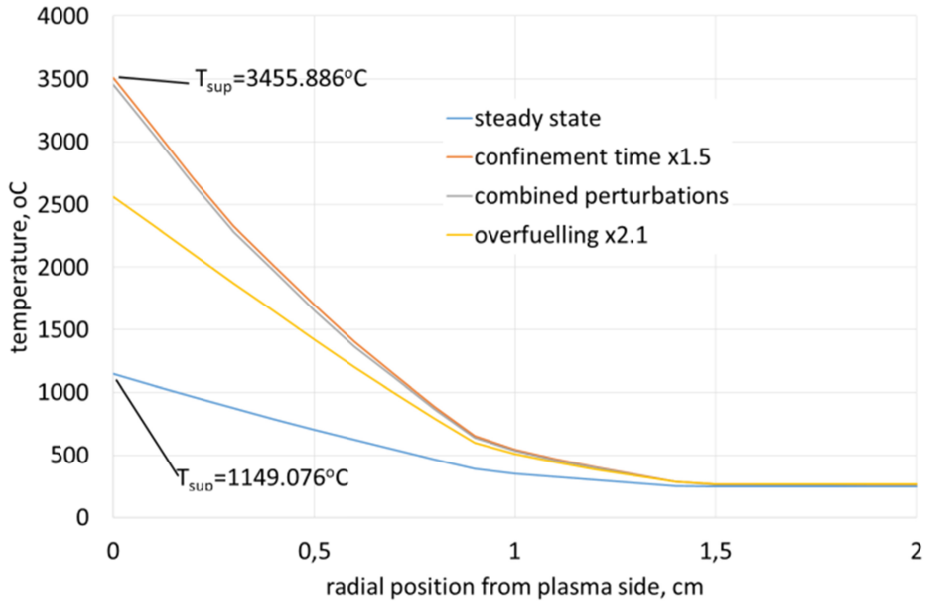

Figure 5-5: Final radial temperature profile of divertor target during reference LOPC transients

[2] Ratio of pedestal value over central value for radial density profile

[3] Overfuelling multiplier

[4] Overheating factor (additive, MW)

[5] Energy confinement time multiplier

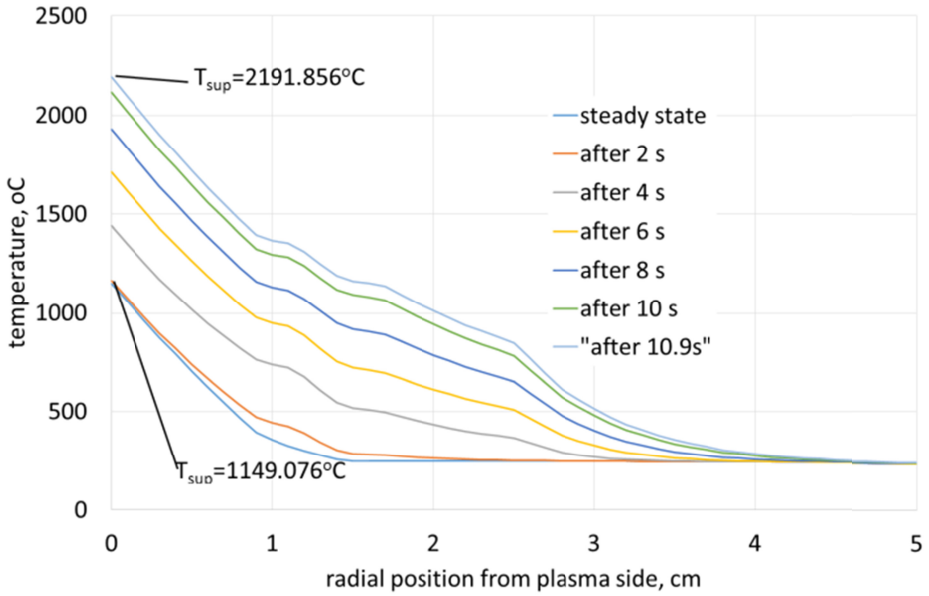

Figure 5-6: Radial thermal profile at outer target, for ex-vessel LOCA with 25% of wall surface affected. Origin of x axis represents surface in contact with plasma

5.4 Discussion

In the case of plasma overpower events, after 200 seconds, breeder temperature reaches up to 1170ºC in the case of overfuelling x 1.35. This effect does not seem to be very severe for the blanket.

In the case of ex-vessel LOCA accident, the structural steel under the First Wall melts after nearly four minutes, without significant effects on plasma impurity fraction.

This result follows a similar evolution pattern to that found in ITER, but in the latter case, evaporation of beryllium in plasma facing components induces a passive plasma shutdown.[RiDF15]

Regarding overfuelling, the transient does not reach the melting temperature at divertor target, and the transient finishes when the structural steel F82H melts at outer breeding blanket. This could be the general case for long transients.

An interesting result is that a modest increase in confinement time, combined with low initial fusion power, ion temperature and a low density pedestal would create great trouble to divertor.

The rest of the reference transients finish with the melting of divertor target in very short time, creating a challenge for the plasma control system.

5.5 Conclusions

As expected, the effect of a Loss Of Plasma Control (LOPC) transient is not very severe for blanket modules but is expected to be more important for divertor. However, divertor models in AINA code need to be upgraded in order to study divertor safety scenarios.

For the LOCA transient, the results seem to show that a passive plasma shutdown is not possible for this DEMO design, and therefore the plasma control system should be considered as a Safety Important Component (SIC). The time for the plasma control system to shutdown the plasma discharge is over 3 minutes.

Future work will include improvements in AINA divertor models, and also a detailed definition of accident scenarios, in order to study ex-vessel divertor LOCA, and Loss Of Flow Accident (LOFA) for both divertor and breeding blanket.

A new version of AINA code has been developed for safety studies of a high aspect ratio Japanese DEMO design. It includes thermal modeling of WCPB breeding blanket and divertor, pedestal-SOL self consistent modeling and an updated erosion model based on wall fluxes calculated with SONIC code.

By changing the objective variable for the determination of reference transients, from maximum fusion power to melting time, and by using global optimisation to find these transients allows taking great profit of the new pedestal-SOL model in the determination of very severe transients that could not be found in past studies.

Initial safety studies have been done with this code, covering LOPC and ex-vessel LOCA transients.

In relation to safety studies, a major breakthrough in the study of Loss Of Plasma Control (LOPC) transients has been the use of an optimisation method to determine the most severe transients in terms of the shortest melting times.

The results of the safety study show that the effects of LOPC transients are not likely to be severe on breeding blankets. In the case of divertor though, they can induce severe melting.

Ex-vessel Loss Of Coolant Accident (LOCA) analysis is severe for both blanket and divertor, but in the first case the transient time until melting is nearly two orders of magnitude higher. The results point out that the recovery time for plasma control system should be at least one order of magnitude lower than confinement time to avoid melting of divertor targets.

Chapter 6: A review study of Loss of Plasma Control transients in ITER

6.1 Introduction

ITER design has as a basic principle that the machine should accommodate the uncertainties of plasma behaviour. Therefore, off-normal plasma transients are studied as safety events.

The most severe plasma transients expected are disruptions, VDEs and runaway electrons. From the safety studies of these events it was concluded that the only consequences affecting the wall integrity would imply the erosion and partial melting of the plasma facing components and, very infrequently, in vessel leaks due to a local perforation of the First Wall by runaway electrons.[Tayl09, TBCC11]

Together with them, the LOPC transients, which postulate a total failure of the plasma control system , have been also studied.[Ayma01b] This is because, as far as the plasma control system is not considered a Safety Important Component, no credit is given to it.

In the ITER Generic Site Safety Report(GSSR),[Ayma01b] the free evolution of plasma discharges in the case of loss of plasma control was studied for possible consequences affecting ITER safety. The methodology used consists of adding a perturbation to the calculated plasma equilibrium and then studying the subsequent transient of the system composed by plasma and in-vessel components, the latter being studied for thermal evolution.

The postulated LOPC transients in GSSR were the following:

- sudden increase in fuelling rate,
- sudden termination of fuelling or auxiliary heating,

- sudden improvement of confinement time,
- sudden increase of auxiliary heating.

The results showed that the plasma discharge would passively shut down once the limits of the plasma operating window are reached, thus bounding the maximum power achievable over the wall.

If the transients last only a few seconds, they will not damage the wall significantly. Otherwise, a long lasting overpower transient would damage the plasma facing components or even melt the copper heat sink.

This chapter covers the results of the most recent work done with AINA for the study of the "Loss of Plasma Control Transients in ITER". It is intended not only to be a review of previous studies on this topic, but also to show the new methodology developed in this thesis work.

6.2 Relevant physics data for this study

For this study, AINA code was configured with ITER plasma models and also with simplified models of in-vessel components, namely blanket modules and divertor modules.

6.2.1 Origin of the data

Most of the data and assumptions to be used for the safety analysis of ITER are summarised in the Safety Analysis Data List document.[Topi08] The Plasma Performance Assessment document[PoSM06b] defines in detail the ITER reference scenarios to be used. The ITER Physics Basis document[Iter99b, Kike07] presents and evaluates the physics rules and methodologies for plasma performance projections. The main input data are shown in Table 6-1and Table 6-2.

6.2.2 Degree of conservatism of the input data:

The plasma safety interface model is based on the work of Uckan.[UPWB96] Regarding the plasma, the operating window is extended in order to assure optimistic plasma operation (and therefore wall heating) and thus assure the robustness of the results from the safety point of view. The beta limit and upper density limit values were raised by >50-100% compared to the nominal values in the Plasma Performance Assessment document.[PoSM06b]

The threshold power value for the confinement mode transition is assumed to be lower than the one calculated from the scaling, to assure optimistic H-mode plasma operation.

The impurity influx to the plasma is also considered conservatively to maintain the plasma as clean as possible. The impurity transport probability is calculated in the steady state equilibrium and is, in any case, more conservative than present tokamak experimental data. The time delay due to the transport was also considered to be the energy confinement time, which is conservative if compared with laser ablation experiment data.[DGLM93]

The wall thermal conductivity is taken as the worst case due to neutron irradiation, and the neutron analysis is performed attending to conservative criteria.

Table 6-1: Inductive plasma operation scenarios [PoSM06b]

Variable	Unit	500 MW	400MW	700MW
		Value	Value	Value
R	m	6.2	6.2	6.2
a	m	2	2	2
k95		1.7	1.7	1.7
d95		0.33	0.33	0.33
Vp	m^3	831	831	831
Bt	T	5.3	5.3	5.3
Ip	MA	15	15	17
q95		3	3	2.7
<ne>19	m^{-3}	11.3	10.1	12.3
<ne>/nG		0.94	0.85	0.91
<Ti>	keV	8.1	8	9.1
<Te>	keV	8.9	8.8	10
Pfus	MW	500	400	700
Pnb	MW	33	33	33
Prf	MW	17	17	2
Poh	MW	1	7	1
Q		10	10	20
Pbrm	MW	26	21	34
Psyn	MW	8	8	10
Plin	MW	27	18	25
Prad	MW	61	47	70
Ploss	MW	104	87	120
Pl-h	MW	51	48	54
Pseparatrix	MW	90	75	103
beta-T	%	2.8	2.5	3.5
beta-N		2	1.8	2.2
beta-p		0.92	0.65	0.69
tauE	s	3.4	3.7	3.6
Wth	MJ	353	320	434
Wfast	MJ	34	32	41
li	H	0.84	0.84	0.77
HH98(y,2)		1	1	1
Ibs/Ip	%	16	15	17
Vloop	mV	75	75	85
tauHe/tauE		5	5	5
Zeff,average		1.72	1.66	1.69
fHe,axis	%	4.4	4.3	5.2
fHe,average	%	3.2	3.2	4.4
fBe	%	2	2	2
fAr	%	0.14	0.12	0.12

Table 6-2: Additional input parameters for plasma configuration

Confinement	HH98(y,2)	-	1
	Ion energy confinement time multiplier	-	1
	Fuel confinement time multiplier	-	2
	Alpha confinement time multiplier	-	5
	Impurities confinement time multiplier	-	5
Operating limits	Troyon G coefficient	-	3.6[Ayma01b]
	Greenwald limit multiplication factor	-	2[Ayma01b]
	H-L mode transition multiplication factor	-	0.2[Ayma01b]
	Locked modes lower density limit	$n^{19}//m^3$	2
Wall fluxes	EM radiation	Ref.	[PoSM06b, RiDi11]
	Neutron radiation	Ref.	[Kike07]
	Conductive losses	Ref.	[Iter99b]
	R-X exchange	Ref.	[Iter99b]
Pedestal-SOL	Initial divertor plasma condition	-	Incipient detachment
	Initial value of peak target heat flux	MW/m^2	10
	Pedestal scalings	Ref.	[John11]
	SOL scalings	Ref.	[AHGG03, GHGA07, PKPJ07]
Operating limits	Max external heating	MW	110
	Isotopic D-T mixture	-	50%
	NB Energy	KeV	1000
	NB Atomic Mass	-	2.5
	NB fraction over total external heating	-	0.66

The neutron deposition model for blanket modules was validated with results from combined neutronics and thermohydraulics data from FEEL-UPC study done in support of AINA development.[Sola05]

6.3 In-vessel systems: design and operating conditions

The plasma-facing components include the blanket system, the divertor system and test blanket modules. AINA thermal analyses consider only blanket divertor. Fuelling and heating systems are also considered as input for the plasma balance calculations. All in-vessel systems are cooled by the Tokamak Cooling Water System (TCWS).[Topi08]

6.3.1 The blanket modules

The blanket system includes an array of shielding blanket modules mounted on the interior wall of the vacuum vessel that absorbs radiation and particle heat fluxes from the plasma. [Topi08]

The main functions of the blanket system are: shielding to reduce heat loads and activation in the vacuum vessel and ex-vessel components; a plasma-facing surface designed for a low influx of impurities to the plasma; and limiting surfaces that define the plasma boundary during start-up and shutdown.

Each shielding blanket module is divided into two parts: the First Wall, at the plasma side, and properly the shielding block.

The First Wall has the function of protecting the shielding from the heat load and erosion coming from the plasma in the form of particles and electromagnetic waves.

It consists of beryllium plasma facing components, arranged in tiles over a surface of copper, which acts as a thermal sink, and which has coolant tubes embedded. The copper sink is supported by a steel plate, which is also cooled, and which has a joint for assembly with the shielding.

The shielding is composed by an approximately 30 cm-wide block of structural low activation steel and by coolant tubes.[Topi08] It has the function of stopping the neutronic flux and evacuate the heat load.

6.3.2 The divertor

The divertor system consists of 54 cassettes located at the bottom of the plasma chamber. The divertor system absorbs radiation and particle heat fluxes from the plasma while allowing neutral particles to be exhausted to the vacuum system. The divertor system minimizes the influx of impurities to the plasma, provides shielding to reduce heat loads and activation in the vacuum vessel and ex-vessel components, and houses an array of diagnostics.

The main functions of the divertor system are: to remove the fusion reaction ash (α-particles), unburnt fuel, and eroded particles from the reactor; to remove heat (~15 % of fusion thermal energy); to withstand a high surface heat flux of up to 15-20 MW/m^2; and to serve as a shield for the magnetic coils behind it. [Iter02]

Each divertor module is covered with tungsten tiles as plasma facing components, arranged over a copper heat sink, which has coolant tubes embedded. The copper sink is supported by a steel plate, which is also cooled.

6.3.3 The fuelling systems

The fuelling systems in ITER comprises two types of fuelling. One is the pellet injection system with a capacity of 50 Pam^3/s and the other is the gas injection system with 200 Pam^3/s. The capacity of the total fuelling rate is limited to 200 Pam^3/s.[Iter02] For pellet fuelling, almost 100 % of fuelled particles will be injected into the plasma. For gas fuelling, a large part of gases injected into the vacuum vessel will be exhausted directly through the vacuum pump.

The fuelling ratio of injected gases into the plasma against the total amount of gases injected into the vacuum vessel depends on the parameters of periphery density and scrape off plasma.

Here, 100 % of injection is assumed as an upper bound, i.e., a maximum fuelling rate is 200 Pam^3/s (~$6.5x10^{19}$ $n/m^3/s$).

6.3.4 The heating systems

The heating and current drive includes the following: Ion Synchrotron Heating and Current Drive (IC H&CD) system; Electron Synchrotron Heating and Current Drive (EC H&CD) system; Neutral Beam Heating and Current Drive (NB H&CD) system; Diagnostic Neutral Beam (DNB); and Neutral Beam Test (NBT) facility.

The maximum capacity of the neutral beam heating system is initially 33MW, located in two ports of 17.5MW each. A third port is allocated son neutral beam heating could amount up to 50MW. The capacity of the radiofrequency heating systems is 80MW in four ports. However the maximum power that can be injected in plasma is 110 MW.[Topi08] As a conservative assumption, a maximum external heating power of 130 MW will be assumed in AINA analyses.[Iter02]

6.4 Calculations framework

6.4.1 Introduction to LOPC transient studies

In the past, the loss of plasma control transients were studied for ITER with an approach based on parameter scans.[HBNS01] In this approach, a scan is done of plasma equilibrium input parameters and of the magnitude of plasma perturbations to determine the maximum fusion power during subsequent plasma transients.

The resulting figures allow estimating trends and possible relative maxima in fusion power. Thus, once decided which one is the most severe transient in terms of fusion power, the effect over wall thermal profile, specifically at divertor target, is studied.

In this chapter, two main changes are introduced for the study of LOPC transients: first, now the objective variable to determine the severity of a transient is not the maximum fusion power but the melting time at any position of poloidal section.

The second change is related to the method for finding the most severe transients. The parameter scan does not cover the full range of variation of the target heat flux in the plasma operating window. Therefore, a new method based on global optimisation constrained by the plasma operating window has been used here.

For completeness, and to check results with previous studies, a sensitivity analysis was also done.

6.4.2 Equilibrium parameters considered in this study

Initial plasma equilibrium has a strong influence on the evolution of the plasma-wall transient simulated with AINA code. Initial ion temperature, fusion power and radial profile of density are considered in these calculations. Other parameters could also be considered in future studies, like magnetic field or poloidal current.

Plasma equilibrium parameters are selected attending to uncertainties in their behaviour. The variation range must be inside the plasma operation window, meaning that values that do not produce a valid equilibrium cannot be selected.

One option to find the solution to this problem would be to map the plasma operation window in order to find those equilibria that produce the most severe condition for in-vessel elements. This way we would avoid calculating plasma transients. But this would not be correct, because during a transient, plasma evolves in a non-equilibrium state, and thus we cannot predict plasma transient states by mapping the plasma operation window. Therefore, it is necessary to study plasma transients.

6.4.3 Perturbations considered in this study

Perturbations considered are step functions that happen at the beginning of the transient. Possible variations could include starting at different simulation time, combined perturbations and progressive increase in a perturbation. However, it is assumed that step perturbations happening at the beginning of the transient will have the most severe effect from the point of view of melting time.

In these calculations, sudden changes in fuelling, in external heating or in energy confinement time are considered. Other possible perturbations could include exhaust pumping or variation in SOL particle fluxes.

a) Overfuelling: Plasma equilibrium calculation in AINA determines necessary fuelling rate. As a validity condition, this fuelling rate must be lower than the maximum ITER fuelling, otherwise plasma equilibrium is not valid. The equilibrium calculation also determines the maximum overfuelling multiplicator applicable in a simulation, and thus the severity of the subsequent transient.
b) Overheating: The maximum auxiliary heating power is limited at 130 MW by the capacity of NB and RF heating, which is determined by the possible maximum upgrade scenarios of the heating system.[Ayma01a]
   Even if the maximum power available simultaneously will be 110 MW, a total value of 130 MW will be assumed as a conservative condition.
c) Increase in confinement time: The sudden change of confinement time will simulate a change in the plasma confinement due to an unidentified cause originated by plasma physics.

6.4.4 Optimisation method

Initially, parametric analyses were done by deciding range of variation for plasma perturbations and for plasma equilibrium parameters. Then, a transient was studied for each of the points specified in the space of parameters and perturbations. Then, a figure of merit, namely fusion power, was studied to find trends and patterns that allow the estimation of where the most dangerous plasma transients are.

This approach has been substituted by one where finding the most dangerous transient is automated, and where the bounds for plasma parameters are defined by the plasma operation window.

In Figure 6-1, the optimisation algorithm is depicted in a flow chart, where the figure of merit is extracted from AINA transients result. This way, AINA transient simulation becomes the function to evaluate.

In this case, it was decided that the figure of merit to minimize would be the melting time. This way, it is possible to give information about time recovery requirements for the plasma control system.

Other figures of merit can be selected, like maximising the tritium inventory, or the thermal energy deposited in the blanket.

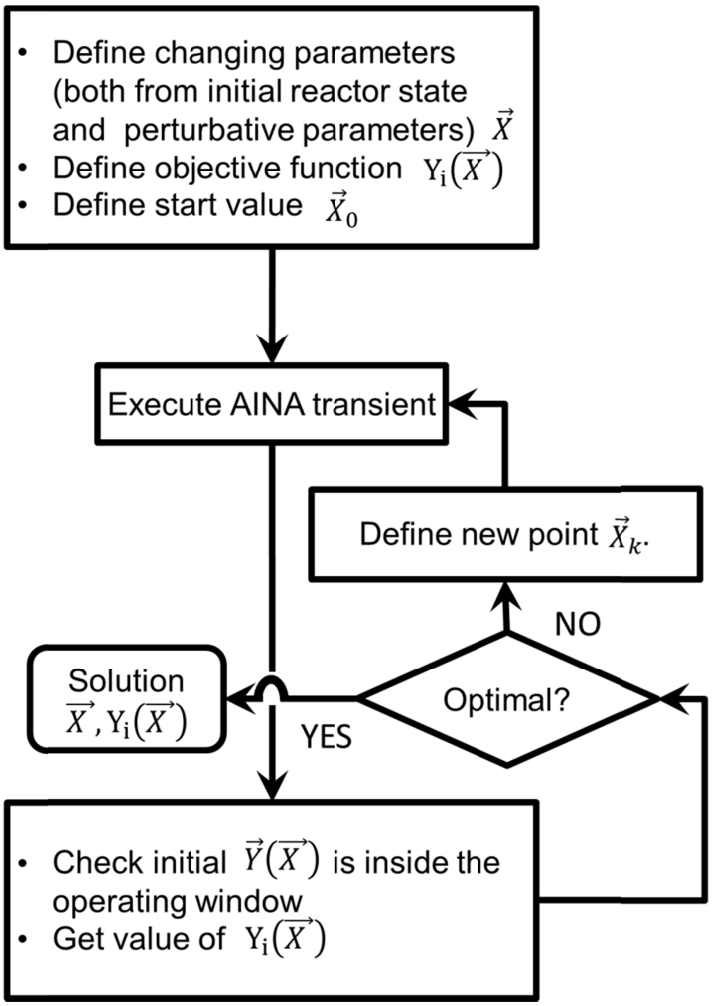

Figure 6-1: Flux diagram of the optimisation process for finding severe transients.

6.5 Safety analysis: numerical results

6.5.1 Parameter scan

The parameters considered in this study were the initial fusion power, the initial ion temperature and the pedestal fraction (over the central value) for the plasma density radial profile.

The perturbations studied were a sudden (step) increase in fuelling (overfuelling), a sudden increase in external heating (overheating) and a sudden increase in confinement time, accounting for unexpected changes in plasma physics, to cover uncertainties in knowledge of plasma transport.

Results were compared with those of GSSR. The comparison shows good agreement.

The parameter scan is reproduced for purpose of comparison with previous GSSR results.[Ayma01b] It follows the same structure shown there. Therefore, parameter scans were done for each combination of plasma equilibrium parameters and plasma perturbations. Nine parameter scans were thus done, as shown in three arrays of figures in Annex 2, starting in Figure A2-2 and ending in Figure A2-10.

6.5.2 Determination and study of reference plasma-wall transients

The parameter scans are useful to get insight into the behaviour of plasma, but to determine the reference transients, global optimisation was used, for each of the three considered perturbations, and also for a case that considers a combination of all of them. The results for the three reference scenarios are shown in Table 6-3, Table 6-4 and Table 6-5, together with the duration of transient and the final consequences for divertor.

Category	Initial plasma equilibrium			Perturbative parameters			Transient duration/final surface temperature /divertor status
	P_{FUS} (MW)	T_i (keV)	$f_{ped,n}$[6]	xOF[7]	+OH[8]	$x\tau_E$[9]	
Overfuelling	-	-	-	-	-	-	It does not melt in the range studied
Overheating	450.0	7.33	0.2	1	54.56	1	2.7s/melting
Confinement time	382.9	6.11	1.0	1	0	1.91	3.1s/melting
Combined[10]	376.7	6.12	1.0	1.80	38.46	2.41	2.0s/melting

Table 6-3: Summary of results from the optimisation process of the 400 MW inductive scenario. The most severe results for each perturbation are listed.

Category	Initial plasma equilibrium			Perturbative parameters			Transient duration/final surface temperature /divertor status
	P_{FUS} (MW)	T_i (keV)	$f_{ped,n}$	xOF	+OH	$x\tau_E$	
Overfuelling	-	-	-	-	-	-	It does not melt in the range studied
Overheating	454.5	6.19	1.0	1	37.63	1	0.7s/melting
Confinement time	518.1	5.70	0.943	1	0	2.52	2.4s/melting
Combined	476.5	5.88	1.0	1	45.84	3	3.2s/melting

Table 6-4: Summary of results from the optimisation process of the 500 MW inductive scenario. The most severe results for each perturbation are listed.

[6] Ratio of pedestal value over central value for radial density profile

[7] Overfuelling multiplier, between 1 and 3

[8] Overheating factor (additive, MW), between 0 and 150MW

[9] Energy confinement time multiplier, between 1 and 3

[10] The best value found by the optimiser until now, but of course it should be lower than overheating value, as the last is a particular case of combined perturbation

Category	Initial plasma equilibrium			Perturbative parameters			Transient duration/final surface temperature /divertor status
	P_{FUS} (MW)	T_i (keV)	$f_{ped,n}$	xOF	+OH	$x\tau_E$	
Overfuelling	-	-	-	-	-	-	It does not melt in the range studied
Overheating	679.9	9.76	1.0	1	95	1	3.3s/melting
Confinement time	674.8	6.33	1.0	1	0	2.1	2.1s/melting
Combined	700.5	6.42	1.0	1.59	44.30	2.67	1.7s/melting

Table 6-5: Summary of results from the optimisation process of the 700 MW inductive scenario. The most severe results for each perturbation are listed.

6.6 Discussion

Regarding the parameter scan, in GSSR study, plasma radial profiles were implemented with parabolic functions. Therefore, scans in radial profile are done by varying the α parameter. Currently, AINA code includes radial profile functions with pedestal. Therefore, the scan in radial profile is done by varying the pedestal height. This means that decreasing evolution of α parameter corresponds to increasing evolution of pedestal height.

In the case of fuelling rate, the X axis corresponds to fuelling rate in GSSR and to overfuelling multiplier in AINA because fuelling varies in every plasma equilibrium, and is a calculated value, while the overfuelling parameter is an input value.

The differences in results are due to the fact that AINA and SAFALY are different codes. AINA includes a more complex plasma geometry, upgraded and updated models for plasma radiation, plasma wall interaction (particles and heat), and all functions included in the plasma balance equation are integrated over the toroidal volume, as shown in Chapter 2.

The agreement is good at a qualitative level. However, some differences can have a strong influence on the results of safety analysis, for example, the scan in confinement improvement (sudden increase in confinement time). While GSSR results show a stabilisation in maximum fusion power as τ multiplier increases, for AINA calculation, maximum fusion power grows near to linearly.

Regarding optimisation, for the three reference scenarios studied, no melting happens in the case of overfuelling during short transients. Melting is likely to happen during long transients and in blanket modules rather than in the divertor. The recovery time for the plasma control system will be long in these cases.

For the rest of perturbations, very short melting times are found for divertor targets in the order of the energy confinement time.

6.7 Conclusions

After the success of new methodology for the analysis of loss of plasma control transients for Japanese DEMO, AINA code has been applied to the study of loss of plasma control transients in ITER with this methodology.

However, for the purpose of comparison with previous GSSR results, parameter scans were also done in maximum fusion power during transients taking combinations of three plasma equilibrium variables (fusion power, ion temperature and density radial profile) and three plasma perturbations (overfuelling, overheating and increase in confinement time). [Ayma01b]

With the new methodology, optimisation has been applied for finding the most severe transients from the point of view of melting time. Results with optimisation methodology show that LOPC transients have severe effects for divertor targets.

According to the results, recovery time for the plasma control system should be at least one order lower than the energy confinement time, because the lower melting times are found to be in the order of energy confinement time.

The exception is long transients where the blanket modules have time for heating up inside. However, for these cases the plasma control system will have a long time for recovery.

Chapter 7: Fusion neutron source model for the systems analysis of a tokamak power plant

7.1 Introduction

In the frame of the conceptual design activities developed under the Spanish Breeding Blanket Technology Programme TECNO FUS,[Perl09] which take as the design starting point the C model of the European Fusion Power Plant Conceptual Study,[NAGI08, NoFo03] one of the tasks was the development of a system's analysis, including a volumetric neutron generation model for a fusion plasma.

The neutron wall loading calculation for tokamaks has been investigated in the past by different works.[ChWu03] Currently, complex models which integrate CAD design and neutronics analysis of the walls with the neutron source have reached a high degree of refinement.[WFFL08]

This neutron source model can be configured with the different plasma and geometry parameters generated by the system's analysis in order to calculate results for neutron wall loading, which is useful as an input for the conceptual design and the systems analysis.

Neutron simulation has been done using Monte Carlo simulation. The problem has been restricted to the calculation of the neutron flux crossing the wall surface without considering its interaction with reactor's wall.

Following the methodology used in a previous work on breeding blanket neutronics analysis, originated from TecnoFUS program,[COSP11] a 60º sector of the toroidal geometry has been considered for the calculations.

Both neutron birth locations and flight directions are considered random variables in this model, and for each neutron the intersection point in the external toroidal surface is calculated.

The model developed in this work can calculate the poloidal wall loading angular distribution. Arbitrary plasma and wall shapes of the poloidal section can be configured.

The model has been validated with previous simulations of ITER wall neutronic poloidal profile, and a parametric study has been performed on different plasma geometries and radial profiles to check the variability of the neutronic poloidal profile.

In this chapter, a model for the neutron generation in a generic tokamak plasma and vessel geometry has been developed on the basis of Monte Carlo simulation, which can calculate the neutron wall loading poloidal distribution.

7.2 Methodology of the analysis

7.2.1 Toroidal geometry and radial profile of the neutron source

The first problem is to define a parameterizable plasma geometry. Tokamak plasma geometry has toroidal symmetry, and the poloidal section contours can be defined[ChWu03, PeRo94] as shown in Eq. 7.1.

$$R = R_0 + r\cos\left(\theta + \delta\frac{r}{a}\sin\theta\right) + \epsilon\, a\left[1 - \left(\frac{r}{a}\right)^2\right]$$
$$z = \kappa\, a \sin\theta$$

where:

R_0: major radius
a: minor radius
r: poloidal radius
θ: poloidal angle
κ: plasma elongation
ϵ: plasma triangularity

Eq. 7.1

Eq. 7.1 describes constant pressure surfaces. At these surfaces, temperatures and densities are taken as constant, and thus radial variations are established, usually with a parabolic profile, but also pedestal and internal transport barriers can be modelled easily. A possible selection of parabolic profile equations can take the form shown in Eq. 7.2.

$$Bare parabolic profile$$
$$x = x_{max}\left(1 - \left(\frac{r}{a}\right)^{\beta_x}\right)^{\alpha_x} \quad (Generic)$$
$$Parabolic profile with pedestal$$
$$x_1 = x_{ped} + (x_{max} - x_{ped})\left(1 - \left(\frac{r}{a}\right)^{\beta_x}\right)^{\alpha_x}$$
$$Parabolic profile with pedestal and ITB$$
$$x = \chi_{[0,r_{ITB}]}\left(\Delta x_{ITB} + \Delta x_{ped} + (x_{max} - \Delta x_{ITB} - \Delta x_{ped})\left(1 - \left(\frac{r}{a}\right)^{\beta_{x,1}}\right)^{\alpha_{x,1}}\right)$$
$$+\chi_{[r_{ITB},a]}\left(x_{ped} + (x_{max} - x_{ped})\left(1 - \left(\frac{r}{a}\right)^{\beta_{x,2}}\right)^{\alpha_{x,2}}\right)$$
$$\chi_{[a,b]}: step function$$

Eq. 7.2

The variable x_{max} is the value at the plasma axis. Figure 7-1 shows examples for the three cases.

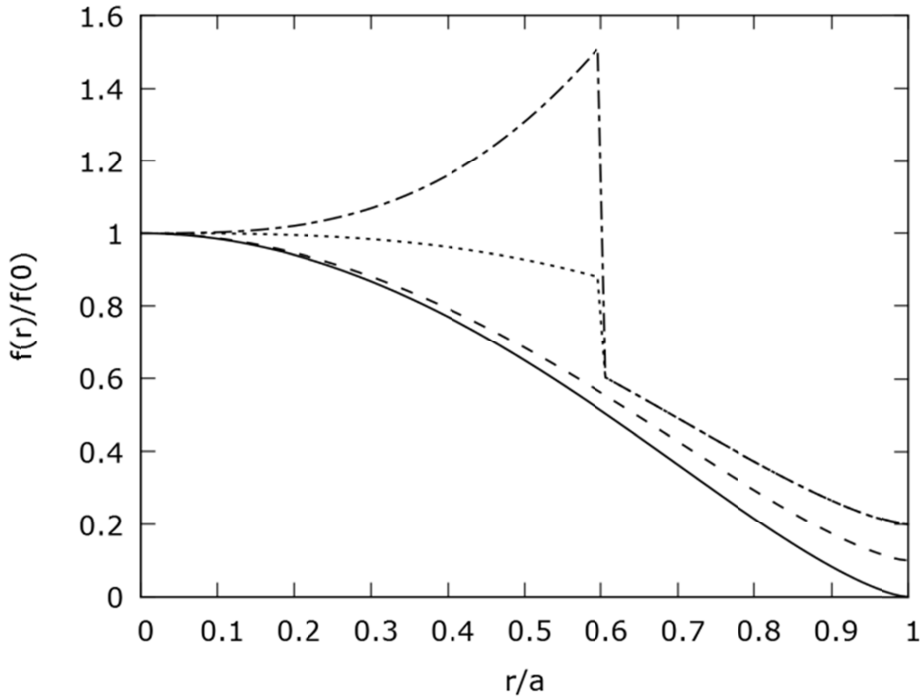

Figure 7-1: Examples of radial parabolic profiles: bare profile (continuous), profile with pedestal (dashed) and two profiles with an ITB, one of them representing a hollow core (dash-dot).

Thus, for a plasma operating in H mode and isotopic control of radial composition, we could have the profiles shown in Eq. 7.3, where ρ is the density of hidrogenic species and Ti is the ion temperature.

$$\rho_{^2H}(r) = \rho_{^2H,max}\left(1-\left(\frac{r}{a}\right)^2\right)^{\alpha_{^2H,ped}}$$
$$\rho_{^3H}(r) = \rho_{^3H,max}\left(1-\left(\frac{r}{a}\right)^2\right)^{\alpha_{^3H,ped}} \qquad \text{Eq. 7.3}$$
$$T_i(r) = T_{i,ped} + (T_{i,max} - T_{i,ped})\left(1-\left(\frac{r}{a}\right)^2\right)^{\alpha_T}$$

Once the radial profiles of ionic temperature and densities are determined, the neutron production is calculated from a known reactivity function. The resulting radial profile of the generated neutrons depends on the radial profiles of T and n. If no pedestals or ITBs are used, we can follow the method outlined by Chen,[ChWu03] to model the neutron source radial profile with a parabolic equation, with exponent $\alpha = 2\alpha_n + \gamma\alpha_T$, where it is assumed that $\langle\sigma v\rangle_{DT} \approx kT_i^{\gamma}$. Otherwise, the individual profiles must be composed as shown in Eq. 7.4.

$$\rho_n(r) = \rho_{^2H}(r)\rho_{^3H}(r)\langle\sigma v\rangle_{DT}(T_i(r))$$
$$\approx \rho_{^2H,max}\left(1-(\frac{r}{a})^2\right)^{\alpha_{^2H,ped}} \cdot \rho_{^3H,max}\left(1-\left(\frac{r}{a}\right)^2\right)^{\alpha_{^3H,ped}} \quad \text{Eq. 7.4}$$
$$\cdot\left(T_{i,ped}+(T_{i,max}-T_{i,ped})\left(1-\left(\frac{r}{a}\right)^2\right)^{\alpha_T}\right)^{\gamma(r)}$$

A comparison of both cases can be seen in Figure 7-2. The resulting neutron generation radial profiles are very similar, because the neutron generation takes place mostly at the high temperature plasma core. Therefore, the temperature pedestal at the edge can be ignored in the calculation.

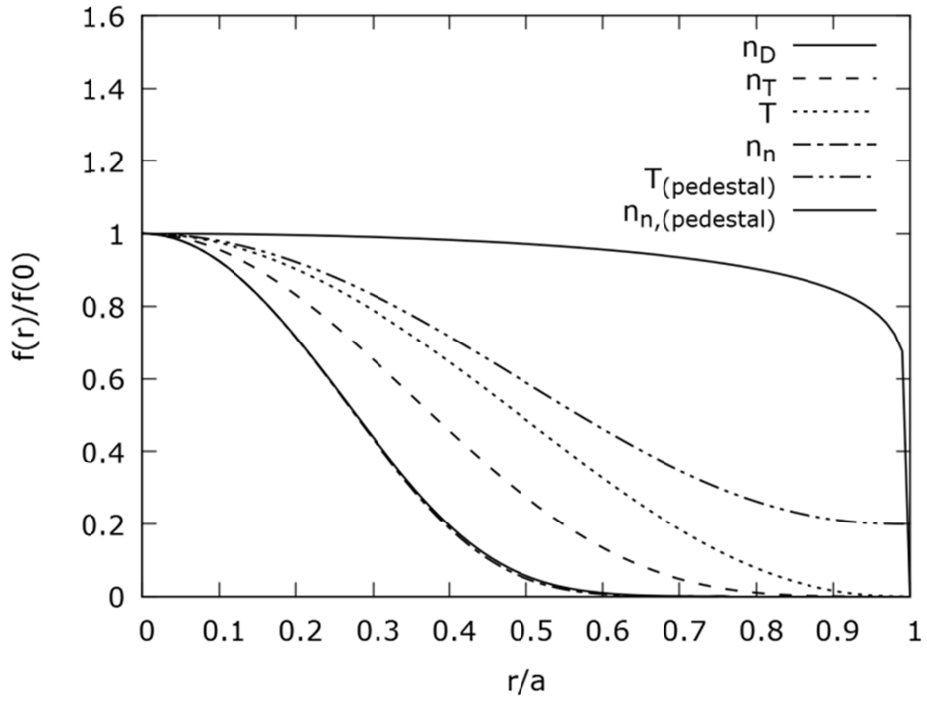

Figure 7-2: Example of normalised radial parabolic profiles, showing the resulting neutron generation profile.

If a scenario with an ITB7 is considered, the resulting neutron source radial profile is affected as shown in Figure 7-3. It can be seen how the sharp fall of the temperature stops the fusion reaction.

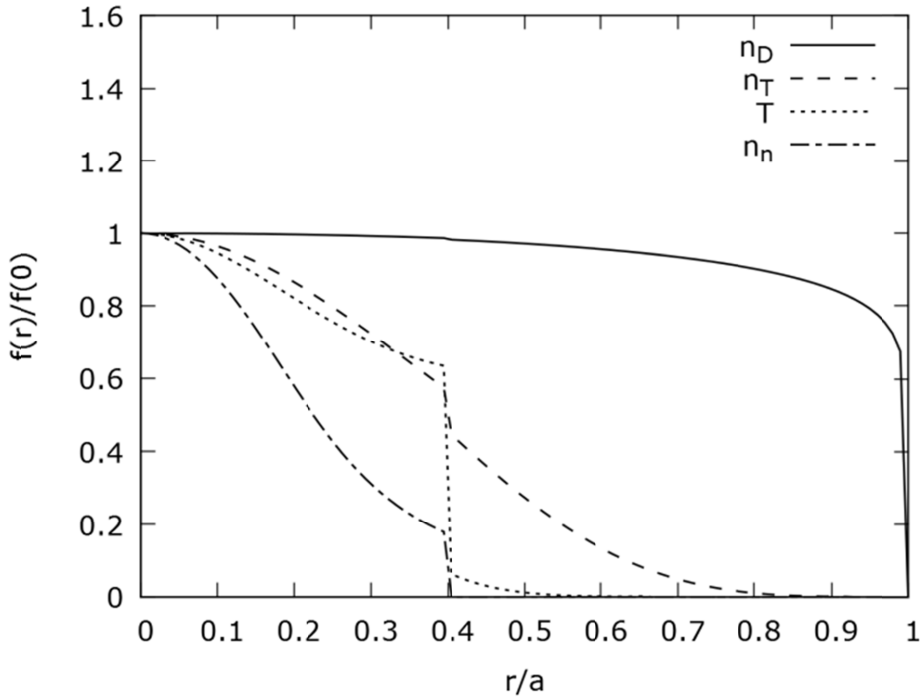

Figure 7-3: Normalised radial profiles for an ITB scenario.

7.2.2 Wall loading calculation

Neutron simulation was done using Monte Carlo methodology. The problem has been restricted to the calculation of the neutron deposition at the border of the plasma poloidal section, or at the wall surface, if geometry information is available. Interaction with reactor wall is not considered.

For the positions of the neutron birth and impact locations, a cartesian system with origin in the center of the torus, x axis crossing the plasma axis at the reference poloidal section, and y axis perpendicular to that section, was selected. The toroidal coordinates in this system are shown in Eq. 7.5.

$$x = \left(R_0 + r\cos\left(\theta + \delta\frac{r}{a}\sin\theta\right) + \epsilon a\left[1 - \left(\frac{r}{a}\right)^2\right]\right)\cos\phi$$
$$y = \left(R_0 + r\cos\left(\theta + \delta\frac{r}{a}\sin\theta\right) + \epsilon a\left[1 - \left(\frac{r}{a}\right)^2\right]\right)\sin\phi \qquad \text{Eq. 7.5}$$
$$z = \kappa r\sin\theta$$
$$\phi: \text{toroidal angle}$$

For each birth location, the flight direction is obtained from a uniform spherical distribution obtained by supposing the coordinates are normally distributed.[Mars72, Merv59] The colision point for each neutron is calculated as the intersection of the straight path

with the external border of the plasma or with the wall surface. When for the impact points only the external plasma surface is used, they can be described as in Eq. 7.6.

$$\text{birth location}$$

$$r_{birth} = R_0 + \rho_{birth}\cos(\theta_{birth} + \delta\sin\theta_{birth}) + \epsilon a\left[1 - \left(\frac{\rho_{birth}}{a}\right)^2\right]$$

$$x_{birth} = r_{birth}\cos\phi_{birth}$$

$$y_{birth} = r_{birth}\sin\phi_{birth}$$

$$z_{birth} = \kappa\rho_{birth}\sin\theta_{birth}$$

$$0 \leqslant \rho_{birth} \leqslant a, 0 \leqslant \theta_{birth} \leqslant 2\pi, -\pi/6 \leqslant \phi \leqslant \pi/6 \qquad \text{Eq. 7.6}$$

$$\text{impact location}$$

$$x_{impact} = \left(R_0 + a\cos(\theta_{impact} + \delta\sin\theta)_{impact}\right)\cos\phi_{impact}$$

$$y_{impact} = \left(R_0 + a\cos(\theta_{impact} + \delta\sin\theta_{impact})\right)\sin\phi_{impact}$$

$$z_{impact} = \kappa a\sin\theta_{impact}$$

To find the collision point, the nearest intersection of the flight path with the outer surface is calculated in the cartesian system, as shown in Eq. 7.7.

$$x_{impact} = x_{birth} + L_{path}\cos\alpha_x$$

$$y_{impact} = y_{birth} + L_{path}\cos\alpha_y \qquad \text{Eq. 7.7}$$

$$z_{impact} = z_{birth} + L_{path}\cos\alpha_z$$

The system of equations in Eq. 7.7 has four unknowns, the missing fourth equation necessary to solve it would be the geometric restriction of the wall surface. The solution is found numerically by varying the path length from the birth location until it touches the wall surface.

7.3 Numerical results

The previously described algorithms were coded in a c++ program, running in a desktop PC machine, and using up to 1,000,000 runs for each simulation.

As a validation, ITER configuration was checked against available ITER neutron wall loading data.[Iter02] It was found that the best fit for simulation results with this plasma geometry equations is obtained using a plasma shift value of -0.55. The calculated neutron flux poloidal distribution was converted to MW/m2 corresponding to the 400MW ITER scenario.

Figure 7-4 shows the comparison between both simulations. ITER1 data represents simulation data available from ITER project,[Iter02] which is very similar to that found in a recent benchmarking work.[WFFL08] ITER2 data represents results from a simulation with the model developed in this work. Part of the differences are due to the geometry used in calculations.

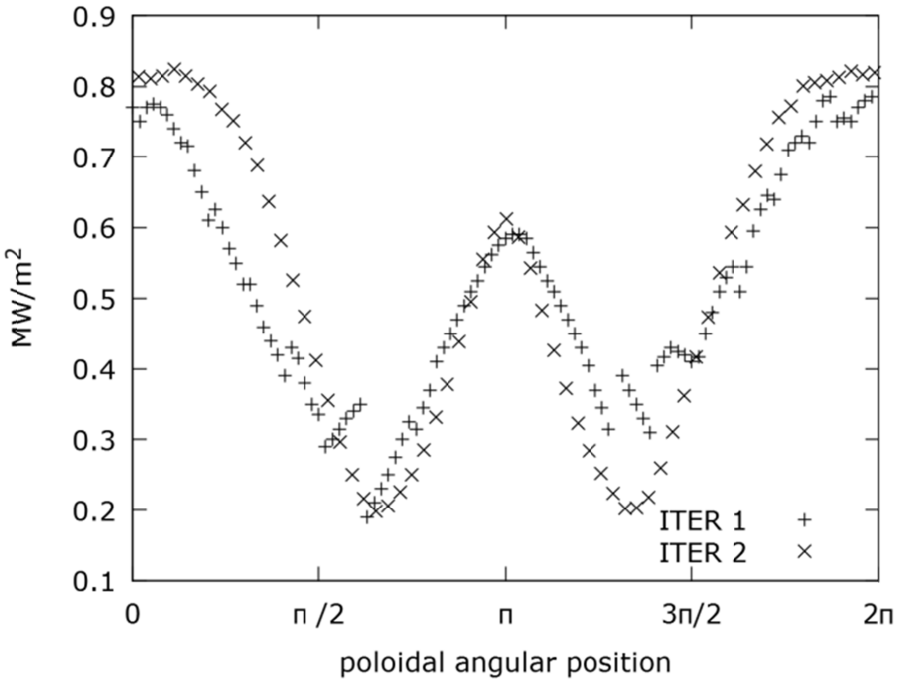

Figure 7-4: Neutron flux distribution for ITER 400MW scenario.

The effect of the geometry parameters on the peaking factor and minimal wall loading has also been checked.. The methodology used was a sensitivity analysis around the plasma geometry parameters used to model ITER scenario, which are R=6.2m, a=2.0m, k=1.7, d=0.33 and e=-0.55. This means that, when a parameter changes, the

rest of the parameters remain unchanged in their reference values. In figures from Figure 7-5 to Figure 7-8, the effects of the aspect ratio, elongation, triangularity and plasma shift on peaking factor and minimum factor are shown.

Peaking factor was selected because it can show the quality of the plasma configuration from the point of view of blanket design. Minimum factor was selected because it can show the variation in the flux affecting the divertor region.

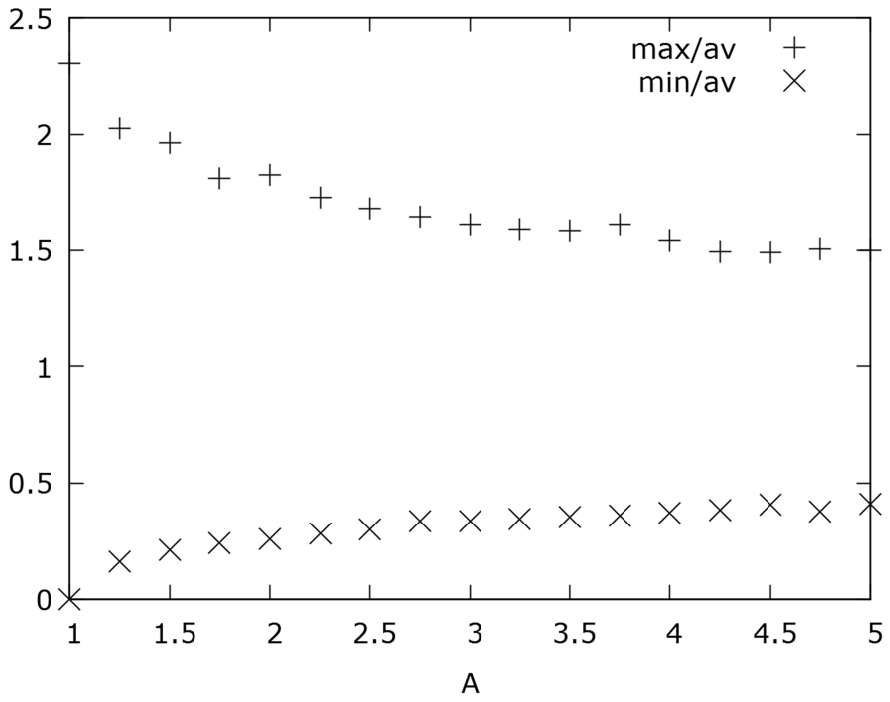

Figure 7-5: Variation of peaking factor and minimum factor of neutron wall loading with the aspect ratio.

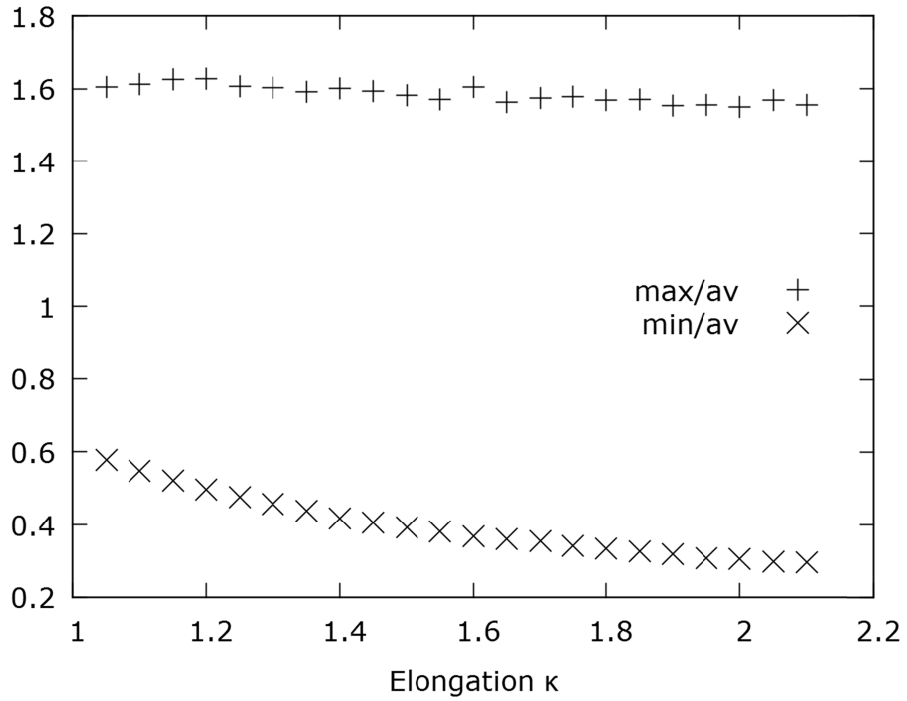

Figure 7-6: Variation of peaking factor and minimum factor of neutron wall loading with the elongation.

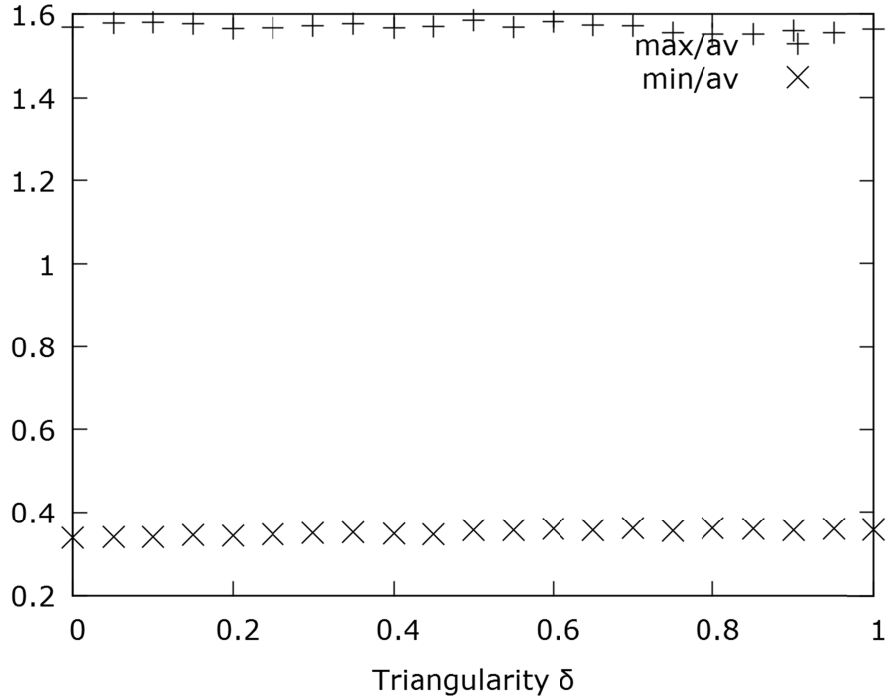

Figure 7-7: Variation of peaking factor and minimum factor of neutron wall loading with the triangularity.

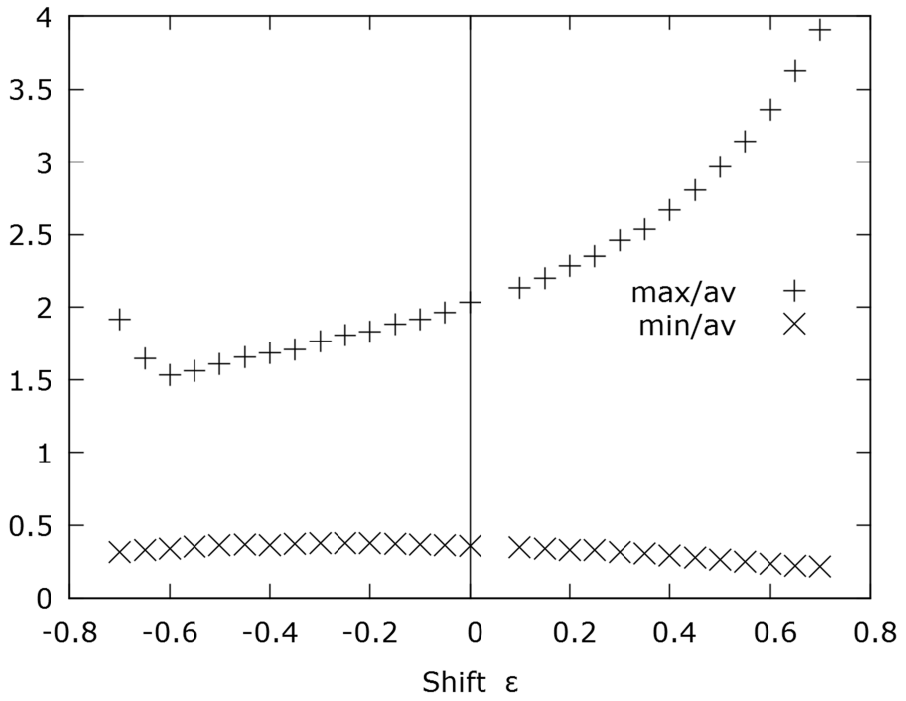

Figure 7-8: Variation of peaking factor and minimum factor of neutron wall loading with the plasma shift.

Low aspect ratio designs have a higher peaking factor, but the increment is moderate. Elongation and triangularity have virtually no effect on the peaking factor. The plasma shift, however, shows a strong influence on the peaking factor.

Plasma shift causes a large increase in the maximum wall loading as it moves the plasma core towards the wall. As it could be expected, the maximum wall loading has a relative minimum for a certain value of ε.

Regarding the minimum factor, an increase in the elongation and a decrease in the aspect ratio seem to have the most relevant effect to minimize it. Triangularity and shift have little effect. From the previous figures from Figure 7-5 to Figure 7-8, it can be seen also that ITER design succeeds in having a low peaking factor.

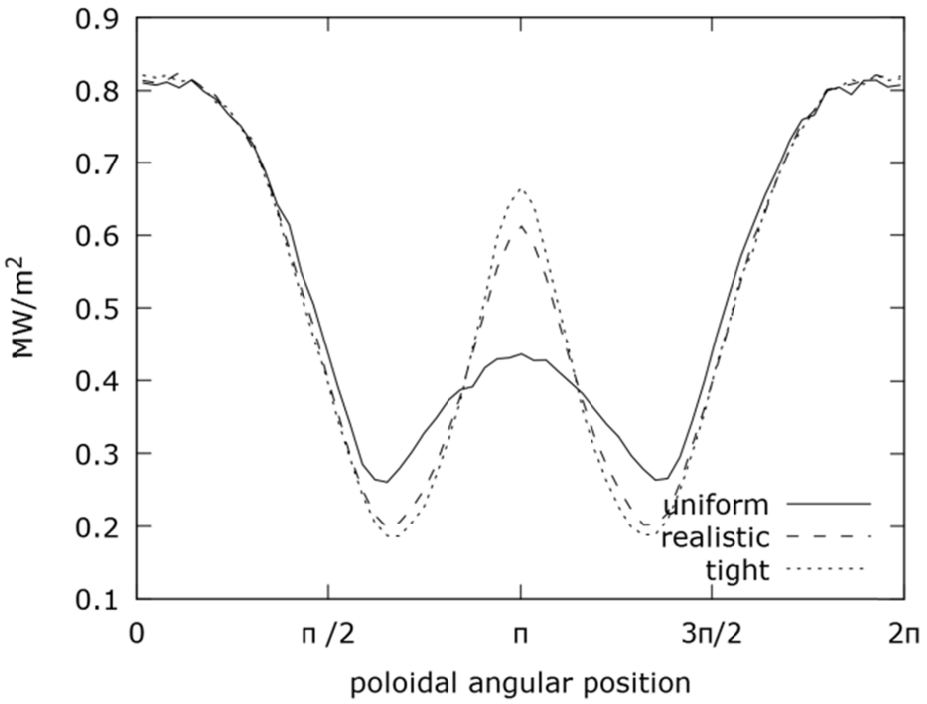

Figure 7-9: Neutron wall loading poloidal profiles corresponding to different neutron source radial profiles.

The effect of the neutron source radial profile is shown in Figure 7-9. In general, neutrons are mainly produced near the hot plasma center, and this effect causes little variation in the final neutron wall loading. However, three distributions have been tested to show the effect. One of them corresponds to a parabolic profile with a high value of α. Another corresponds to a uniform distribution. The realistic one corresponds to an intermediate value of α which in fact is the one that fits better with the ITER wall loading data, and was used for the rest of the calculations.

7.4 Conclusions

A neutron source model has been developed which can calculate the fusion neutron source for arbitrary tokamak and plasma poloidal shapes using a 3-D Monte Carlo algorithm. Results have been compared with simulations from other codes for the ITER 400 MW scenario.

Plasma density and temperature radial profiles have been characterised by variations of parabolic profiles which can represent an edge pedestal and internal transport barriers. The neutron generation radial profile has been characterised with the previous density and temperature profiles. Two examples have been shown, one corresponding to an ITER-like H-mode scenario, and the other to an advanced scenario with an ITB, which has been characterised from a previous work.[Yama09]

The effect of different plasma geometry parameters in the wall loading has been checked. Low aspect ratio designs increase the difference between maximum and minimum of wall loading. An increase in elongation maintains constant the maximum wall loading while decreasing the minimum. Triangularity variation does not affect significantly the wall loading poloidal profile. Plasma shift raises greatly the maximum wall loading as it moves the plasma core towards the wall. Therefore, the maximum wall loading has a relative minimum for a certain value of ε. Plasma shift has a small influence on the minimum wall loading in comparison.

The developed model has the purpose of serving as a tool for flexible, parametric studies, and can be coupled with other codes for systems analysis and conceptual design activities.

Chapter 8: Summary and conclusions

8.1 Conclusions

Safety in nuclear devices is of the outmost importance, especially in regards to the acceptance of the public. The concept of nuclear fusion by magnetic confinement shows some characteristics that make it safe against runaway accidents like Fukushima or Chernobyl, due to the small amount of fuel and to the inherent instability of the burning process. Therefore, an uncontrolled power excursion that induces significant radiological consequences is very unlikely.

Besides, the activity does not generate long term activated residues. Safety studies generally focus on minimising the inventory of tritium, radioactive dust and corrosion activated products that can be released during an accident.

In the context of safety studies for ITER and DEMO devices, AINA code is used for the calculation of plasma-wall transients and its consequences for in-vessel components. It is a very small area of safety studies, but to develop this work a complex code is necessary.

The work of this thesis has consisted basically on the development of AINA code, and the safety studies performed with the code. Additionally, systems studies were performed in the frame of Tecno_FUS program and also as a contribution to the development of a systems code.

The work has not been sequential. In fact there was a lot of feedback, as new models and understanding were developed. Also several small codes were developed in support of AINA calculations.

There is no doubt that the most important block of work done in this thesis was the development of AINA code. It involved the implementation of many different numerical, physical and engineering models, in a simple enough way, sometimes with scalings derived from other, more specialized codes and with a higher degree of detail.

The main motivation for developing a new code was a revision of previous results of LOPC analysis with AINA in 2007, done at the request of request of ITER Safety, because they detected some strange results. The subsequent validation activity of former AINA code showed some problems in the old fortran code that were very difficult to solve just by adding small changes. Therefore, a re-engineering activity started that eventually gave birth to a new C++ code.

The development of a scientific code implies the use of a lot of different skills. It is necessary to know about coding, about algorithms, and about the field of research. This is true for every small scientific code, but in the case of AINA, which is composed of about 15,000 lines of C++ code, and of many models accounting for very complex phenomena, it is a very poor description of the content of the work.

Regarding coding, it was necessary to establish a development framework, comprising tools, activities, and skills.

- A design activity was setup, comprising requirements definition, search and study of models; code structure design; and mockup testing.
- Coding activity was based on object oriented programming in C++ and use of *Design by Contract* checking code everywhere in the code.
- Debugging activity, including number of fault, date of occurrence, time used to solve it and other relevant data, was registered to check reliability growing.

Regarding algorithms, the code was divided in four different blocks:

- Structural code, comprising interface, input and output of data, and parts of the code executing the main flux diagram.
- Numerical models, comprising numerical algorithms used during the simulation.
- Physical models, comprising the plasma core models, the pedestal-SOL models and the erosion models.

Regarding the field of research, the development of AINA code took years of study, and still the activity continues.

The conclusion is that a scientific code reflects the scientific knowledge of its developer or developers. In the case of AINA code, which is the main outcome of this thesis, it reflects the knowledge that I learned during the last eight years from this marvellous congregation of skilled geniuses that compose the world of fusion research.

One of the purposes of safety studies with AINA code is to offer confidence about the behaviour of plasma in off-normal transients. It is very important then to assure the conservativeness of results. This is particularly difficult when it comes to plasma physics because of the uncertainties remaining.

The methodology for assuring conservativeness in relation to plasma has been the expansion of the limits of the operation window, the range where the plasma is stable. This way, it is assured that the discharge will last more time and thus the melting risk for in-vessel components is increased.

The calculation unit of AINA work is a plasma transient. To calculate it, an equilibrium configuration is provided, and also a perturbation, which will consist in a plasma perturbation or a thermohydraulic accident. The result is the evolution of plasma variables, and also of temperatures of in-vessel components.

To cover the uncertainties of plasma behaviour, many different transients are analysed. In previous studies it was done through parametric scans, but now the study is performed by optimisation. The optimisation algorithm decides the next transient on the basis of results of a previous analysed transient. This methodology is very similar to that used in systems studies, and is an example of the synergies that both activities had during this thesis.

Due to the delay in having access to PROCESS code, systems study activity was started at UPC-FEEL in the frame of Tecno_FUS research programme. A requirements study showed that AINA code models could be used as the core of a future systems analysis, and thus several studies were done to promote this task.

Simple 0D plasma equilibrium equations were identified as suitable for the plasma core equations, and several simple models for engineering systems were developed and integrated in Scilab, producing results such as a map of plasma operation window and results for plant efficiency calculations.

In addition, a simple Montecarlo code was developed for calculation of neutron wall loading for varying toroidal geometries and plasma pressure radial profiles. The purpose was to obtain wall loadings in a fast way for different reactor designs. Results of this code were compared with ITER wall loading results with acceptable agreement.

The development of systems studies in the frame of this thesis came from the fact that AINA code has many similarities with a fusion systems code. Both are complex codes with many models implemented in a simplified way to minimize the computational effort of calculations.

In fact, future safety studies could take models currently implemented in systems analysis to study new cases including variables like magnetic field and plasma current variation, that can have a strong influence on the development of a plasma transient.
A systems study with PROCESS code was developed at CCFE Culham, where a python script was developed to automate the calculations with PROCESS code. The results were also interesting to acquire more insight into the systems study area.

The python script developed for PROCESS group was based on an Excel macro developed for automation of AINA execution. This kind of productivity code is of outmost importance when developing parametric studies with codes like AINA or PROCESS, because they allow the computer to run a long series of simulations autonomously.

AINA code is used in a context of high uncertainty about plasma physics and also about the final engineering design of in-vessel components. The purpose of its use is to obtain conservative results that can be used in the context of accident sequence analysis or, generally speaking, to provide useful results for safety or conceptual design activities.

Systems studies are also being explored in relation to AINA code because both areas of research have synergies that can be used to improve the code and the results.

The study of two simultaneous perturbations in the development of a plasma transient was not demanded by ITER, but served to the purpose of exploring new methodologies for finding answers in relation to the study of plasma transients.

The results showed that, if a transient is considered where the plasma evolves in quasi-static equilibrium, then it is possible to predict in a relatively simple way the characteristics of the transient just knowing the initial state and the characteristics of the perturbations.

Even if the application of this study is rather limited, it served to the purpose of exploring a new methodology of work, and to get insight in the behavior of a 0D plasma transient inside the operation window.

A new study of the Passive Plasma Termination for Beryllium Evaporation was done in 2013-2014 with the new AINA code. This study was the first task of this thesis

work in 2008. Initially it consisted of developing a new erosion model for the existing AINA code and to apply the new code to the study of the ITER safety case "Passive plasma termination for beryllium evaporation".

The task included the study of the reference case and also a sensitivity analysis on some parameters that showed uncertainty. The results were not conclusive about the possibility of melting of beryllium First Wall before passive shutdown, but this is not relevant for safety, just for the protection of investment. What the results showed clearly is that, attending to AINA simulations, plasma discharge would end passively.

This time, a Matlab code for the calculation of view factors between faces of different in-vessel components, including divertor, was developed. The code can calculate view factors for different toroidal geometries and with arbitrary degree of detail.

With the new configuration and with the new AINA code, the study was repeated, and was able to show melting at some points of the First Wall before the end of the discharge. Again, due to the uncertainties of the calculation, and to the fact that plasma discharge will end passively in any case, these results are not relevant from the point of view of safety, just from the point of view of investment protection.

For 2014, AINA safety studies were demanded for the conceptual design activity of a Japanese DEMO reactor. The objective was to give an estimate for the plasma control system recovery time in the case of a malfunction followed by a plasma transient or by a thermohydraulic accident like an ex-vessel LOCA.

Therefore, a new version of AINA code was developed for safety studies of this Japanese DEMO design. This version included a thermal model for WCPB (water cooled pebble bed) breeding blanket and also for divertor. A new model for plasma, including an integrated pedestal-SOL model, [AHGG03, GHGA07, PKPJ07, John11] based on parametric equations obtained from simulations with SOLPS code, was also included. This model will hopefully allow to make a better estimation of the evolution of the peak heat fluxes over targets. Other models were also changed, like the erosion and impurity transport models.

Of course, there are big uncertainties about these models, but at least a systematic approach was established to implement new improvements in the future, based on parametrisations of results from specialised codes.

During this work, a new approach to the analysis of plasma transients was developed. The new approach is based on the use of global optimisation of plasma

transients in the plasma operating window to find the most severe ones from the point of view of a figure of merit that we are interested in.

In our case, what was demanded was the melting time of the in-vessel components. Therefore, optimisation was done for this output variable considering a range of plasma equilibrium variables and plasma perturbations.

This is clearly an improvement upon previous work, which proceeded by parameter scanning, and which uses a very limited set of samples.

A new methodology has been developed that is clearly better than the previous one. In the past, parametric scans were performed for giving an estimation of the most severe transients. These transients were studied in detail later to extract insight for safety studies.

This had several problems:

First, the parametric scan calculations were only performed for plasma transient, while keeping a static wall. This was done to save time and computational power.

This effect produced very high values of maximum fusion power, which would not be possible if the transient calculations stopped after melting.

Now, calculations always include the thermal equilibrium at the Wall, and therefore the maximum fusion power reached is lower than before.

Besides, the selection of a figure of merit was not optimal. In previous studies, fusion power was taken to select the most severe transients, but this is only true if we consider blankets, where power deposition comes mainly from neutronic flux.

However, in this study the objective was to find the lowest melting temperature transient. These transients are located at the divertor, because the operating conditions of targets make them very vulnerable to changes in plasma regime.

Because of that, fusion power is not the best figure of merit for estimating transients with low melting time. Peak heat flux at target could be a good candidate, but the maximum magnitude reached during a transient is not necessarily related with the duration of this transient, because it can decrease to rise later. Therefore, the final time to melting was taken as figure of merit.

Additionally, objective transients were decided based on expert criterion from the results of the parametric scan. Because of the non-linear nature of the plasma balance equations, with values for the derivatives that can vary very sharply, the estimation of the most severe transient could be inaccurate.

Therefore, a non-linear global optimisation algorithm (basing hopping) has been implemented, bounded by the operation window of plasma. This algorithm uses a figure of merit taken from AINA code output as optimising function.

This way, it is possible to argue that the solution obtained is the most severe in the range of analysis, which should be decided by attending to the uncertainties we attribute to plasma equilibrium and to the magnitude of plasma perturbations.

The final study was the application of the methodology developed for Japanese DEMO safety studies to the ITER case of "Loss of Plasma Control Transients". This case was not studied again since the validation study done in 2009 for request of ITER Safety, because the approach for solving it was not found good enough. Now, the new methodology was applied to this case and yielded different results. Even if they could be improved on in the future, the most important step is to establish a systematic approach for finding the most severe cases of these plasma-wall transients.

8.2 Summary

8.2.1 The following codes have been developed during this thesis:

- AINA code, a safety code for the analysis of plasma-wall transients in nuclear fusion reactors of tokamak type. It is composed of about 15,000 lines of C++ code, and the main features are listed in summary of Chapter 2. The following versions were developed in the frame of this thesis:
  - ITER version
  - Japanese DEMO version
- SimSched, simulation scheduler, is an Excel macro for automating calculations with AINA code. It allows making large series of simulations without supervision, increasing productivity.
- Code in Matlab for calculation of view factors of arbitrary toroidal geometries, useful for configuring AINA code. This code was developed by a graduate student under my supervision.
- Montecarlo code for the calculation of neutron wall loading from a plasma source.
- Python script for parametric studies with PROCESS code.
- Python script for optimisation studies with AINA code.
- Scilab code for calculation of systems studies.

8.2.2 The following studies were done:

1. The development of the new AINA code was started in the frame of a contract between FEEL-UPC and ITER for the development of a Quality plan for AINA. It turns out that, after an unsuccessful process of validations of the previous code, the result was a new code.
2. The following safety studies have been performed in the frame of different research contracts as mentioned in the framework:
   - Study of passive plasma termination for beryllium evaporation during and ex-vessel LOCA transient in ITER
   - Study of Loss of Plasma Control transients in ITER
   - Safety studies for Japanese DEMO, considering plasma perturbations or thermohydraulic accidents and assuming loss of plasma control.
3. The following developments have been done in the frame of Tecno_FUS program:

- Parametric studies with PROCESS code.
- Study of neutron wall loading of a tokamak plasma for arbitrary geometry.

8.2.3 The following innovations were produced by this thesis:

Regarding the passive plasma termination for beryllium evaporation case, the sensitivity study has shown that beryllium can melt.

Regarding LOPC studies, it has been shown that parametric scan method is not appropriate to find the most severe plasma transients. An optimisation method has been proposed to substitute it. Besides, optimisation is done over the melting time instead of the fusion power used in previous studies.

Regarding Japanese DEMO safety studies, the results of this work are that AINA project has been consolidated, and methodology for safety studies has been improved. The result of this research is useful for Japanese DEMO research program, as it gives information about the recovery time for plasma control system.

Regarding Tecno_FUS research program, the results consolidate the path towards a new systems code, where physics and many engineering models are already developed, and only need integration and validation.

Regarding AINA project, this work represents an important consolidation of this research line.

References

[AERG92] A. Sykes, E. Del Bosco, R.J. Colchin, G. Cunningham, R. Duck, T. Edlington, D.H.J. Goodall, M.P. Gryaznevich, J. Holt, J. Hugill, J. Li, et al.: First results from the START experiment, Nucl. Fusion, 32(4), 694–699, 1992.

[AHGG03] A.S. Kukushkin, H.D. Pacher, G.W. Pacher, G. Janeschitz, D. Coster, A. Loarte and D. Reiter: Scaling laws for edge plasma parameters in ITER from two-dimensional edge modelling, Nucl. Fusion, 43(8), 716–723, 2003.

[AJDU01] Albajar Viñas, F., Johner, J., Dies Llovera, J., Universitat Politècnica de Catalunya. and Departament de Física i Enginyeria Nuclear.: Radiation transport modelling in a tokamak plasma application to performance prediction and design of future machines, [online] Available from: http://www.tdx.cat/TDX-0114104-103202/, 2001.

[AlJG01] Albajar, F., Johner, J. and Granata, G.: Improved calculation of synchrotron radiation losses in realistic tokamak plasmas, Nucl. Fusion, 41(6), 665, 2001.

[Aman96] Amano, T.: Passive shut-down of ITER plasma by Be evaporation, National Institute for Fusion Science, Nagoya., 1996.

[Ayma01a] Aymar, R.: Generic Site Safety Report, final version., International Atomic Energy Agency. Vienna. ITER Joint Central Team, Garching., 2001.

[Ayma01b] Aymar, R.: Generic Site Safety Report, final version., International Atomic Energy Agency. Vienna. ITER Joint Central Team, Garching., 2001.

[Bart00] Bartels, H. .: Shutdown temperature due to Be evaporation from FW for ITER FEAT, ITER Garching Joint Work Site., 2000.

[BEHK11] Barabash, V., Eaton, R., Hirai, T., Kupriyanov, I., Nikolaev, G., Wang, Z., Liu, X., Roedig, M. and Linke, J.: Summary of beryllium qualification activity for ITER first-wall applications, Phys. Scr., 2011(T145), 014007, 2011.

[Beth39] Bethe, H. A.: Energy Production in Stars, Phys. Rev., 55(5), 434–456, doi:10.1103/PhysRev.55.434, 1939.

[Bohd84] Bohdansky, J.: A universal relation for the sputtering yield of monatomic solids at normal ion incidence, NIMB Nucl. Inst Methods Phys. Res. B, 2(1), 587–591, 1984.

[ChWu03] Chen Yi-xue and Wu Yi-can: Effect of Fusion Neutron Source Numerical Models on Neutron Wall Loading in a D-D Tokamak Device, Plasma Sci. Technol., 5(2), 1749–1754, 2003.

[CMDG00] Cook, I., Marbach, G., Di Pace, L., Girard, C., Rocco, P. and Taylor, N. P.: Results, conclusions, and implications of the SEAFP-2 programme, Fusion Eng. Des., 51–52, 409–417, doi:10.1016/S0920-3796(00)00271-4, 2000.

[COSP11] Catalán, J. P., Ogando, F., Sanz, J., Palermo, I., Veredas, G., Gómez-Ros, J. M., Sedano, L. and Porto Portugal 20100927-20101001: Neutronic analysis of a dual He/LiPb coolant breeding blanket for DEMO, FUSION Fusion Eng. Des., 86(9-11), 2293–2296, 2011.

[DaDI00] Dapena, M., Dies, J. and Izquierdo, J.: Estudios de seguridad deterministas de ITER. Contribución al desarrollo del código SAFALY. UPC Research Report, (2007)., n.d.

[DBKS05] Doerner, R. P., Baldwin, M. J., Krasheninnikov, S. I. and Schmid, K.: High temperature erosion of beryllium, J. Nucl. Mater., 337(1), 877, 2005.

[DGLM93] Denne-Hinnov, B., Giannella, R., Lauro-Taroni, L., Magyar, G., Mattioli, M. and Pasini, D.: Evidence of an edge impurity transport barrier in JET L-mode plasmas, in Europhysics Conference Abstracts, vol. 17C, pp. I–55–I–58, Lisboa., 1993.

[DiRB10a] Dies, J., Rivas, J. C. and Bargallo, E.: AINA safety code, v2.0 – Volume 1: Quality Assurance Project Memory and Team Process Description., 2010.

[DiRB10b] Dies, J., Rivas, J. C. and Bargallo, E.: AINA safety code, v2.0 – Volume 2: Code Description., 2010.

[DRBD10a] Dies, J., Rivas, J. C., Bargallo, E., Dapena, M., Izquierdo, J. and Garcia, J.: AINA safety code, v2.0 – Volume 3: Code Assessment., 2010.

[DRBD10b] Dies, J., Rivas, J. C., Bargallo, E., Dapena, M., Izquierdo, J. and Garcia, J.: AINA safety code, v2.0 – Volume 4: Code Manuals., 2010.

[Elgu10] El-Guebaly, L. A.: Fifty Years of Magnetic Fusion Research (1958–2008): Brief Historical Overview and Discussion of Future Trends, Energies, 3(6), 1067–1086, doi:10.3390/en30601067, 2010.

[Ener58] Energy, I. C. on the P. U. of A.: Proceedings of the second United Nations International Conference on the peaceful uses of atomic energy, held in Geneva, 1 September-13 September, 1958, United Nations. [online] Available from: http://ci.nii.ac.jp/ncid/BA08435791 (Accessed 10 May 2015), 1958.

[Fabb14] Fabbri, M.: Neutronics analysis of WCPB blanket, FEEL-UPC., 2014.

[Frei07] Freidberg, J. P.: Plasma Physics and Fusion Energy, Cambridge University Press., 2007.

[FRHS84] F Troyon, R Gruber, H Saurenmann, S Semenzato and S Succi: MHD-Limits to Plasma Confinement, Plasma Phys. Control. Fusion, 26(1A), 209–215, 1984.

[FSBC01] Federici, G., Skinner, C. H., Brooks, J. N., Coad, J. P., Grisolia, C., Haasz, A. A., Hassanein, A., Philipps, V., C.S. Pitcher, Roth, J., Wampler, W. R., et al.: Plasma-material interactions in current tokamaks and their implications for next step fusion reactors, Nucl. Fusion, 41(12), 1967, 2001.

[FZZZ09] Feng, K. M., Zhang, G. S., Zheng, G. Y., Zhao, Z., Yuan, T., Li, Z. Q., Sheng, G. Z. and Pan, C. H.: Conceptual design study of fusion DEMO plant at SWIP, Fusion Eng. Des., 84(12), 2109–2113, doi:10.1016/j.fusengdes.2009.01.104, 2009.

[GABC07] Glugla, M., Antipenkov, A., Beloglazov, S., Caldwell-Nichols, C., Cristescu, I. R., Cristescu, I., Day, C., Doerr, L., Girard, J.-P. and Tada, E.: The ITER tritium systems, Fusion Eng. Des., 82(5–14), 472–487, doi:10.1016/j.fusengdes.2007.02.025, 2007.

[GaER95] Garcia-Rosales, C., Eckstein, W. and Roth, J.: Revised formulae for sputtering data, J. Nucl. Mater., 218(1), 8, 1995.

[GCMS07] Gulden, W., Ciattaglia, S., Massaut, V. and Sardain, P.: Main safety issues at the transition from ITER to fusion power plants, Nucl. Fusion, 47(9), 1391, doi:10.1088/0029-5515/47/9/C01, 2007.

[GHGA07] G.W. Pacher, H.D. Pacher, G. Janeschitz, A.S. Kukushkin, V. Kotov and D. Reiter: Modelling of DEMO core plasma consistent with SOL/divertor simulations for long-pulse scenarios with impurity seeding, Nucl. Fusion, 47(5), 469–478, 2007.

[GoRu95] Goldston, R. J. and Rutherford, P. H.: Introduction to plasma physics, Institute of Physics Pub., Bristol, UK; Philadelphia., 1995.

[GrRu58] Grad, H. and Rubin, H.: Hydromagnetic equilibria and force-free fields, J. Nucl. Energy 1954, 7(3), 284–285, 1958.

[GuRC00] Gulden, W., Raeder, J. and Cook, I.: SEAFP and SEAL: safety and environmental aspects, Fusion Eng. Des., 51–52, 429–434, doi:10.1016/S0920-3796(00)00291-X, 2000.

[HASN14] Hoshino K., Asakura N., Shimizu K., Nakano T. and Takizuka T.: The influence of the radial particle transport on the divertor plasma detachment, J Nucl Mater J. Nucl. Mater., 2014.

[HBNS01] Honda, T., Bartels, H.-W., Neyatani, Y., Shimada, M. and Sartori, R.: Safety-related plasma events for ITER-FEAT, Fusion Eng. Des., 58–59, 1043–1046, doi:10.1016/S0920-3796(01)00545-2, 2001.

[HBUS97a] Honda, T., Bartels, H.-W., Uckan, N. A., Seki, Y. and Okazaki, T.: Development of Safety Assessment Method for Plasma Anomaly Events in Fusion Reactors, J. Fusion Energy, 16(1-2), 175–179, doi:10.1023/A:1022593803350, 1997.

[HBUS97b] Honda, T., Bartels, H. W., Uckan, N. A., Seki, Y. and Okazaki, T.: Development of time dependent safety analysis code for plasma anomaly events in fusion reactors, J. Nucl. Sci. Technol., 34(3), 229–239, 1997.

[HKAN99] H. Takenaga, K. Nagashima, A. Sakasai, N. Asakura, K. Shimizu, H. Kubo, S. Higashijima, T. Oikawa, H. Shirai, T. Fujita, Y. Kamada, et al.: Particle confinement and transport in JT-60U, Nucl. Fusion, 39(11Y), 1917–1928, 1999.

[Holm97] Holman, J. P.: Heat transfer, McGraw-Hill Companies, New York., 1997.

[Hond00] HONDA, T.: Transients of passive shutdown under loss of coolant events, Task Report, Japanese ITER Home Team., n.d.

[HsGm92] H.-S. Bosch and G.M. Hale: Improved formulas for fusion cross-sections and thermal reactivities, Nucl. Fusion, 32(4), 611–631, 1992.

[IDEU08] Izquierdo Villena, J., Dies Llovera, J., Escola Tècnica Superior d'Enginyers Industrials de Barcelona., Universitat Politècnica de Catalunya. and Departament de Física i Enginyeria Nuclear.: ITER safety assessment : in-vessel simulation of tokamak events and component reliability approach., 2008.

[IiKP06] Iida, H., Khripunov, V. and Petrizzi, L.: Nuclear Analysis Report, Nuclear Analysis Group, ITER Garching Joint Work Site., 2006.

[Inte91] International Atomic Energy Agency: ITER conceptual design report, International Atomic Energy Agency, Vienna. [online] Available from: http://books.google.com/books?id=0RZOAQAAIAAJ (Accessed 10 May 2015), 1991.

[Iter01] ITER Council: Final report of the ITER engineering design activities, IAEA EDA Doc. Ser., (21) [online] Available from: http://scholar.google.com/scholar?cluster=13298201764039443612&hl=en&oi=scholarr (Accessed 10 May 2015), 2001.

[Iter02] ITER Team: ITER Technical Basis., IAEA, Vienna., 2002.

[Iter99a] ITER, E.: documentation series no. 16, Tech. Basis ITER Final Des. Rep. Cost Rev. Saf. Anal. FDR IAEA Vienna [online] Available from: http://scholar.google.com/scholar?cluster=3090762476167333407&hl=en&oi=scholarr (Accessed 10 May 2015), 1999.

[Iter99b] ITER Team, and others: ITER physics basis, Nucl Fusion, 39, 2137, 1999.

[Izqu06] Izquierdo, J.: Safety assessment ofenergy fluxes on in-vessel components with SAFALY, 2006.

[John11] Johner, J.: HELIOS: A Zero-Dimensional Tool for Next Step and Reactor Studies, Fusion Sci. Technol., 59(2), 308–349, 2011.

[KeBl46] Kern, W. F. and Bland, J. R.: Solid mensuration. [With answers.]., New York & London., 1946.

[KGGL99] Keilhacker, M., Gibson, A., Gormezano, C., Lomas, P. J., Thomas, P. R., Watkins, M. L., Andrew, P., Balet, B., Borba, D., Challis, C. D., Coffey, I., et al.: High fusion performance from deuterium-tritium plasmas in JET, Nucl. Fusion, 39(2), 209, doi:10.1088/0029-5515/39/2/306, 1999.

[Kike07] K. Ikeda: Progress in the ITER Physics Basis, Nucl. Fusion, 47(6), 2007.

[King00] KING, D. et al.: Conclusions of the Fusion Fast Track Experts Meeting Held on 27 November 2001 on the Initiative of Mr. De Donnea, President of the Research Council, n.d.

[KLKR09] Kotov, V., Litnovsky, A., Kukushkin, A. S., Reiter, D. and Kirschner, A.: Numerical modelling of steady-state fluxes at the ITER First Wall, J. Nucl. Mater., 390(1), 528, 2009.

[Kmmc95] K M McGuire, H. A.: REVIEW OF DEUTERIUM-TRITIUM RESULTS FROM THE TOKAMAK FUSION TEST REACTOR, Phys. Plasmas, 2, 2176–2188, 1995.

[KNHC08] Kwon, M., Na, Y. S., Han, J. H., Cho, S., Lee, H., Yu, I. K., Hong, B. G., Kim, Y. H., Park, S. R. and Seo, H. T.: A strategic plan of Korea for developing fusion energy beyond ITER, Fusion Eng. Des., 83(7–9), 883–888, doi:10.1016/j.fusengdes.2008.06.009, 2008.

[KPKR05] Kukushkin, A. ., Pacher, H. ., Kotov, V., Reiter, D., Coster, D. and Pacher, G. .: Effect of neutral transport on ITER divertor performance, Nucl Fusion Nucl. Fusion, 45(7), 608–616, 2005.

[Laws57] Lawson, J. D.: Some Criteria for a Power Producing Thermonuclear Reactor, Proc. Phys. Soc. Sect. B, 70(1), 6, doi:10.1088/0370-1301/70/1/303, 1957.

[Loar08] Loarte, A.: Guidelines on load specifications for ITER plasma facing components in steady and transient phases., 2008.

[MAAG97] Matthews, G. F., Allen, S., Asakura, N., Goetz, J., Guo, H., Kallenbach, A., Lipschultz, B., McCormick, K., Stamp, M., Samm, U., Stangeby, P. C., et al.: Scaling radiative plasmas to ITER, J. Nucl. Mater. J. Nucl. Mater., 241-243, 450–455, 1997.

[Mars72] Marsaglia, G.: Choosing a Point from the Surface of a Sphere, Ann Math Stat., 43(2), 645–646, 1972.

[Mart02] Martin Greenwald: Density limits in toroidal plasmas, Plasma Phys. Control. Fusion, 44(8), R27–R53, 2002.

[MCPL06] Maisonnier, D., Cook, I., Pierre, S., Lorenzo, B., Luigi, D. P., Luciano, G., Prachai, N. and Aldo, P.: DEMO and fusion power plant conceptual studies in Europe, Fusion Eng. Des., 81(8–14), 1123–1130, doi:10.1016/j.fusengdes.2005.08.055, 2006.

[Mead10] Meade, D.: 50 years of fusion research, Nucl. Fusion, 50(1), 014004, doi:10.1088/0029-5515/50/1/014004, 2010.

[Merv59] Mervin Muller: A note on a method for generating points uniformly on n-dimensional spheres, Commun ACM Commun. ACM, 2(4), 19–20, 1959.

[NAGI08] Norajitra, P., Abdel-Khalik, S. I., Giancarli, L. M., Ihli, T., Janeschitz, G., Malang, S., Mazul, I. V. and Sardain, P.: Divertor conceptual designs for a fusion power

plant, Fusion Eng. Des., 83(7-9), 893 – 902, doi:DOI: 10.1016/j.fusengdes.2008.05.022, 2008.

[Naka13] Nakajima, N.: IFERC Annual report, JA Home Team., 2013.

[NITS14] Nakamura, M., Ibano, K., Tobita, K., Someya, Y. and Tanigawa: Analysis of Accident Scenarios of a Water-Cooled Tokamak DEMO, Saint Petersburg, Russia., 2014.

[NLFJ98] Nakamura, H., Ladd, P., Federici, G., Janeschitz, G., Schaubel, K. M., Sugihara, M., Busigin, A., Gierszewski, P. J., Hiroki, S., Hurzlmeier, H. S., Kuan, W., et al.: ITER fuelling, pumping, wall conditioning systems and fuel dynamics analysis, Fusion Eng. Des., 39–40, 883–891, doi:10.1016/S0920-3796(98)00275-0, 1998.

[NoFo03] Norajitra, P. and Forschungszentrum (Karlsruhe).: Conceptual design of the dual-coolant blanket within the framework of the EU power plant conceptual study (TW2-TRP-PPCS12) : final report, FZKA, Karlsruhe., 2003.

[Pata80] Patankar, S. V.: Numerical heat transfer and fluid flow, Hemisphere Pub. Corp. ; McGraw-Hill, Washington; New York., 1980.

[Perl09] Perlado, J. M.: TECNO_FUS: A Breeding Blanket NFT programme developing dual functional He/Pb15.7Li systems engineering & associated underlying technologies, Ericeira, Portugal., 2009.

[PeRo94] Pedretti, E. and Rollet, S.: Exact and approximate geometric calculations for toroidalD-shaped plasmas : Application to Ignitor-Ult., 1994.

[PJTG77] Post, D. E., Jensen, R. V., Tarter, C. B., Grasberger, W. H. and Lokke, W. A.: Steady-state radiative cooling rates for low-density, high-temperature plasmas, At. Data Nucl. Data Tables, 20(5), 397–439, doi:10.1016/0092-640X(77)90026-2, 1977.

[PKPJ07] Pacher, H. D., Kukushkin, A. S., Pacher, G. W., Janeschitz, G., Coster, D., Kotov, V. and Reiter, D.: Effect of the tokamak size in edge transport modelling and implications for DEMO, NUMA J. Nucl. Mater., 363-365, 400–406, 2007.

[PoSM06a] Polevoi, A. R., Shimada, M. and Mukhovatov, V. S.: ITER plasma performance assessment on the basis of newly-proposed scalings, Plasma Phys. Control. Fusion, 48(5A), A449, doi:10.1088/0741-3335/48/5A/S46, 2006.

[PoSM06b] Polevoi, A. R., Shimada, M. and Mukhovatov, V. S.: ITER plasma performance assessment on the basis of newly-proposed scalings, Plasma Phys. Control. Fusion, 48(5A), A449, doi:10.1088/0741-3335/48/5A/S46, 2006.

[Pres07] Press, W. H.: Numerical recipes : the art of scientific computing, Cambridge University Press, Cambridge, UK; New York., 2007.

[Rama14] Ramanujan, S.: Modular Equations and Approximations to π, Quart J Pure App Math, 45, 350–372, 1914.

[ReTT07] Reyes, S., Topilski, L. and Taylor, N.: Accident Analysis Specifications, Environment, Safety & Health Section , Cadarache ITER Joint Central Team., 2007.

[RFBP97] Raffray, A. ., Federici, G., Barabash, V., Pacher, H. ., Bartels, H. ., Cardella, A., Jakeman, R., Ioki, K., Janeschitz, G. and Parker, R.: Beryllium application in ITER plasma facing components, Fusion Eng. Des. Fusion Eng. Des., 37(2), 261–286, 1997.

[RiDF15] Rivas J.C., Dies J. and Fajarnes X.: Revisiting the analysis of passive plasma shutdown during an ex-vessel loss of coolant accident in ITER blanket, Fusion Eng Fusion Eng. Des., 98-99, 2206–2209, 2015.

[RiDi11] Rivas, J. C. and Dies, J.: Upgrading of Plasma Wall Interaction Model for Tokamak Transient Modeling Code AINA 2.0, Used in Safety Studies of ITER Plasma Instability Events, Fusion Sci. Technol., 60(2), 825–829, 2011.

[RiDi13] Rivas, J. C. and Dies, J.: Safety studies: Review of loss of plasma control transients in ITER with AINA 3.0 Code, Fusion Eng. Des., 88(9-10), 2709–2713, 2013.

[Rma15] RMA: ITER and Fusion Energy, Belg. Portal ITER Fusion Energy Res. [online] Available from: http://iter.rma.ac.be/en/community/Worldwide/index.php (Accessed 22 May 2015), 2015.

[RNSH15] Rivas, J. C., Nakamura, M., Someya, Y., Hoshino, K., Asakura, N., Takase, H., Miyoshi, Y., Utoh, H., Tobita, K., Dies, J., Blas, A. de, et al.: Safety Studies of Plasma-Wall Events with AINA code for Japanese DEMO, Jeju, South Korea., 2015.

[RNST14] Rivas, J. C., Nakamura, M., Someya, Y., Takase, H., Tobita, K., Dies, J., Blas, A. de, Fabbri, M. and Riego, A.: Safety studies for Japanese demo design with AINA code, Niigata, Japan., 2014.

[Roth99] Roth, J.: Chemical erosion of carbon based materials in fusion devices, J. Nucl. Mater., 266/269, 51–57, 1999.

[RuIP00] Ruvutuso, G., Iida, H. and Petrizzi, L.: Nuclear Heat Deposition in the Blanket and Vacuum Vessel, Nuclear Analysis Group, ITER Garching Joint Work Site., 2000.

[SaOb15] Sadiku M.N.O. and Obiozor C.N.: A simple introduction to the method of lines, Int J Electr Eng Educ Int. J. Electr. Eng. Educ., 37(3), 282–296, 2015.

[Sola05] Sola, A.: Contribución al estudio de seguridad de ITER. Determinista y probabilista., 2005.

[SSHV09] Sánchez, J., Sedano, L. A., Hodgson, E. R., Victoria, M., Sanz, J., Chuimenti, M. and others: CONSOLIDER TECNO_FUS: a nuclear fusion technology programme developing dual functional helium/Pb15. 7Li breeding blanket systems engineering and associated underlying technologies, 23th Symp. Fusion Eng. San Diego USA [online] Available from: http://scholar.google.com/scholar?cluster=15702634115254157044&hl=en&oi=scholarr (Accessed 10 May 2015), 2009.

[Stac10] Stacey, W. M.: The Quest for a Fusion Energy Reactor: An Insider's Account of the INTOR Workshop, 1 edition., Oxford University Press, New York., 2010.

[Stan00] Stangeby, P. C.: The Plasma Boundary of Magnetic Fusion Devices, CRC Press, Bristol u.a., 2000.

[STUT15] Someya, Y., Tobita, K., Utoh, H., Tokunaga, S., Hoshino, K., Asakura, N., Nakamura, M. and Sakamoto, Y.: Design study of blanket structure based on a water-cooled solid breeder for DEMO, FUSION Fusion Eng. Des., 98-99, 1872–1875, 2015.

[TaMB01] Takenaga, H., Mahdavi, M. A. and Baker, D. R.: Comparison of particle confinement in the high confinement mode plasmas with the edge localised mode of the Japan Atomic Energy Research Institute Tokamak-60 Upgrade and the DIII-D tokamak, Phys Plasmas Phys. Plasmas, 8(5), 1607, 2001.

[Tamm58] TAMM, I. E.: Teoriya Magnitnogo Termoyadernogo Reaktora (Theory of the Magnetic Thermonuclear Reactor)., Fiz. Plazmy Probl. UTS Plasma Phys. CTF Probl. Akad Nauk SSSR Ed, 1(1), 3, 1958.

[Tayl09] Taylor, N.: Preliminary Safety Analysis of ITER, FUSION Sci. Technol., 56(2), 573–580, 2009.

[TBCC11] Taylor, N., Baker, D., Ciattaglia, S., Cortes, P., Elbez-Uzan, J., Iseli, M., Reyes, S., Rodriguez-Rodrigo, L., Rosanvallon, S., Topilski, L. and Porto Portugal

20100927-20101001: Updated safety analysis of ITER, FUSION Fusion Eng. Des., 86(6-8), 619–622, 2011.

[THNH98] Takuro Honda, Hans-Werner Bartels, Nermin A. Uckan and Honda Takuro: Transient Behaviors of Plasma and In-vessel Components when Considering Divertor Plasma State Transition in a Fusion Reactor, J. Nucl. Sci. Technol., 35(12), 916–927, 1998.

[TNEK09] Tobita, K., Nishio, S., Enoeda, M., Kawashima, H., Kurita, G., Tanigawa, H., Nakamura, H., Honda, M., Saito, A., Sato, S., Hayashi, T., et al.: Compact DEMO, SlimCS: design progress and issues, Nucl. Fusion, 49(7), 075029, doi:10.1088/0029-5515/49/7/075029, 2009.

[Topi08] Topilski, L.: Safety Analysis Data List., 2008.

[Tous00] Tous, J.: Interfaz gráfica para el código de seguridad SAFALY de reactores de fusión. Aplicación a ITER., n.d.

[TrKu58] TRUBNIKOV, B. and KUDRIAVTSEV, V.: Plasma radiation in a magnetic field, J. Nucl. Energy 1954 J. Nucl. Energy 1954, 7(3-4), 301–301, 1958.

[Tsun09] Tsunematsu, T.: Broader Approach to fusion energy, Fusion Eng. Des., 84(2–6), 122–124, doi:10.1016/j.fusengdes.2009.02.029, 2009.

[UcOC91] Uckan, N., Oak Ridge National Lab., T. (United S. and Conference: 14. IEEE symposium on fusion engineering, S. D. CA (United States), 30 Sep - 3 Oct 1991: ITER physics design guidelines at high aspect ratio, United States., 1991.

[UPWB96] Uckan, N. A., Putvinski, S., Wesley, J., Bartels, H.-W., Honda, T., Amano, T., Boucher, D., Fujisawa, N., Post, D. and Rosenbluth, M.: ITER physics-safety interface: models and assessments, Oak Ridge National Lab., TN (United States). Funding organisation: USDOE, Washington, DC (United States). [online] Available from:

http://inis.iaea.org/Search/search.aspx?orig_q=RN:28020445 (Accessed 14 February 2015), 1996.

[WeCa04] Wesson, J. and Campbell, D. J.: Tokamaks, Clarendon Press ; Oxford University Press, Oxford; New York., 2004.

[WFFL08] Wilson, P. P. H., Feder, R., Fischer, U., Loughlin, M., Petrizzi, L., Wu, Y., Youssef, M. and Heidelberg Germany 20070930-20071005: State-of-the-art 3-D radiation transport methods for fusion energy systems, FUSION Fusion Eng. Des., 83(7-9), 824–833, 2008.

[Wu08] Wu, Y.: Conceptual design of the China fusion power plant FDS-II, Fusion Eng. Des., 83(10–12), 1683–1689, doi:10.1016/j.fusengdes.2008.06.048, 2008.

[YaII83] Yamamura, Y., Itikawa, Y. and Itoh, N.: Angular dependence of sputtering yields of monatomic solids, Institute of Plasma Physics, Nagoya University, Nagoya, Japan., 1983.

[Yama09] Yamazaki, K.: Impurity Behavior in ITER and Helical Burning Plasmas with Internal Transport Barriers, J Plasma Fusion Res Ser., 8, 338–341, 2009.

Papers and contributions

Journal papers

Safety studies of plasma-wall events with AINA code for Japanese DEMO
Rivas, J. C.; Nakamura, Makoto; Someya, Yoji; Takase, Haruhiko; Tobita, Kenji; Dies, J.; Blas, A. de; Fabbri, M.; Riego, A.
Fusion Engineering and Design, Accepted 29 October 2015, DOI:10.1016/j.fusengdes.2015.10.037

Revisiting the analysis of passive plasma shutdown during an ex-vessel loss of coolant accident in ITER blanket
J.C. Rivas, J. Dies, X. Fajarnés
Fusion Engineering and Design, **98–99** (2015) 2206-2209

ITER safety studies: the effect of two simultaneous perturbations during a loss of plasma control transient
Rivas, J.C.; Dies, J.
Fusion engineering and design **89** no. 9-10, (2014) 2043-2047

Fusion neutron source model for the systems analysis of a tokamak power plant
Rivas, J.C.; de Blas, A.; Dies, J.; Sedano, L.
Fusion science and technology **64** no. 3, (2014) 687-691

Safety studies: Review of loss of plasma control transients in ITER with AINA 3.0 Code
Rivas, J.C.; Dies, J.
Fusion engineering and design **88** no. 9-10, (2013) 2709-2713

Upgrading of Plasma Wall Interaction Model for Tokamak Transient Modeling Code AINA 2.0, Used in Safety Studies of ITER Plasma Instability Events
Rivas, J.C.; Dies, J.
Fusion science and technology **60** no. 2, (2011) 825-829

AINA Safety Code, A Review of Loss of Plasma Control Transients in ITER: Sudden Increase in Fuelling Rate, Sudden Increase of Auxiliary Heating
Dies, J.; Dapena, M.; Ramon, M.; Lopez, R.; Garcia, J.; Rivas, J.C.; Calvo, A.; Reyes, S.
Fusion science and technology **56** no. 1 (2009) 31-37

Developing the IFMIF RAM planning
Tapia, C.; Dies, J.; Calvo, A.; Rivas, J.C.; Ibarra, A.
Fusion engineering and design **84** no. 7-11, (2009) 1823-1826

Conference papers

Safety studies of plasma-wall events with AINA code for Japanese DEMO
Rivas, J. C.; Nakamura, Makoto; Someya, Yoji; Takase, Haruhiko; Tobita, Kenji; Dies, J.; Blas, A. de; Fabbri, M.; Riego, A.
12th International Symposium on Fusion Nuclear Technology, Jeju (South Korea) September 2015

Revisiting the analysis of passive plasma shutdown during an ex-vessel loss of coolant accident in ITER blanket
Rivas, J.C.; Dies, J.; Fajarnes, X.
28th Symposium of Fusion Technology, San Sebastian (Spain) September 2014

Safety studies for Japanese DEMO design with AINA code
Rivas, J. C.; Nakamura, Makoto; Someya, Yoji; Takase, Haruhiko; Tobita, Kenji; de Blas, A.; Dies, J.; Fabbri, M.; Riego, A.
Plasma Conference 2014 Niigata (Japan) November 2014

ITER Safety Studies: The effect of two simultaneous perturbations during a Loss of Plasma Control Transient
Rivas, J.C.; Dies, J.
11th International Symposium on Fusion Nuclear Technology, Barcelona (Spain), September 2013

Estudios de Seguridad para ITER: El efecto de dos perturbaciones simultáneas durante un Transitorio de Pérdida de Control del Plasma
Rivas, J.C.; Dies, J.
39ª Reunión Anual de la Sociedad Nuclear Española, Reus, September 2013

Fusion Neutron Source Model for the Systems Analysis of a Tokamak Power Plant
J. C. Rivas, A. de Blas, J. Dies, L. Sedano
20th Topical Meeting on the Technology of Fusion Energy Nashville (USA) August 2012

Safety studies: Review of loss of plasma control transients in ITER with AINA 3.0 Code
Rivas, J.C.; Dies, J.
27th Symposium on Fusion Technology, Liege (Belgium), September 2012

Plant engineering models for a Tokamak Power Plant systems analysis
Rivas, J.C.; Dies, J.
27th Symposium on Fusion Technology, Liege (Belgium), September 2012

ITER safety studies: deployment of quality plan for AINA code
Dies, J.; Rivas, J.C.; Mora, P.; Bargalló, E.
26th Symposium on Fusion Technology, Oporto (Portugal), September 2010

Upgrading of Plasma Wall Interaction Model for Tokamak Transient Modeling Code AINA 2.0, Used in Safety Studies of ITER Plasma Instability Events
Jose-Carlos Rivas, Javier Dies
19th Topical Meeting on the Technology of fusion Energy, Las Vegas (USA), September 2010

AINA safety code, a review of Loss of Plasma Control Transients in ITER: fuelling and/or auxiliary heating cut off, increase in confinement time
Dies, J.; Dapena, M.; Ramon, M.; Lopez, R.; Garcia, J.; Rivas, J.C.; Calvo, A.
18th Topical Meeting on the Technology of fusion Energy, San Francisco (USA), September 2008

Loss of Plasma Control Transients in ITER: a review with AINA Safety code.
J. Dies, M. Dapena, M. Ramon, R. López, J.García, J.C. Rivas, A. Calvo, S. Reyes
25th Symposium on Fusion Technology, Rostock (Germany), September 2008.

Annex 1: List of common symbols

Plasma balance

A_k	Atomic mass of k-th impurity species
B_T	Toroidal magnetic field
β_{lim}	Beta limit
β_P	Poloidal beta
β_T	Toroidal beta
β_N	Normalised beta
C_{bs}	Bootstrap constant
E	Electron charge
E_α	Energy due to fusion reaction going to alpha particle
ε_0	Vacuum permittivity
H	Plasma resistivity (averaged)
η_0	Spitzer resistivity
η_S	Spitzer resistivity corrected for impurities
HH98	Scale factor for energy confinement time scaling
$f_{bootstrap}$	Bootstrap current fraction
f_{ext}	Fraction of external power absorbed by ions
f_{ripple}	Ripple loss factor
f_α	Fraction of alpha power absorbed by ions
G_{Troyon}	Troyon constant
γ_{NC}	Neoclassical correction factor
I_P	Poloidal current
j_{bs}	Bootstrap current density
j_P	Poloidal current density
j_{CD}	Current density due to current drive
j_Ω	Ohmic current density
$\ln\Lambda$	Coulomb logarithm
m_e	Electron mass
n_i	Fuel particle density
n_α	Alpha particle density
$n_{z,j}$	j-th impurity species particle density
n_e	Electron particle density
n_D	Deuterium particle density
n_T	Tritium particle density
P_{ext}	External power
P_α / p_α	Alpha power/power density
$P_{i,e}$ / $p_{i,e}$	Ion-electron exchange power/power density
P_Ω/ p_Ω	Ohmic power/power density
P_{brem}/ p_{brem}	Bremsstrahlung power/power density
P_{li}/ p_{li}	Line power/power density
P_{cy}/ p_{cy}	Synchrotron power/power density
P_{con}	Conductive power losses

Psep	Power flux crossing the separatrix
P_{THR}	Threshold power for confinement mode transition
Q	Amplification factor of fusion power
q_{95}	Safety factor, 95% flux
q_0	Safety factor at plasma axis
S_H	Fuel particle source
S_α	Alpha particle source
$S_{Z,j}$	j-th impurity species particle source
$\langle\sigma v\rangle_{DT}$	DT fusion reaction velocity averaged cross section
Ti	Ion temperature
Te	Electron temperature
τp,H	Fuel particle confinement time
$\tau_{p,\alpha}$	Alpha particle confinement time
$\tau_{p,z}$	j-th impurity species particle confinement time
$\tau_{E,i}$	Ion energy confinement time
$\tau_{E,e}$	Electron energy confinement time
$\tau_{i,e}$	Ion-electron heat exchange time
V_{loop}	Resistive loop voltage
Z_{eff}	Effective charge of plasma ions
Z_j	Atomic number of j-th impurity species

Plasma geometry

R	Major radius
A	Minor radius
δ, $\delta_X^{(u)}$, $\delta_X^{(l)}$	Triangularity, triangularity at upper X point, triangularity at lower X point
κ, $\kappa_X^{(u)}$, $\kappa_X^{(l)}$	Elongation, elongation at upper X point, elongation at lower X point
V,S,p	Plasma volume, surface, poloidal perimeter
R	Radial position in poloidal section (absolute)
P	Radial position in poloidal section (relative)
α_x	Generic plasma variable dimensionless parameter for radial parabolic profile
x	Generic plasma variable
$\langle x\rangle$	Volume average of generic plasma variable
$\bar{x}$	Line average of generic plasma variable
B	Beta function

Wall thermal model

C_p	Specific heat of node i
f_{ij}	Geometrical view factor between PFC regions i and j
$k_{T,i}$	Thermal conductivity of node i
k_{GAP}	Thermal conductance at a contact surface
h_∞	Film coefficient at cooling channel
L_v	Evaporation heat
$P_{neut,i}$	Neutronic power for node i
P_{rad}, $\dot{q}_h$	Radiative power at PFC surface
$\dot{q}_{subl}$	Heat flux lost by sublimation of PFC
Q	Heating source
ρ,ρ_i	Material density at node i

SOL model

$\dot{q}_{h,module}$	Surface heat flux to a calculation región
P_{EM}	Electromagnetic power
$f_{r,module}$	EM radiation peaking factor in a calculation region
S_{tot}	Total inner area
$P_{part,module}$	Thermal power due to particles in a calculation region
$\dot{q}_{n,module}$	Volume (neutron) heat flux to a calculation region
$f_{n,module}$	Neutron flux peaking factor in a calculation region
S_{module}	Area of a calculation region
$\dot{q}_{tot,module}$	Total heat flux to a calculation region
Γ_{module}	Particle flux to a calculation region
c_s	Ion sound speed
$n_e(a)$	Electron density t the plasma edge
$\dot{q}_d$	Heat flux to divertor
E_i	Ion bombardment energy
Φ	Wall electric potential
Γ_S	Sheath flux
n_S	Sheath particle density
q_i	Ion energy flux over surface (sheath model)
q_e	Electron energy flux over surface (sheath model

Impurities model

A_p	Surface area of the plasma
C_{screen}	Screening coefficient
$D_\perp$	Cross-field diffusion coefficient
$\dot{\delta}_{sublimation}$	Impurity source by thermal sublimation
$\dot{\delta}_{erosion}$	Impurity source by erosion
$\dot{\delta}_{TOTAL}$	Total impurity source
E_0	Incident particle energy
E_{th}	Threshold energy
E_{TS}	Thomas-Fermi energy
E_S	Surface binding energy
λ_z	Mean free path for ionisation of the impurity
λ_n	Plasma density decay length
m_d	Dust production
$S(t)_{imp}$	Impurity source
τ_d	Duration of impurity transport
$Y(t)_e$	Impurity production rate
Y^{ad}	Adatom yield
Y^{chem}	Chemical erosion yield
Y^{dam}	Erosion yield due to damage caused by incident ions
Y^{phy}	Physical erosion yield
Y^{RES}	Beryllium RES yield
Y^{surf}	Surface term yield in chemical erosion
Y^{therm}	Thermal term yield in chemical erosion

Annex 2: LOPC transients in ITER: Figures

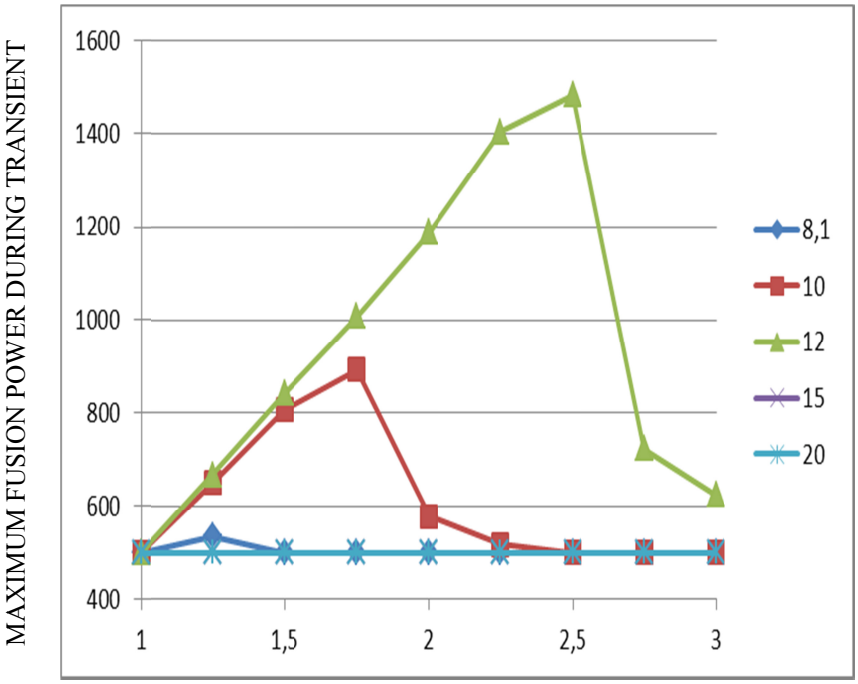

Figure A2-1: Maximum fusion power in case of increase in fuelling rate for different ion temperatures, AINA calculations for ITER 500MW inductive scenario.

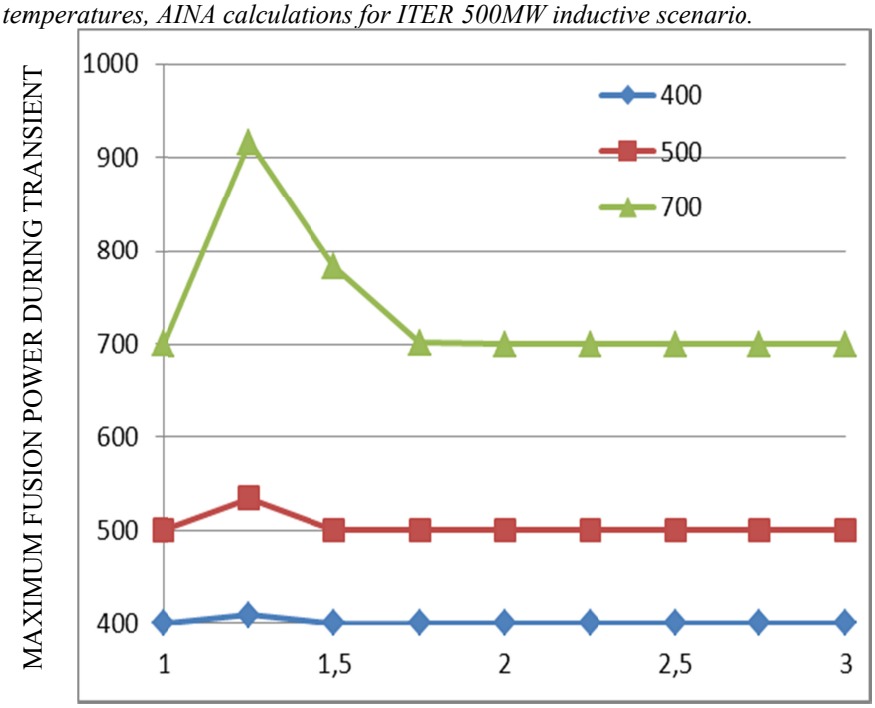

Figure A2-2: Maximum fusion power in case of increase in fuelling rate for different initial fusion power, AINA calculations for ITER inductive scenarios.

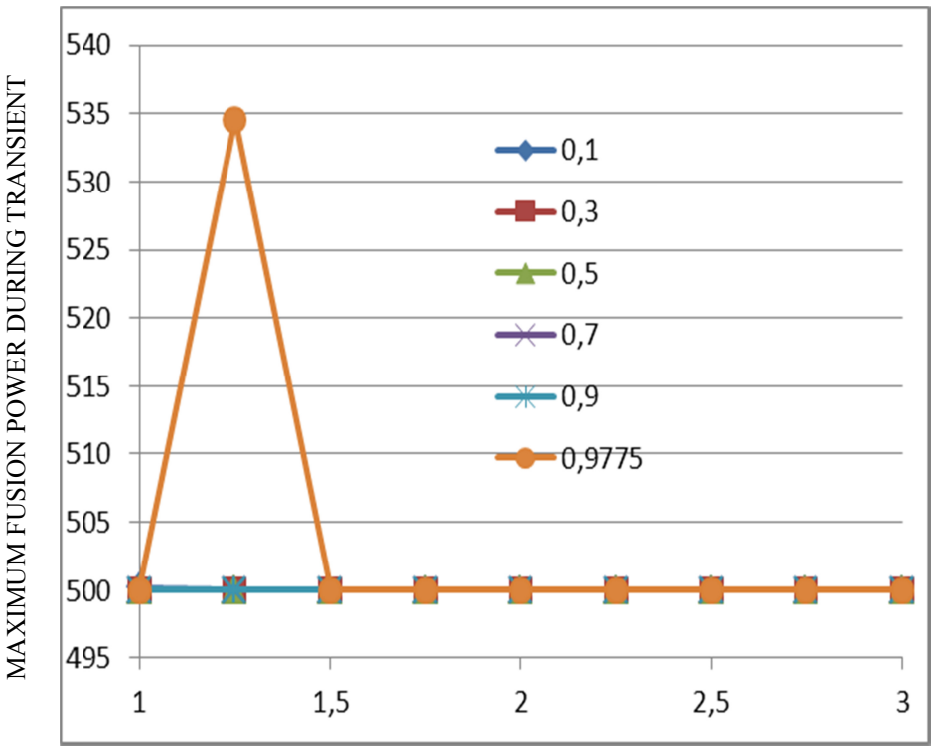

Figure A2-3: Maximum fusion power in case of increase in fuelling rate for different initial density profile, AINA calculations for ITER 500MW inductive scenario.

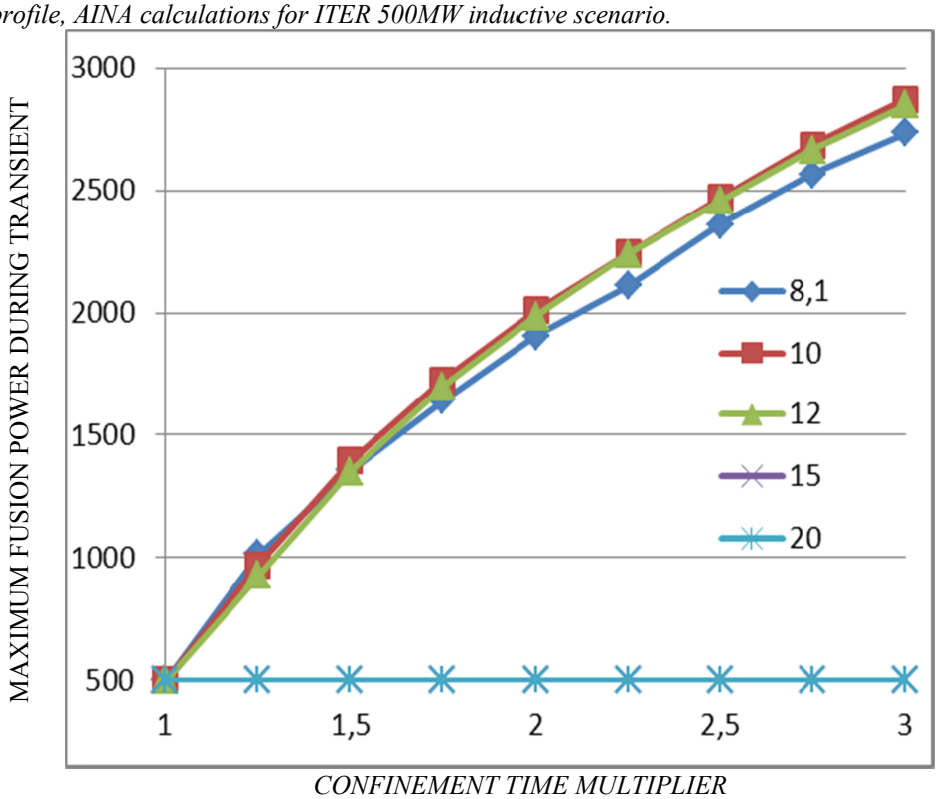

Figure A2-4: Maximum fusion power in case of confinement improvement for different initial ion temperature, AINA calculations for ITER 500MW inductive scenario.

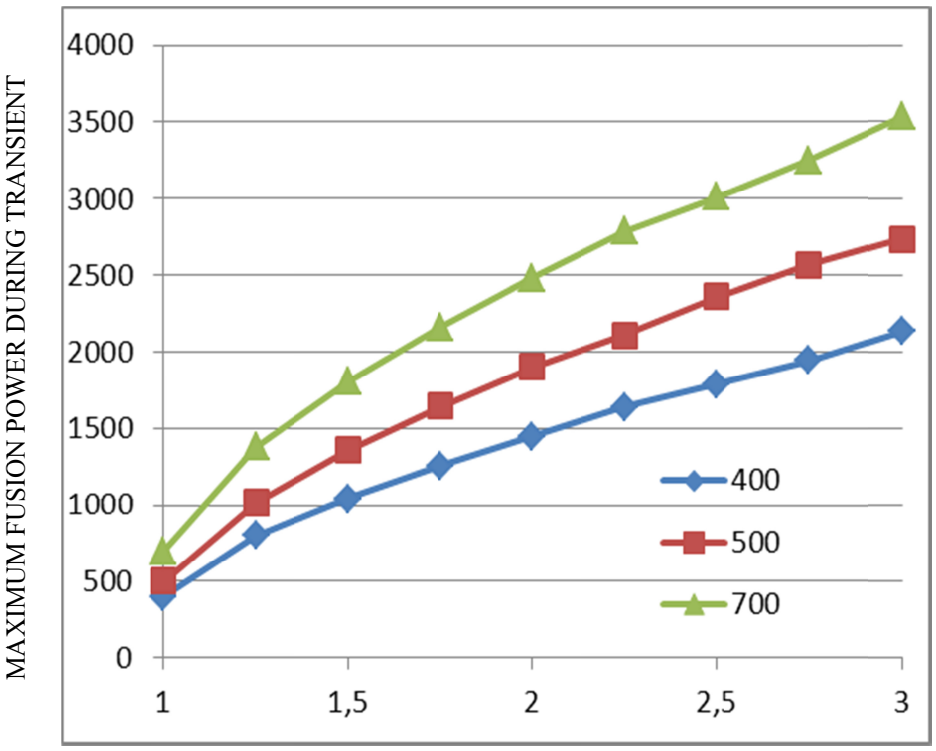

Figure A2-5: Maximum fusion power in case of confinement improvement for different initial fusion power, AINA calculations for ITER inductive scenarios.

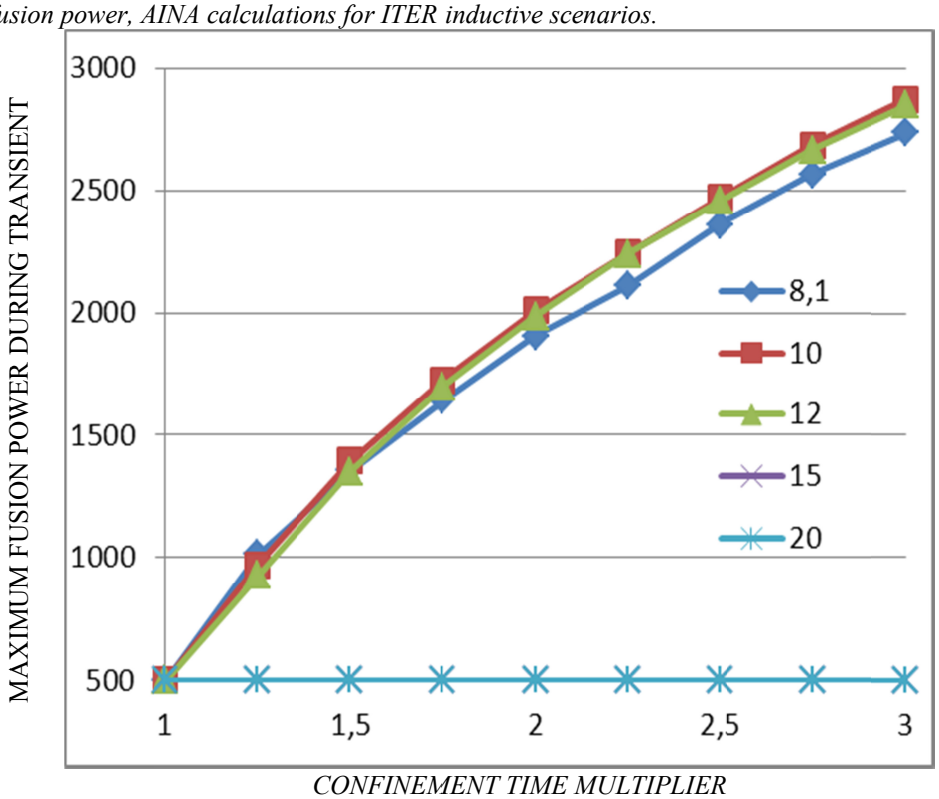

Figure A2-6: Maximum fusion power in case of confinement improvement for different initial density profile, AINA calculations for ITER 500MW inductive scenario.

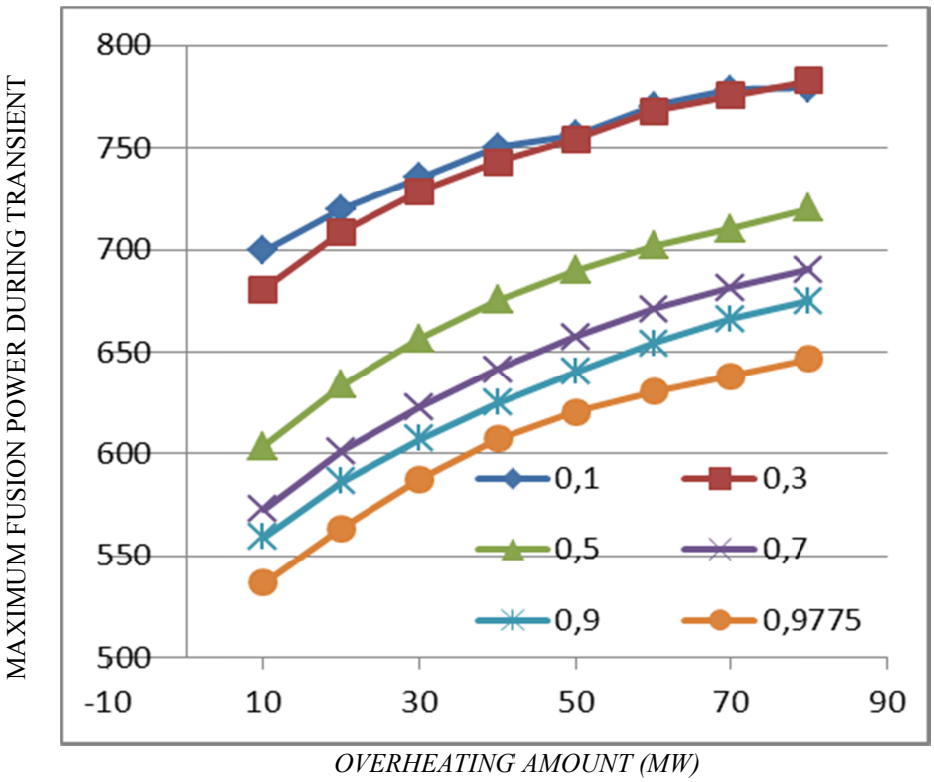

Figure A2-7: Maximum fusion power in case of increase of external heating for different initial density profile, AINA calculations for ITER 500MW inductive scenario.

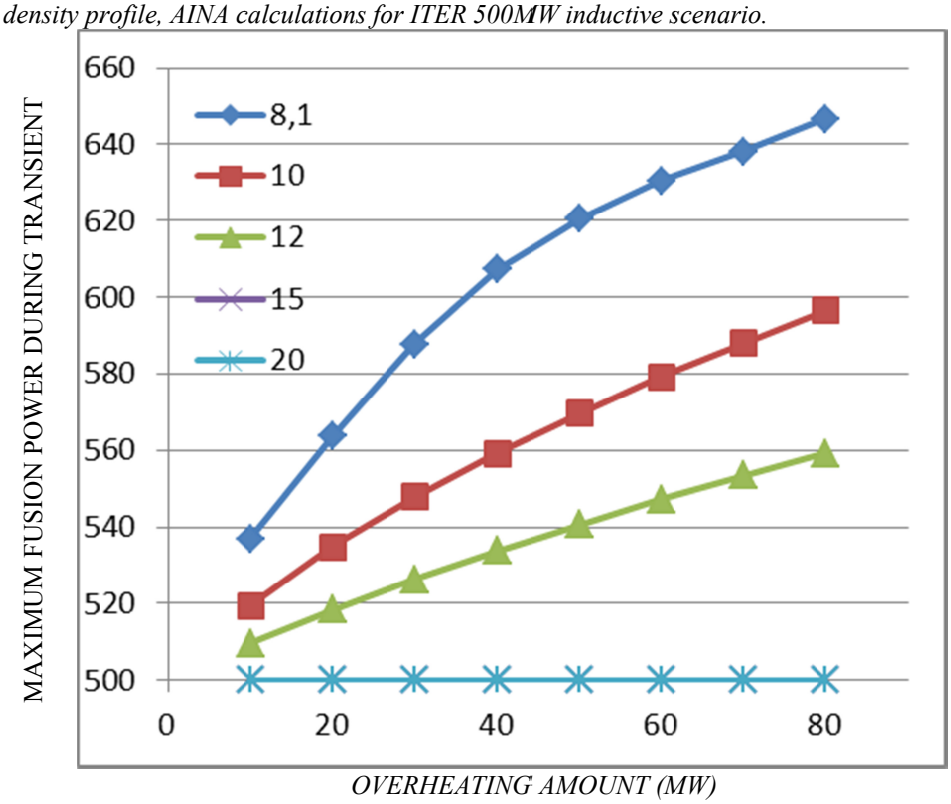

Figure A2-8: Maximum fusion power in case of increase of external heating power for different initial ion, AINA calculations for ITER 500MW inductive scenario. temperature. In GSSR case,

[Ayma01b] *only the case of 80MW overheating is shown*

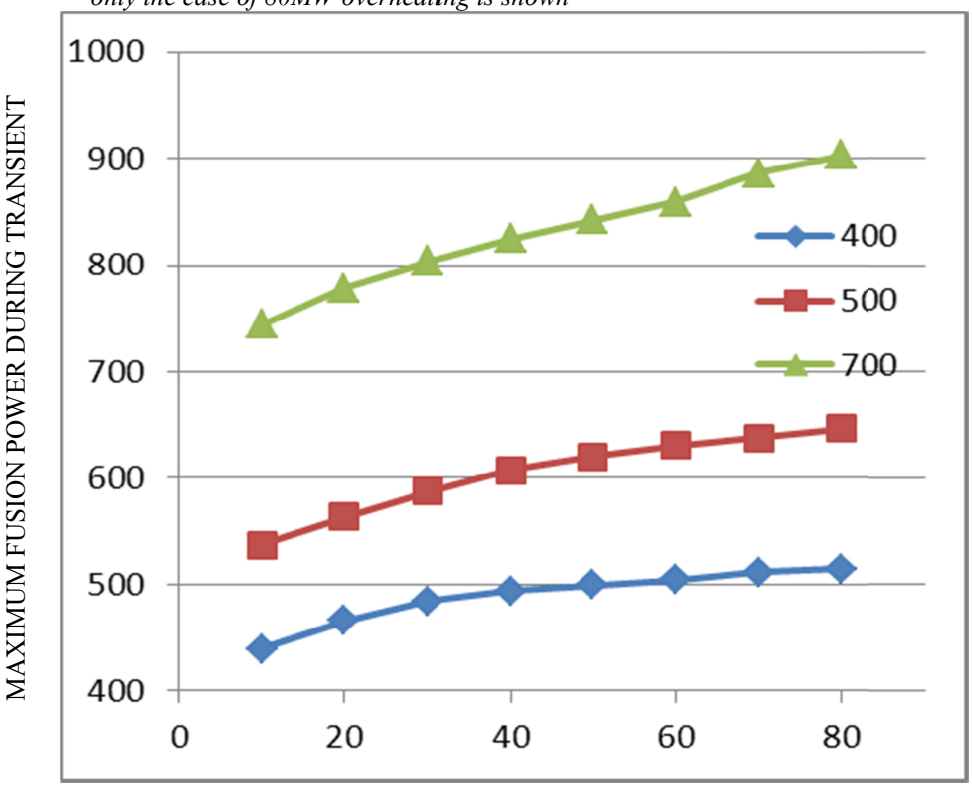

Figure A2-9: Maximum fusion power in case of increase of external heating power for different initial fusion, AINA calculations for ITER inductive scenarios. power. In GSSR case, [Ayma01b] *only the case of 80MW overheating is shown*

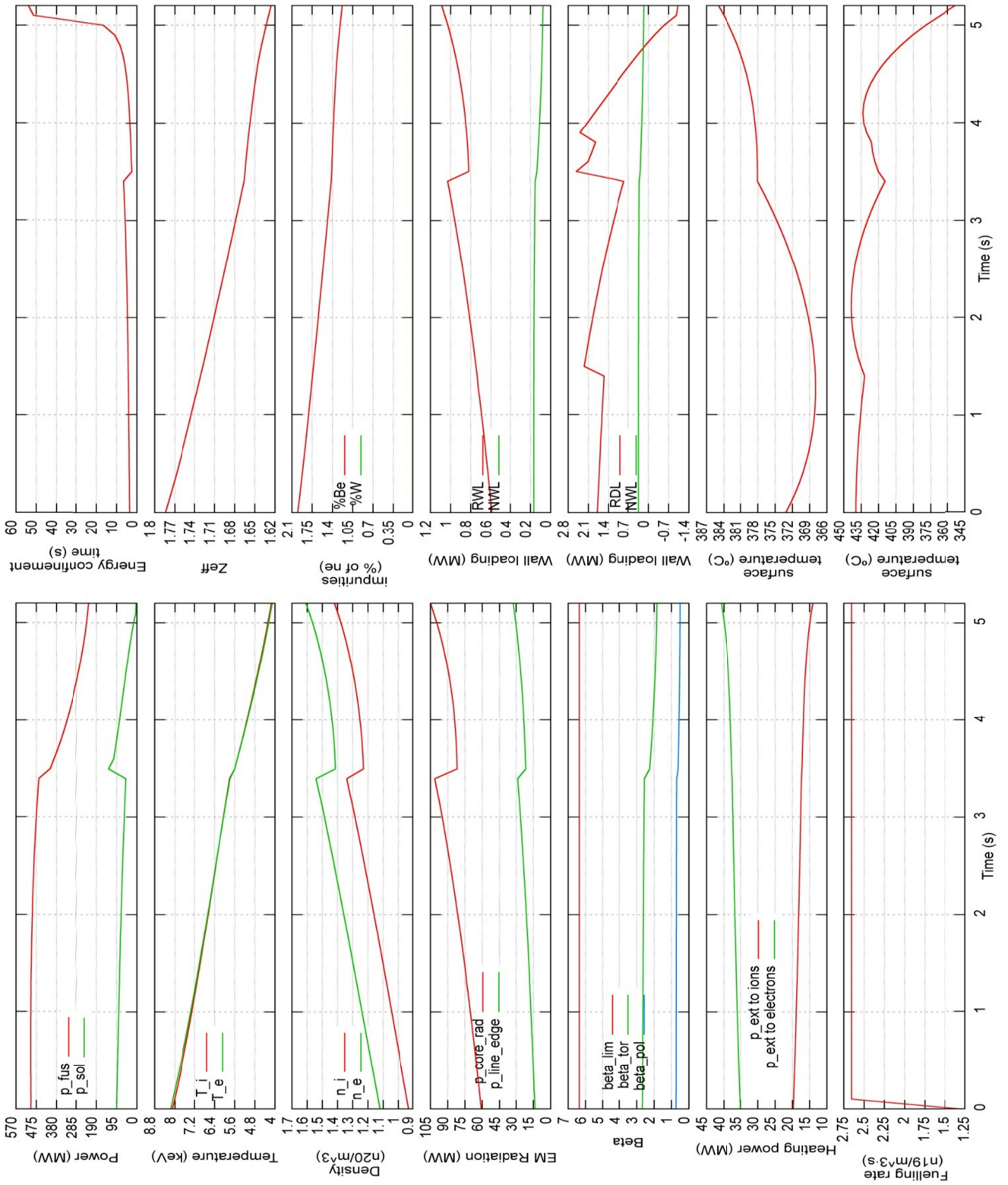

Figure A2-10: Sudden increase of fuelling by factor 2.0, Ti=8.1 keV, PFUS=500MW

Annex 3: SimSched, an application to perform multiple simulations with AINA code

SimSched, which stands for "Simulation Scheduler", is an Excel spreadsheet containing a visual basic macro, able to process multiple simulation requests.

AINA user only must specify the values of parameters that change among simulations, and SimSched will change the configuration files, execute the corresponding AINA simulations and store the output files with an appropriate name, in both text and excel format.

At the beginning of this thesis work, simulations were executed one by one, and results were compiled by the user. A parameter scan for the study of LOPC transients could take weeks using several desktop computers and needing a team of users. With this macro, calculations are executed autonomously, without supervision.

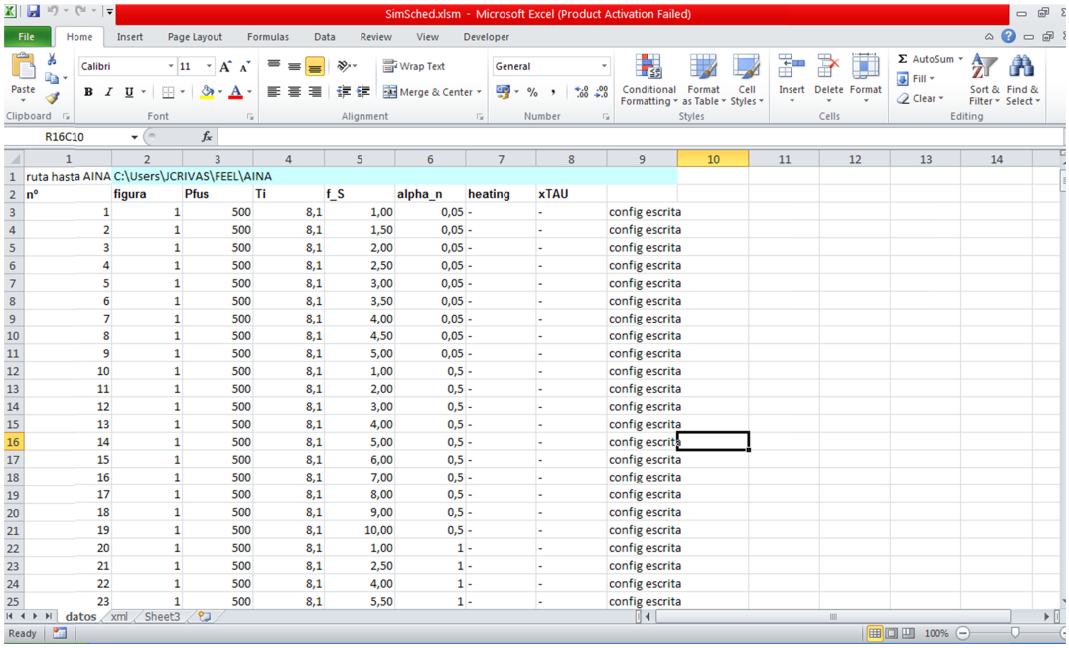

Figure A3-1: Main sheet in SimSched

It includes three stages:

- Preprocessing: configuration files are created from parameters specified in each row of the spreadsheet, and stored in a configurations folder.

- Processing: simulations are executed sequentially for each configuration file, and output files are stored in an output folder.

- Postprocessing: output files are read to extract statistics like maxima, minima or average values for all the output variables, and these value are stored in a statistics spreadsheet.

In Figure A3-1, the main input sheet is shown. Here, the AINA user must configure the path to AINA application directory. The simulations are configured in individual rows. The two first columns are auxiliary fields, for information purposes. In this case, the number of simulation and a code for the figure that will include the results. The next columns are variables to be modified in the file input_vars.xml.

The last column must be blank to change the configuration file. Otherwise, SimSched will skip it.

SimSched application uses a special version of AinaGui application named AinaGuiAuto, that starts execution immediately, and exits after finishing calculations. Besides, it uses a directory structure composed by the folder “SCRIPT”, containing template configuration files and the subfolders “configuraciones” and “resultados”, where configuration files and results are stored.

Annex 4: View factor calculation code

The results of the view factor code are used to configure AINA simulations, improving previous studies and also allowing the configuration of arbitrary geometries of next-step reactors.

Features

Figure A4-1 shows an example of results from this code, with the original surface marked as the isolated red point in the left. Green points represent the centers of surfaces that can be seen from the origin and red points representing the centers of hidden surfaces.

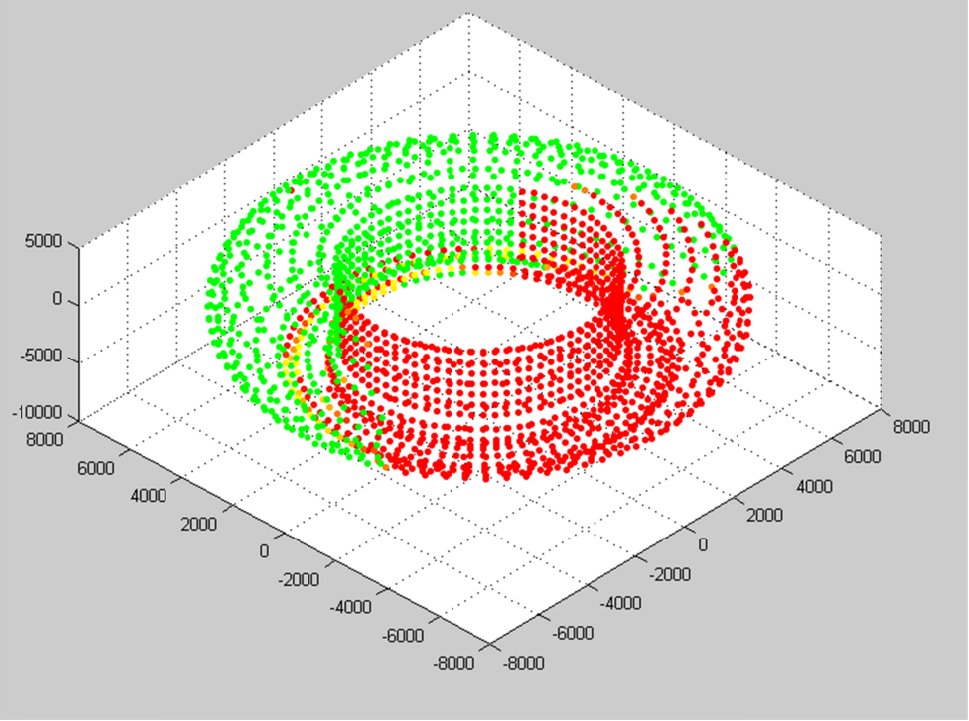

Figure A4-1: Example of results from calculation of view factor between ITER in-vessel components. Dimensions are in mm.

The code allows using any poloidal configuration, with a variable number of sections. It makes possible to increase the number of sections on regions of interest for more accurate studies about the critical section where, for example, the higher FW temperature is achieved in a LOCA accident.

In addition the code can calculate the view factor matrix for future shapes of symmetric fusion reactors like DEMO, and also can calculate the view factor from module to module for none toroidally symmetric reactors.

Algorithm of the code

First of all, the user is asked about the poloidal configuration of the reactor. It can be introduced either by writing the length of the sections and its poloidal orientation or also by writing the Cartesian coordinates. The user should also write the number of modules on the toroidal direction for each section.

Then, the code determines the toroidal and poloidal position of each section and calculates the vertices, center and surface of each module.

Once the code has the 3D configuration of the reactor, it starts the calculations. Two functions are used, one for calculating the view factor of two isolated faces, and the other to calculate the interference of other surfaces.

Symmetry considerations allow to simplify calculations, because the view factors on the right side will be the same as in the left side.

Finally, a sum of the view factor from the first module of a certain section A to all modules corresponding to section B is done. That is how the code can finally give a 2D matrix of view factors from a 3D configuration, that can be used as input for AINA simulations.

Symmetry assumption

Symmetry considerations allow to simplify calculations, because the view factors on the right side will be the same as in the left side.

Other consideration is that the distribution of the view factors of one module is the same that any other module situated on the same poloidal section, that is why the code only calculate the view factor from one module for each section to all the modules.

Finally, even there is no symmetry in the matrix calculated it can be related and if the surfaces of the sections are known is possible to calculate just half of the matrix, because Fa->b*Sa/Sb=Fb->a. However, the code doesn't use that propriety just for the reason of checking that is working properly all around the reactor.

Limitations of the code

Some limitations of the algorithm impose limits to the accuracy of the solution. For example:

The calculation uses discrete surfaces, which make results less accurate. However, it makes calculations faster.

The treatment of overlapping of surfaces is approximate, because overlapping is detecting by ray tracing and thus partial overlapping treatment depends on the number of vertices that are hidden. The accuracy could be improved by dividing overlapping modules in submodules.

The computational time in a desktop computer with this Matlab script could be approximated as y=0.0028x, where y is the amount of hours spent on the simulation and x the number of submodules to analyze. So for 4000 submodules, that is not so much the simulation spends about 12 hours.

ITER configuration simplifications

The following simplifications are considered:

- The gap between the modules is not taken into account, but it is actually of about 10 mm.
- All faces are considered flat, but in fact they are convex.
- The divertor is modeled with nine straight modules but in fact it is a curved surface.
- Configuration is purely symmetric when in the real configurations some modules are substituted by some ports

Annex 5: Python script for 2D parametric scans with PROCESS code

Code description

In the frame of systems studies done for the Tecno_FUS project at CCFE, a python script was developed which can be used to perform a 2D scan over selected input variables, and give outputs for different variables and error codes, which can be helpful to map the behaviour of both the operational space and the PROCESS solver.

The script is configured through a simple text file, so there is no need for the user to change the python source code. Other features include:

- Feedback of the previous output data to the current iteration input file, in order to improve the convergence.

- Generation of error files showing convergence problems and changes in the vector of saturated variables, which can help to interpret unexpected changes in the solutions.

A lot of work was still remaining to make this script functional for PROCESS users, however this initial version showed the potential of this technique in performing sensitivity analyses with PROCESS.

Future work can include:

- Use of the script with different INPUT files, currently it has been only tested with the last version of DEMO 2013 input file.

- More complete error checking for the configuration and input files, to avoid undesired effects on the code function.

- Direct generation of figures from the data output.

Some results generated with the script:

DEMO 2013 sensitivity analysis

On the basis of DEMO2 2013 IN.DAT file, several sensitivity studies were done by performing 2D parametric scans over two variables simultaneously with the python script and PROCESS code. The sensitivity analyses are described in the following:

1.- Change the current drive efficiency multiplier (FEFFCD) and wallplug efficiency (ETANBI) in a systematic way, and see how the solution changes, bearing in

mind that PROCESS is trying here to find a minimum major-radius machine that still gives 500MW net electric power, so more current drive power will require more electrical power, and more fusion power, and therefore a bigger machine.

The script was configured to perform a parametric scan over both variables. The results are shown plotting the product ETANBI x gammaNBI against the major radius. It can be seen that, as the global performance of the NBI system increases, the reduction in the major radius due to a better efficiency reaches saturation.

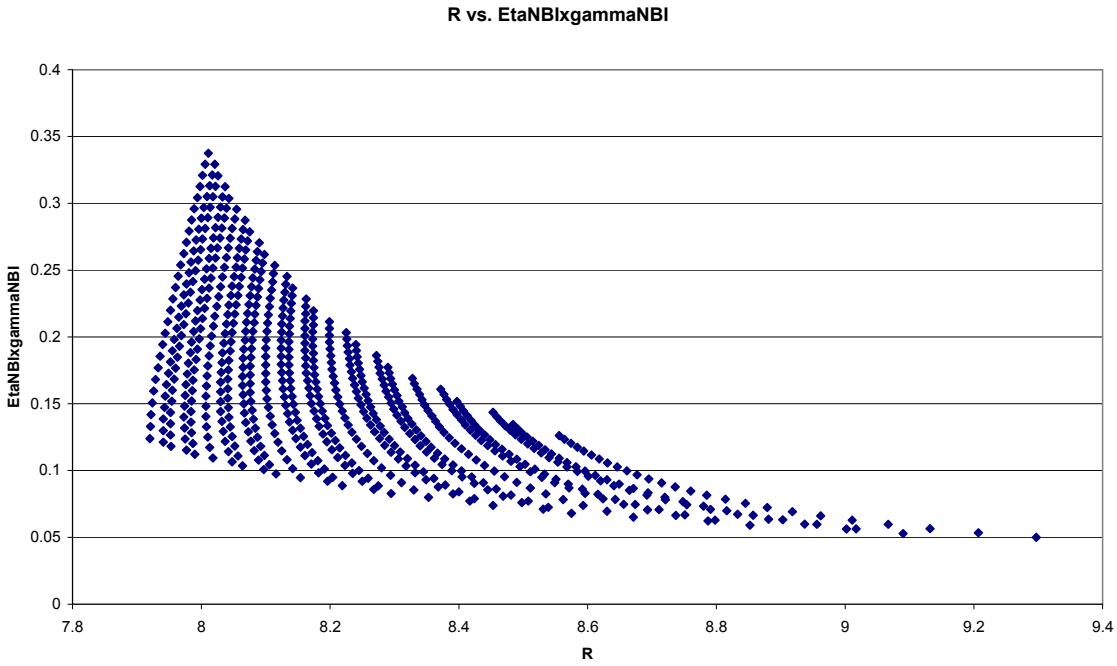

Figure A5-1: product ETANBI x gammaNBI against the major radius

2.- In addition we want to protect the divertor by limiting the exhaust power which gets to it (output pdivt). As injected and fusion powers increase, this will go up, so we will want to increase the radiation from the plasma to compensate. We do this by increasing (or decreasing, if pdivt is acceptable) the seeded impurity fraction CFE0 in the input file. This can also be iron (ZFEAR=0 (default)) or argon (ZFEAR=1). Changing this will again affect the radiation and the plasma dilution.

For this analysis, the script was configured to perform a parametric scan with the fraction of impurities (CFE0) and the type of impurities (ZFEAR), and taking as output variables the exhaust power (pdivt) and the major radius. The selected figure of merit to plot was pdivt/rmajor, and a threshold value of 12 MW/m was considered as optimum.

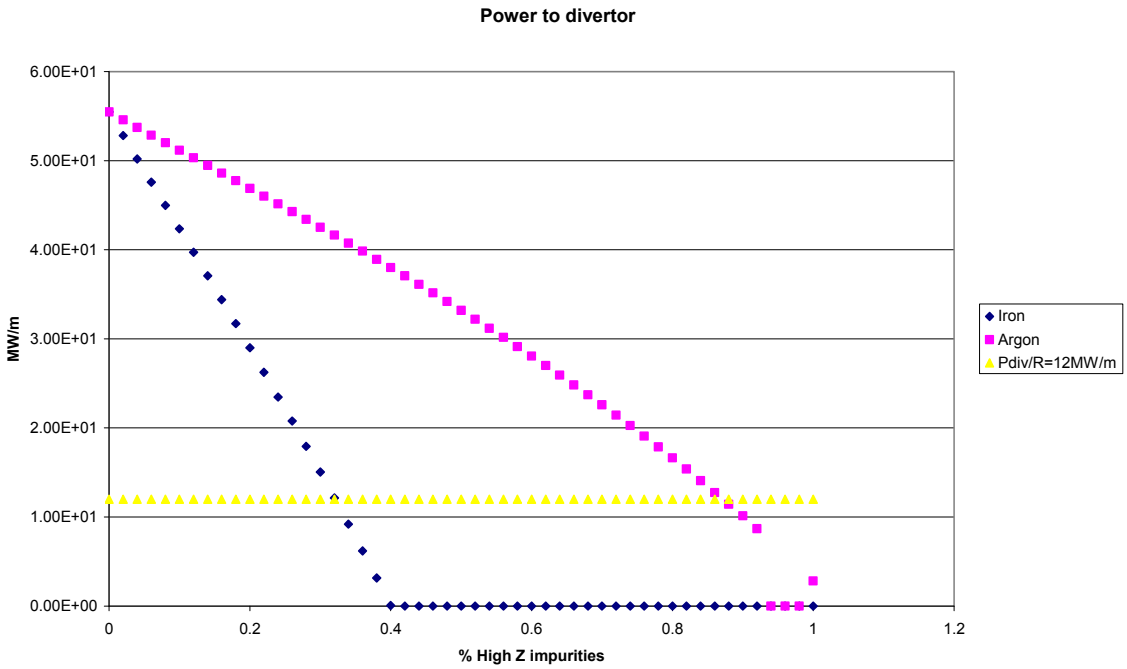

Figure A5-2: parametric scan with the fraction of impurities (CFE0) and the type of impurities (ZFEAR). The selected figure of merit to plot was pdivt/rmajor, and a threshold value of 12 MW/m was considered as optimum.

In the figure, it can be seen how for the argon curve there are three anomalous points. These are due to numerical Problems when finding the solution. However, the general tendency of the curve is clear. From the results it can be seen that iron needs a lower impurity fraction in plasma to reach the threshold value for divertor load, so it is more efficient than argon.

3.- It is also worth exploring a little advanced plasma scenarios. What happens if we allow H to increase (increase BOUNDU(10))? What happens if we change the plasma profiles to represent decreasing collisionality (compare alphan = 0.1, 0.3, 0.5)? Does allowing a higher beta limit (set DNBETA) help? (If not, what other factors are preventing us from reaching the beta limit?)

In the two next figures we see the results of a 2D scan in HH98 and alphaN variables.

For the first figure we can see how, as HH98 increases, the major radius decreases until reaching a saturation value. It is due to the beta limit being reached, what blocks further improvement.

In the second figure we can see how, for alphaN>0.23, the major radius reach a saturation curve, due also to the beta limit being reached.

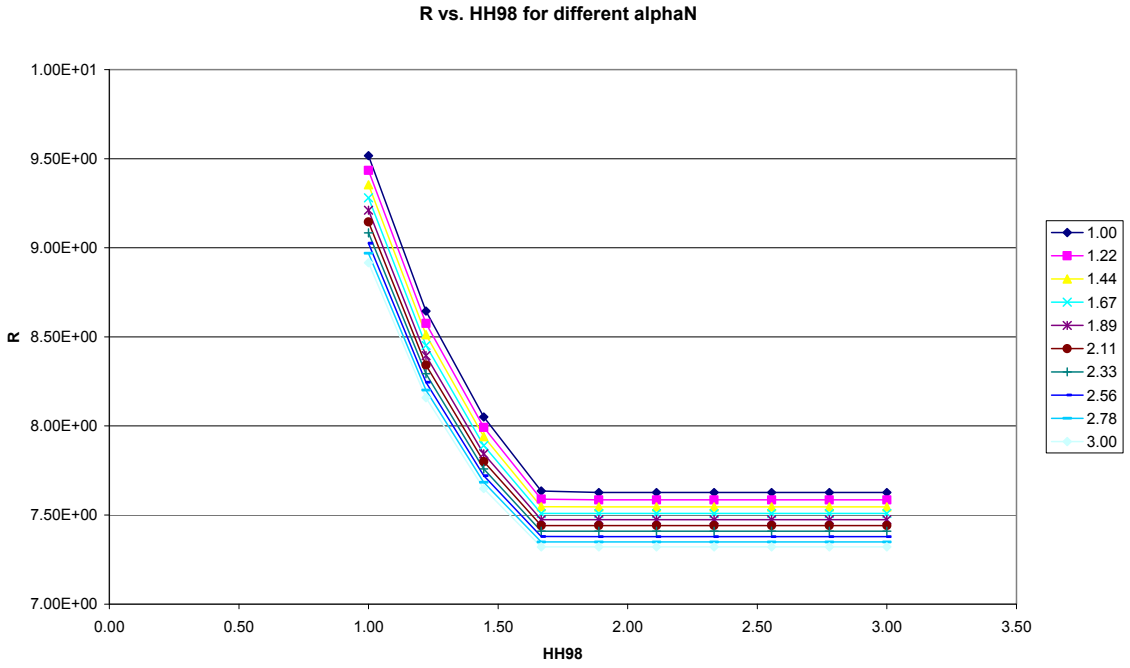

Figure A5-3: 2D scan in HH98 and alphaN variables

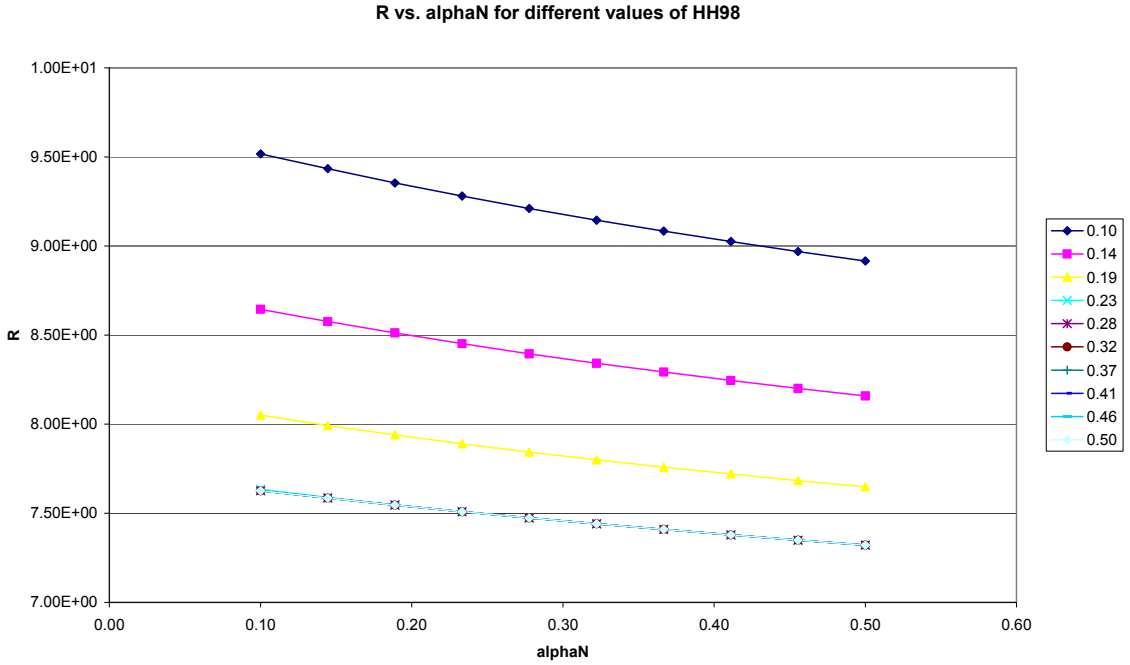

Figure A5-4: 2D scan in HH98 and alphaN variables

In the next two figures we see the effect of increasing the beta limit allowed over the major radius.

Combined increase in HH98 and DNBETA allow the major radius to decrease. And a liomit in te value of any of the two variables block the decreasing of the major radius.

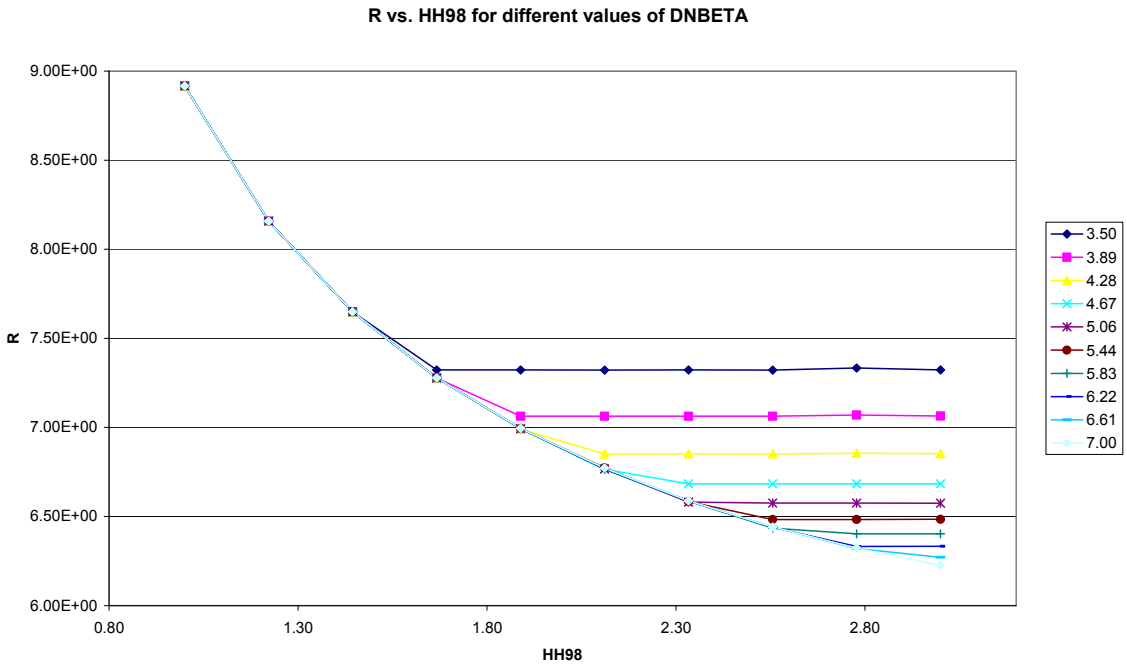

Figure A5-5: effect of increasing the beta limit allowed over the major radius

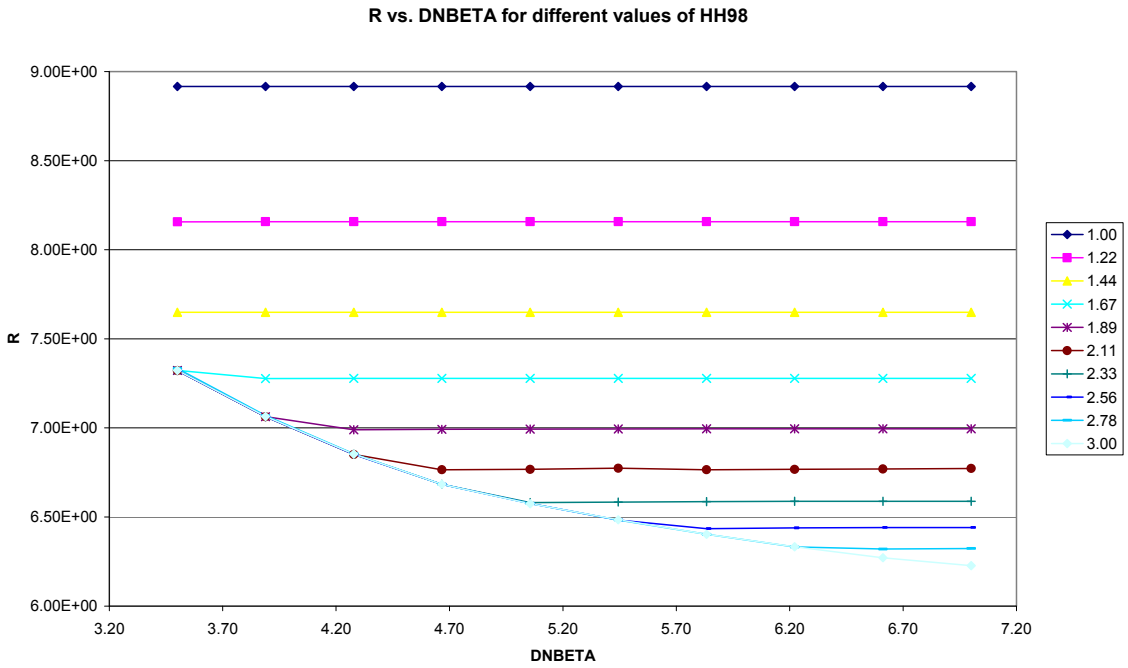

Figure A5-6: effect of increasing the beta limit allowed over the major radius